Self-assembly of POSS-Containing Materials

Anna Kowalewska

Abstract Polyhedral oligomeric silsesquioxanes (POSS) are unique nanoscale compounds that play a very important role in nanotechnology and materials science. The three-dimensional hybrid molecular clusters can form a range of well-defined supramolecular structures, owing to their intrinsic ability for aggregation. The organization of POSS in the solid state provides a non-covalent "crystalline template" approach. Understanding the mechanisms behind the cooperative interactions in POSS-based materials allows for the tailored performance of the building blocks and is essential for the development of novel hierarchical hybrid materials. Numerous reports have been published on various aspects of POSS chemistry and technology. This chapter presents an overview of selected contributions to the field of POSS-based nanostructured materials and the phenomena operating at the nanolevel in the truly beautiful world of the self-assembling polyhedra.

Keywords Polyhedral silsesquioxanes · Self-assembly · Crystal packing Interface · Templating · Surfactants · MOF · Liquid crystals · Optoelectronics Advanced materials · Biomaterials

1 Introduction

Polyhedral oligomeric silsesquioxanes (POSS) are structurally well-defined, three-dimensional hybrid molecular clusters with a rigid inorganic nanocore surrounded by organic groups that can be modified to achieve the desired physicochemical properties. The term *silsesquioxane* describes their characteristic stoichiometry, where each silicon atom (*sil-*) is bonded to one-and-a-half oxygen (*-sesquiox-*) and to a hydrocarbon moiety (*-ane*). Octasilsesquioxane ($R_8Si_8O_{12}$, T_8) is POSS molecule, with quasi-spherical geometry of the siloxane core (Scheme 1). Species with spherosilox-

A. Kowalewska (✉)
Centre of Molecular and Macromolecular Studies, Polish Academy of Sciences, Sienkiewicza 112, 90-363 Łódź, Poland
e-mail: anko@cbmm.lodz.pl

S. Kalia and K. Pielichowski (eds.), *Polymer/POSS Nanocomposites and Hybrid Materials*, Springer Series on Polymer and Composite Materials,
https://doi.org/10.1007/978-3-030-02327-0_3

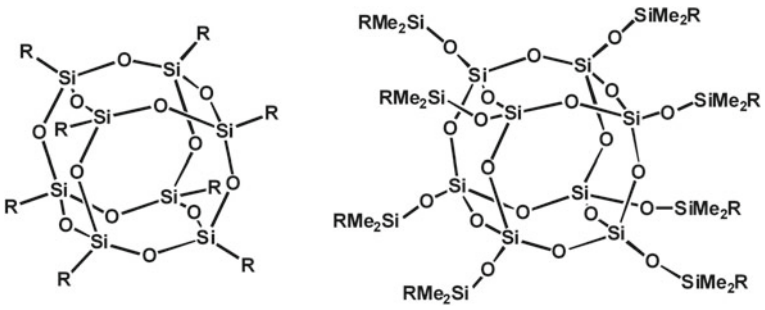

Scheme 1 Molecular structure of octahedral silsesquioxanes T_8R_8 and dimethylsiloxyspherosiloxanes Q_8MR_8

ane cage $(SiO_{4/2})_8$ surrounded by functionalized dimethylsiloxy groups ($OSiMe_2R$) (Q_8MR_8) also belong to the family of POSS compounds.

Over the last two decades, POSS have received an exceptional attention in macromolecular science and nanoengineering as building blocks for the synthesis of various organic–inorganic hybrids. Apart from their high symmetry and nanosize of the chemically robust framework, POSS are non-toxic and biocompatible. POSS show also excellent thermal characteristics [1], ultralow dielectric constant [2] and extraordinary oxygen plasma etching resistance [3, 4]. Well-defined structural features and tailor-made physicochemical properties make POSS ideal nanofillers for polymer composites [5, 6]. They can be blended into polymer matrices, grafted as side chains or acting as cross-linking sites. Their incorporation improves physicochemical properties of the material and its processing (glass transition temperature, thermal stability, mechanical performance) [7–13]. POSS can also influence the crystalline morphology of polymers facilitating or hindering the crystallization process [14, 15]. Polyhedral silsesquioxanes have been also used for the synthesis of more advanced materials such as light-driven artificial enzymes [16], biomaterials for tissue engineering [17], biocomposites [18], optical sensors [19] or scaffolds for controllable 3D π-conjugated luminophores [20].

Hierarchical structures are present in a range of POSS-based advanced materials, including amphiphilic macromolecules, nanoparticles and liquid crystals [21–24]. The structure of POSS and most POSS-derived shape amphiphiles is accurate without polydispersity. As a result, hierarchical nanoassemblies can be obtained with sharp interfaces between different domains and low defect density. It makes POSS ideal elemental building blocks for the preparation of diverse inorganic–organic hybrid materials by the bottom-up approach. Self-assembly is one of the methods most frequently used to obtain ordered structures. Non-covalent interactions such as intermolecular hydrogen bonding, π–π stacking and hydrophobic interactions are typically used as driving forces in the construction process. Understanding the phenomena directing the molecular packing of POSS is crucial for the effective design and control of hierarchical structures as well as physicochemical properties of POSS-based hybrid materials.

2 POSS Crystal Packing and Hierarchical Structures in the Solid State

The ability of POSS for self-assembling and formation of well-defined superstructures in solid state should be reviewed in the context of their morphology. Silsesquioxanes can be easily functionalized, and the respective synthetic methods for their preparation have been recently reviewed [25–31]. The nature of the organic periphery affects the molecular packing of POSS as well as their characteristic mesomorphic behaviour [32, 33]. The highest symmetry arrangement for octahedral silsesquioxanes with functional groups in each octant of Cartesian space would be the one with side substituents pointing away from the vertices of the core. In fact, the preferred way of organization and packing morphology of POSS molecules depend on several factors. The most important one is the type, size and structure of the organic substituents [34]. The way of side group distribution around the silsesquioxane core, closest distances and contacts between arms in the same molecular cage as well as other neighbouring cages can play a significant role in self-assembled systems. Monofunctional POSS (T_8R_8) bearing the same organic groups at each of silicon atoms and multifunctional (bifunctional or heterofunctional) POSS ($T_8R_{8-x}R'_x$) with more than one type of organic substituents can form completely different supramolecular assemblies.

2.1 Monofunctional POSS

A range of crystal-packing types and polymorphic forms have been described for silsesquioxanes bearing the same type of organic groups at each of silicon atoms. Majority of solid T_8R_8 crystallize in the triclinic space group *P*-1; nevertheless, monoclinic, tetragonal and rhombohedral structures have been also reported. X-ray diffraction studies revealed that T_8R_8 with relatively small alkyl or aryl substituents have molecular symmetry close to octahedral (O*h*), and their packing patterns are governed by the inorganic core [35–39]. Such species can be treated as spheres that are arranged hexagonally in the crystal structure in ABCA sequence [38, 40–42]. In such a pattern, molecules in one layer lie above the interstitial spaces in adjacent layers. The tiniest POSS molecules of T_8H_8 pack most closely in the trigonal *R*-3 ($^2C_{3i}$) crystal lattice [43, 44]. Organic substituents at silicon atoms prevent such close packing. Characteristic diffraction peaks in a single-crystal X-ray spectrum of an octahedral silsesquioxane appear at 2θ values corresponding to overall dimension of the molecules, body diagonal of the silsesquioxane cage [(1–11) plane, ~5.4 Å] and the distance between its opposite faces [(300) plane, ~3.1 Å] [25, 45]. The diffraction patterns of T_8R_8 with R = Me, Ph, vinyl or allyl suggest that the average value of the length of Si–O bonds in silsesquioxane cages is independent of the nature of the organic substituent [46]. Polymorphism phenomenon, which is the ability of

chemical compounds to exist in more than one crystalline structure, was observed for many POSS [39, 47–50].

T_8R_8 molecules bearing elongated side groups at the inorganic core exhibit a "rod-like" uniaxial symmetry [39, 47, 51–53]. In most cases symmetrical, radial arrangement of side substituents around the silsesquioxane cube is unfavourable for efficient packing in the crystal structure. Long side chains are much better accommodated if aligned orthogonally to the two opposite faces of the inorganic cube. Despite the rod-like structure and the arrangement in solid state similar to that of mesogenic groups along *b*-axis in liquid crystals, rod-like POSS do not belong to the class of smectic/nematic compounds. Side substituents control the type of packing of POSS in the crystal lattice. $T_8(n\text{-}C_nH_{2n+1})_8$ ($n = 7$, 8–14, 16, 18) are crystalline solids at room temperature owing to the intermolecular interactions and van der Waals attraction forces between *n*-alkyl chains [39, 47, 51–53]. The molecules are stacked in a lamellar or bilayer arrangement in triclinic (*P*-1) crystals. Similar structures are formed by *n*-alkanes C_nH_{2n+2} (n(even) = 6–26) [54]. The same type of solid-state packing (triclinic, *P*-1) was found for POSS with hetero-organic side groups, e.g. $T_8(CH_2CH_2CH_2SH)_8$ [55, 56], $T_8(CH_2CH_2CH_2Cl)_8$ [57, 58] and T_8(3-paramethoxyphenylpropyl)$_8$ [39]. Molecules of $T_8(CH_2CH_2CH_2SH)_8$ are additionally bound by weak S–H–S hydrogen bonds [56].

Side alkyl groups in rod-like $T_8(n\text{-alkyl})_8$ also crystallize in conformations similar to those characteristics for *n*-alkanes. Some POSS bearing *n*-alkyl groups are also polymorphic. The most efficiently packed crystal lattice is formed when alkyl chains are stacked parallel to each other in low-energy trans zigzag conformation. In some cases [e.g. $T_8(n\text{-alkyl})_8$, $n = 4$, 6], the alkyl arms can be distorted away from the molecular axis and interdigitated between the layers [47]. Molecular packing of $T_8(n\text{-}C_5H_{11})_8$ is quite unique. Side arms are spaced radially out of the core, giving rise to a "disc-like" arrangement of molecules in two-dimensional columnar structures [47]. A similar structure can be induced under appropriate crystallization conditions for otherwise rod-like $T_8(n\text{-}C_7H_{15})_8$ [47]. In the case of POSS with longer side chains [$T_8(n\text{-}C_8H_{17})$ and $T_8(n\text{-}C_{10}H_{21})$], an adjustment of molecules in the crystal network is required in order to obtain the most compact structure [47]. Side alkyl chains do not interdigitate but are tilted to the basal plane of POSS cages and aligned antiparallel to each other with respect to the layers that are separated by well-defined gaps.

Interestingly, despite all similarities, the hierarchical structures and packing morphologies of octasilsesquioxanes T_8R_8 and dimethylsiloxyspherosiloxanes Q_8MR_8 can differ significantly. It was found that the type of packing can be strongly altered if the size of the inorganic core increased. Moreover, flexible siloxane linkers (-$OSiMe_2$-) between alkyl groups and siloxane cages allow for greater mobility of side arms and larger distance between the free chain ends. It results in lower melting temperatures (T_m) of Q_8MR_8 compared to their T_8R_8 analogues. The effect seems to be more pronounced for species with small organic substituents. For example, ideally symmetric molecules of T_8Me_8 form rhombohedral crystals (space group *R*-3) [59] but those of only slightly larger $T_8(OMe)_8$ are triclinic (space group $P1\text{-}C_i$) [35, 60], while both T_8H_8 [43] and Q_8MH_8 [35, 37, 61] crystallize within trigonal-rhombohedral lattices (space group *R*-3). Interactions between substituents in Q_8MR_8

with long alkyl groups are more important than the increased mobility of side arms due to the presence of flexible dimethylsiloxane linker. Consequently, they govern the crystal packing of such molecules. For example, side alkyl arms of $T_8(n\text{-}C_{18}H_{37})_8$ and $Q_8M(n\text{-}C_{18}H_{37})_8$ point away in parallel way from the polyhedral core [51]. Both molecules are of rod-like shape, but crystals of Q_8MR_8 are more compact due to the interdigitation of long alkyl chains. Dimethylsiloxyspherosiloxanes octasubstituted with $R = -(CH_2)_2S(CH_2)_2(CF_2)_nCF_3$ ($n = 5, 7$) and their T_8R_8 analogues also belong to the same crystal group (triclinic $P1$) [37, 62].

The type of packing defines the course of melting of $T_8(n\text{-}C_nH_{2n+1})_8$. Melting temperatures are higher for species with longer side chains [36, 47, 53]. It can be ascribed to a larger extent of intermolecular interactions and more efficient packing. Yet, the increase in T_m exhibits an odd–even number effect due to the differences in packing geometry (parallelograms or trapezoids) and efficiency of intermolecular contacts, analogously to *n*-alkanes [54]. However, contrary to *n*-alkanes, $T_8(n\text{-}C_nH_{2n+1})_8$ ($n = 4$–11) did not show the odd–even effect in their experimentally (X-ray diffraction) estimated densities. The crystal density decreases on augmenting the length of side chains [47]. The effect was attributed to the separation of organic fraction by inorganic cubes and more efficient interdigitation of shorter side arms. For the same reason, the type of crystal packing determines thermal stability of $T_8(n\text{-}C_nH_{2n+1})_8$ [36, 47] and $Q_8M(n\text{-}C_nH_{2n+1})_8$ (linear, $n = 3$–8; and branched, $n = 5$–7) [37].

It was also found that melting temperatures of some rod-like POSS grafted with heterorganic side groups [56, 63] are higher than T_m of their *n*-alkyl analogues [53]. The effect was explained by strengthening the interactions between side chains due to the formation of hydrogen bonds.

2.2 *Heterofunctional POSS*

There are various synthetic pathways available for the preparation of heterofunctional POSS bearing more than one type of organic substituents at silicon atoms. Most reports published to date are focussed on octahedral silsesquioxanes of the T_8R_7R' type [29], sometimes named "monofunctional" due to the fact that only one of eight organic groups can be chemically modified.

Development of a synthetic procedure that would result in the desired heterofunctional silsesquioxanes is not an easy task. Co-hydrolysis of two different trifunctional organosilanes ($RSiX_3$, $X = Cl, OR'$) typically results in complicated, statistical mixtures of products [64]. T_8R_7R' are most often prepared in reactions of substitution or addition to one of eight reactive corner groups on the silsesquioxane core or by corner-capping of truncated trisilanol POSS [$T_7R_7(OH)_3$]. The latter procedure provides molecules of defined structure [65]. The majority of POSS obtained by the corner-capping strategy have seven chemically inert groups (e.g. Ph, *i*-Bu, *i*-Oct) and only one functional substituent that can be used for further modifications. However, the functionalization of the remnant organic moieties (if possible) leads to more elaborated systems. $T_8(CH{=}CH_2)_8$ is an ideal molecule for the preparation of

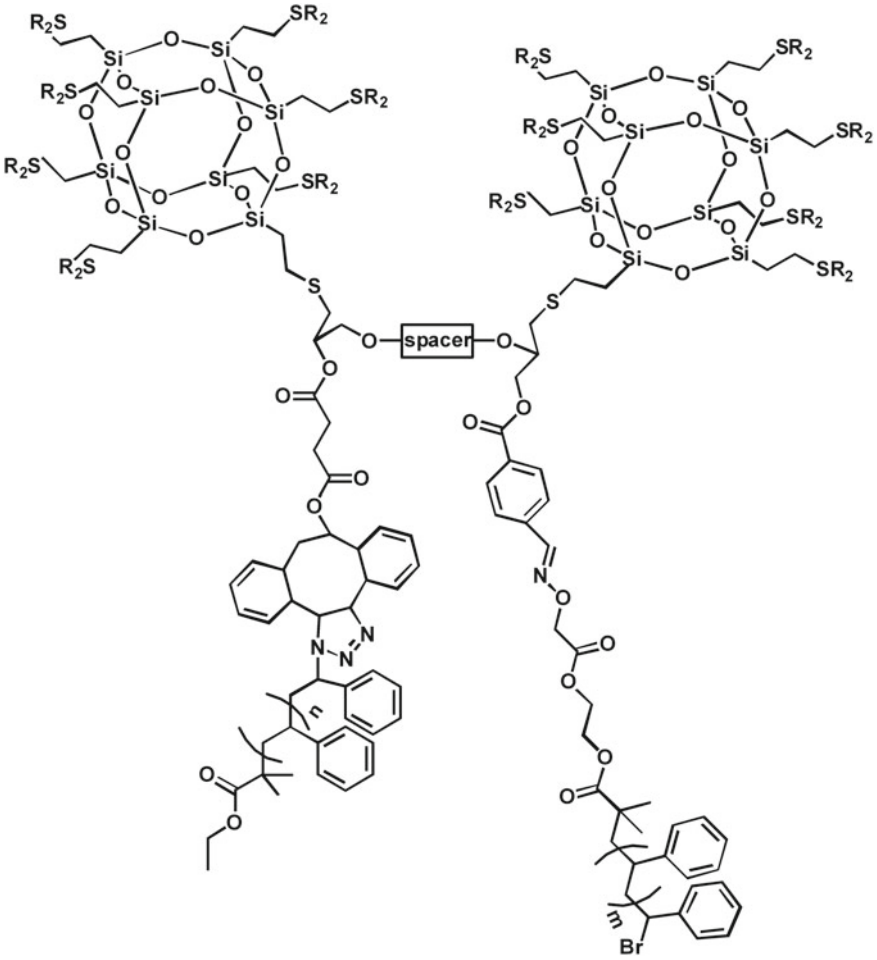

Scheme 2 Molecular structure of an asymmetric gemini surfactant (R = tert-butyl mercaptoacetate) [71]

such multifunctional products via "one corner" modification of the silsesquioxanes [66]. Procedures for anisotropic functionalization of $T_8(CH{=}CH_2)_8$ through reaction with triflic acid [30] or via thiol–ene chemistry [31] were developed. The resulting T_8R_7R' amphiphiles contain chemically distinct segments (e.g. hydrophilic and hydrophobic) connected via a covalent chemical bond. The products were used for the synthesis of various unsymmetrical macromolecules, such as shape amphiphiles based on polymer-tethered POSS [67–69], or asymmetric giant gemini surfactants (AGGS) of complex macromolecular structures (Scheme 2) [70–72]. The strategies for the preparation of such giant species can involve both "grafting-from" and "grafting-onto" procedures [22].

Other octafunctional POSS can be also selectively functionalized by monosubstitution at one of silicon atoms. For example, giant surfactants with acryloxyl-functionalized silsesquioxane heads were constructed from commercially available POSS and polystyrene. The head was subsequently functionalized with bulky ligands via thiol-Michael and thiol–ene addition of 2-mercaptoethanol, 1H,1H,2H,2H-perfluoro-1-decanethiol, 1-thio-β-D-glucose tetraacetate and 2-naphthalenethiol [73]. T_8H_7 monofunctionalized with a side group bearing azobenzene moiety was prepared by hydrosilylation of 4-butyl-4′-allyloxyazobenzene with T_8H_8 [74]. It was found that the bulky POSS ligands played an important role in the formation of cylindrical assemblies that were transformed into a mesostructured silica-like film. The *trans–cis* photoisomerization of azobenzene groups upon UV irradiation was also facilitated in the hybrid molecules.

Grafting of multiple functional groups onto POSS in two consecutive thiol–ene reactions resulted in a mixture of regioisomers (*para*-, *meta*-, *ortho*-) of bis-adducts that could be separated by flash column chromatography and isolated at synthetically useful quantities [31, 75, 76]. They were transformed into giant surfactants by the attachment of polystyrene chains [77]. Evidence was found for the influence of the tethering positions on the contributions of the system free energy (interfacial energy, head-to-head interactions and entropic energy of the tails). Upon increasing the temperature, the order–order transitions from lamellae to double gyroids were noted in the metaisomer, and from double gyroids to hexagonal cylinders in the orthoisomer (Fig. 1). It was observed that the order–disorder transition temperatures decreased in the order of *ortho*-, *meta*- and *para*-isomers.

POSS with cubic symmetry seem to be ideal candidates for the preparation of well-defined, bifunctional Janus-type "nanobricks". The term "Janus particle" (named after the two-faced Roman god of beginning and ending) was used for the first time by Pierre-Gilles de Gennes to define dissymmetric nanoscale objects with two distinct sides [78]. The structural directionality of each single particle results in unique physicochemical properties and is exceptionally promising for applications in nanoengineering, sensing, optical imaging and catalysis [79]. The synthesis of structurally well-defined and monodispersed Janus POSS is extremely challenging. Preparation of such molecules has been attempted from "half-cage" cyclic tetrasiloxanetetraol precursors [80–82]. However, the pioneering synthetic routes led to rather complex statistical mixtures of multifunctional cubes.

Recently, two reports have been published on the synthesis of true Janus POSS with a two-face substitution of silicon atoms in the inorganic core (Scheme 3). A structurally well-defined Janus nanocube of two chemically distinct opposed faces was obtained via symmetry controlled multiclick CuAAC functionalization of $T_8(CH_2CH_2CH_2N_3)_8$ with a conformationally constrained tetra-alkyne having an appropriate geometry and spatial orientation of the C≡C bonds [83]. Another nanometre-scale Janus silsesquioxane was synthesized through the cross-coupling of a "half-cube" cyclic sodium siloxanolate with another "half-cage" cyclic fluorosiloxane [84]. The structure of the isolated compound (triclinic, space group *P*-1) was confirmed by X-ray crystallography.

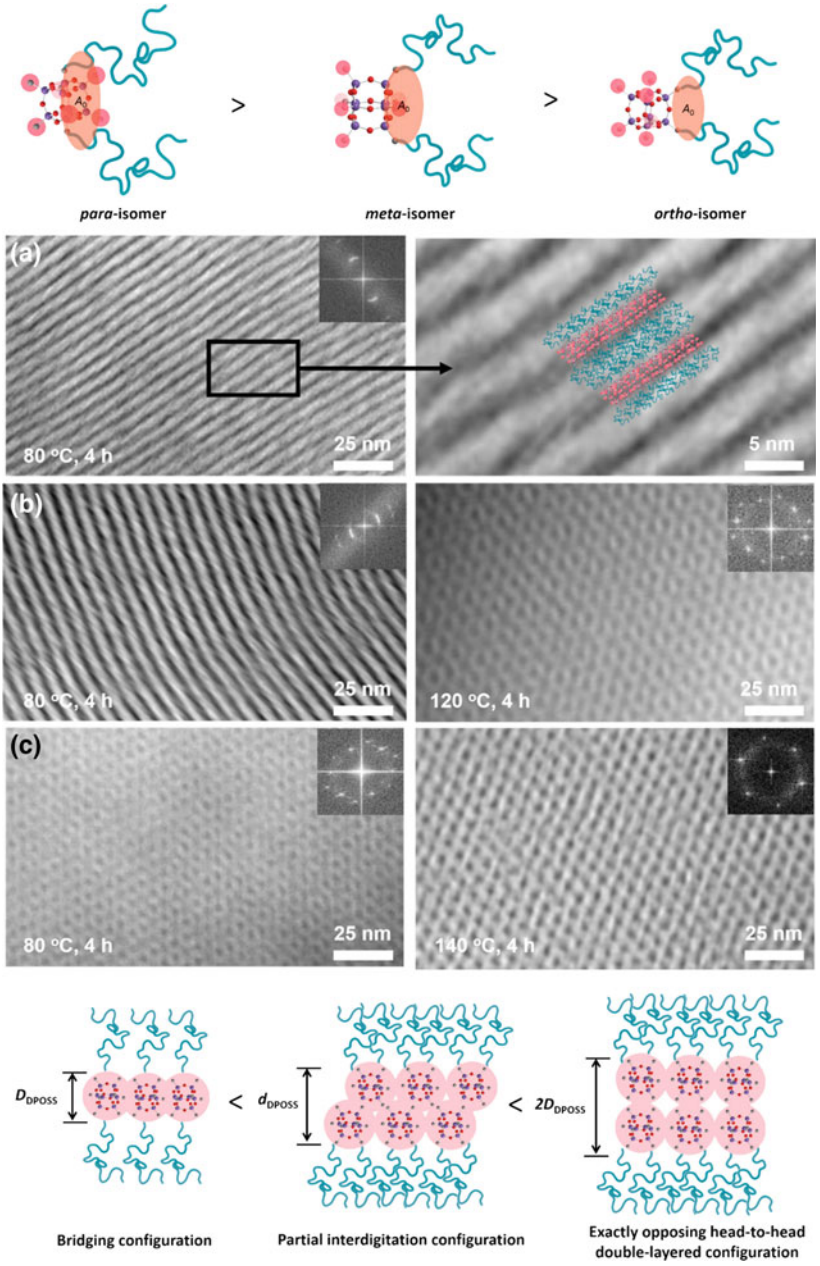

Fig. 1 Packing schemes of giant surfactant regioisomers with two PS chains and hydroxyl-functionalized POSS head, and variable temperature TEM images of microtomed samples and the corresponding diffraction patterns obtained from fast Fourier transformation of the images for **a** LAM phase of paraisomer at 353 K (the zoom-in view and the molecular packing model); **b** LAM phase of metaisomer at 353 K (left), and DG phase (right) of metaisomer at 393 K; **c** DG phase (left) of orthoisomer at 353 K and HEX phase (right) at 413 K. Adapted with permission from [77]. Copyright 2018 American Chemical Society

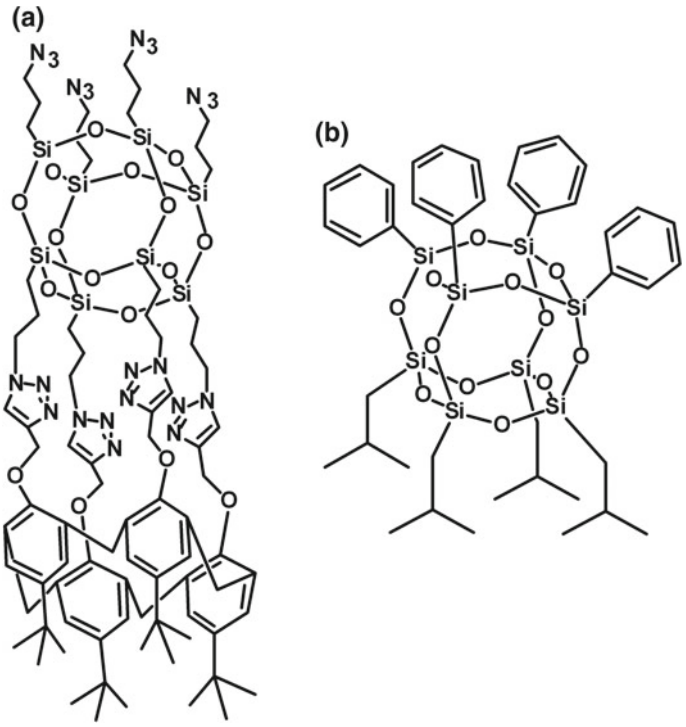

Scheme 3 Structure of octahedral "Janus" silsesquioxanes **a** 1,3,5,7-tetraazidopropyl-9,11,13,15-tetratriazolyl-calixarene-pentacyclo-[9.5.1.13,9.15,15.17,13]-octasiloxane [83] and **b** 1,3,5,7-tetraphenyl-9,11,13,15-tetraisobutyl-pentacyclo-[9.5.1.13,9.15,15.17,13]-octasiloxane [84]

3 Mesomorphic Behaviour of POSS Crystals

Thermally induced packing polymorphism due to the conversion from a metastable to a stable crystal structure can be observed for a range of polyhedral silsesquioxanes. It is an exceptionally important phenomenon that can be used for the design of self-assembled hierarchical systems based on crystal structures formed by POSS. The major solid–liquid phase transition of melting/crystallization can be accompanied for some octahedral silsesquioxanes by specific transformations in the solid state, involving changes of their crystal structure. For example, $T_8(n\text{-Pr})_8$ can exist in two forms: hexagonal (space group *R*3) above 272 K and triclinic (space group *P*1) below 272 K [42]. Three different crystal structures varying in unit cell dimensions, the space group and the conformation of cyclohexyl rings were observed for $T_8(\text{cyclohexyl})_8$ (*P*-1 triclinic, *R*3 rhombohedral and *P*4/n tetragonal) [39]. The packing morphology and thermal behaviour of some aryl-substituted POSS are also dictated by molecular interactions between the side groups [85]. For example, two

crystal structures [triclinic (*P*1 or *P*-1) and monoclinic (space group *P*2/m or *P*m)] were found for T_8Ph_8 [42].

The phenomena can be caused by increased molecular motions within the crystallites involving rotations in side groups or by a minor structural reordering of alkyl chain arms (without changes in the long-range order of the molecules). Compounds that exhibit such behaviour are known in organic chemistry as "plastic crystals" [86]. They interact weakly in the solid state and can be dynamically disordered with respect to the orientational degrees of freedom, e.g. by jump diffusion between a restricted number of possible orientations [87]. The term "rotor phase" or "rotatory phase" is also used if rotation of molecules is involved in the process. Classic plastic crystals are most frequently of globular shape, which provides little steric hindrance for reorientation and free tumbling about points of 3D crystal lattices.

Octahedral silsesquioxanes of spherical shape [e.g. $T_8(Me)_8$, $T_8(Et)_8$ and $T_8(i\text{-}Bu)_8$] are capable of free tumbling about their axes of symmetry which give rise to solid–solid state transitions that can be detected by a range of analytic methods (X-ray crystallography, calorimetry, Raman spectrometry and solid-state NMR spectroscopy). It was found that triclinic crystals of $T_8(i\text{-}Bu)_8$ undergo transformation into symmetric rhombohedral structures on heating via transitional formation of a monoclinic crystal cell [88, 89]. The phase transition involves fast and cooperative rotation of CH_3 units in *i*-Bu groups, as was shown by solid-state NMR experiments and Raman analysis [89]. The rotation helps POSS molecules to adopt a spheroid-like shape compatible with D3h symmetry and to fit into a rhombohedral lattice of *R*-3m space group.

$T_8(CH{=}CH_2)_8$ exists as a mixture of conformers with a small energy difference [90]. Vinyl groups at the silica core are fairly unhindered, and the methylene groups can rotate between three minimum-energy positions. It results in a change of crystal structure from triclinic (*P*-1) characteristic at $T < 233$ K [91] to hexagonal (space group *R*-3) at $T > 233$ K, leading also to the expansion of unit cell volume, which is characteristic to phase transitions of first order [90, 92–94]. Thermal solid–solid phase rearrangements were also noted for $T_8(n\text{-}Pr)_8$ [42], T_8Et_8 and $T_8(CDCH_2D)_8$ [95]. Four different crystal phases were observed at different temperatures for $T_8(CDCH_2D)_8$ [95]. The largest change in packing symmetry was noted at 257 K ($\Delta H = 47$ J/mol K) leading to the transition from asymmetric triclinic (space group *P*-1) to a highly symmetric rhombohedral unit cell (space group *R*-3). It involved also the expansion of the cell volume and a decrease in the number of molecules per unit. The motions of side groups in $T_8(CDCH_2D)_8$ became increasingly anisotropic if the temperature was lowered past the transition point, as indicated by solid-state ^{1}H NMR spectroscopy [95]. A similar phenomenon was observed for T_8Et_8 (at 253 K, $\Delta H = 28$ J/mol K) [95]. The transition from triclinic to a closely packed hexagonal (space group *R*-3) arrangement of molecules in the crystal structure was observed as well for $T_8(n\text{-}Pr)_8$ (272 K) [42], $T_8(i\text{-}Bu)_8$ (330 K) [89] and $T_8(CH_2CH_2CH_2Cl)_8$ (~400 K) [94]. Thermal characteristics of other T_8R_8 systems bearing heteroatoms in their side alkyl chains (e.g. $T_8(CH_2CH_2CH_2SH)_8$ [56] and octa(3-decanamidopropyl)-silsesquioxane [63]) suggest analogous behaviour. Surprisingly, plastic crystal phase transitions were not detected for T_8Me_8, $T_8(i\text{-}Pr)_8$ nor

$T_8(n\text{-Bu})_8$ [42]. However, neutron powder diffraction studies indicated a strongly temperature-dependent rotational dynamics of methyl groups in the crystal of T_8Me_8 [96]. The results exhibited different average lengths and vibrational energies of C–H bonds in methyl groups. Two methyl groups with shorter C–H bond lengths are situated the hexagonal *c*-axis and have C_3 site symmetry, while the other six methyls (not placed on symmetry axes or planes) are of C_1 site symmetry.

Rod-like polyhedral silsesquioxanes of elongated structure do not meet the criteria of classic "plastic crystals". Despite of this, POSS grafted with long *n*-alkyl groups (both $T_8(n\text{-alkyl})_8$ [47, 51, 53, 95] and $Q_8M_8(n\text{-alkyl})_8$ [37] derivatives) can exhibit specific solid–solid phase transitions in solid state due to increased mobility of their side chains. Thermally induced structural reordering can involve segmental motions including kinking and chain twisting out of the plane. Such mesomorphic transitions are usually of a small consequence. Most often only reversible change of unit cell size is observed, and the long-range crystal structure is not affected [53]. In the case of their $Q_8M_8(n\text{-}C_{18}H_{37})_8$ counterparts, no evidence of a thermally induced solid–solid phase transition was found despite a reversible lattice expansion before melting [51]. Such a solid-state behaviour can be ascribed to the presence of the flexible $OSiMe_2$ spacers between the inorganic core and the alkyl chains. Nevertheless, Q_8MMe_8, Q_8MH_8 and Q_8MVi_8 of spherical shape behave as plastic crystals and show endothermic rotor phase transitions at low temperatures [35].

Multitechnique (DSC, DRS, PALS, NMR and POM) variable temperature studies have been carried out to explain the differences in the "plastic crystal" behaviour between spherical and rod-like octahedral silsesquioxanes [94]. $T_8(CH{=}CH_2)_8$ and $T_8(CH_2CH_2CH_2Cl)_8$ were chosen as the respective models (Scheme 4). The pattern of multiple phase transitions in $T_8(CH_2CH_2CH_2Cl)_8$ can be also found for other POSS, such as $T_8(CH_2CH_2CH_2SH)_8$, but in the case of the octa(3-chloropropyl)silsesquioxanes they are well separated. It enabled much more precise analysis of their nature. It was found that both POSS undergo reversible thermally induced phase transitions in the solid state (Fig. 2) due to increased dynamics of the side groups. The mechanisms leading to the best position of molecules in most symmetrical crystal lattices vary for the species of different symmetry (Scheme 5). In the case of spherical $T_8(CH{=}CH_2)_8$, the thermal energy was used to increase dynamics of side groups. The single phase transition observed at 233 K is of first order. It leads to a change in the permittivity due to α-type structural relaxation (Fig. 3), as well as expansion of the crystal lattice and thermochromism of the material.

The respective low-temperature transition (at 250 K) for rod-like $T_8(CH_2CH_2CH_2Cl)_8$ involved a unique negative thermal expansion of crystals and their self-actuation. The effect is opposite to that observed for $T_8(CH{=}CH_2)_8$; nevertheless, both observed lattice expansion and contraction are of first order, as indicated by the respective changes of heat capacity. High-temperature transitions (350–400 K) of $T_8(CH_2CH_2CH_2Cl)_8$ are of a completely different nature. The increased mobility of side groups at elevated temperatures resulted in a gradual change of crystal structure and formation of a highly symmetric system. The observed transitions are of second order, as suggested by the gradual increase in ΔCp in the corresponding temperature range. The complex behaviour was reflected

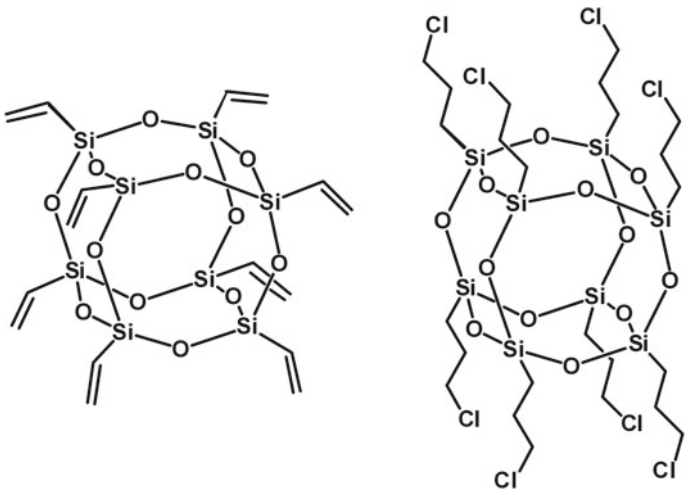

Scheme 4 Molecules of spherical $[T_8(CH{=}CH_2)_8]$ and rod-like $[T_8(CH_2CH_2CH_2Cl)_8]$ octasilsesquioxanes

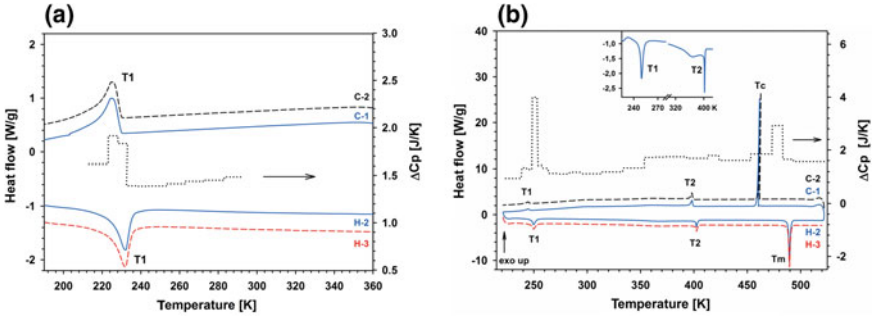

Fig. 2 DSC studies (heating and cooling runs) of phase transitions and changes of heat capacity (ΔC_p) recorded for **a** $T_8(CH{=}CH_2)_8$ and **b** $T_8(CH_2CH_2CH_2Cl)_8$ ([94]—reproduced by permission of the PCCP Owner Societies)

in unusual changes in the capacitance (Fig. 3) and fractional free volume of the material. The relaxation process due to the increased dynamics of 3-chloropropyl groups has a linear temperature dependency with low activation energy. The observed phenomena are important for molecular engineering of POSS-based well-defined hybrid materials capable of thermally induced structural transformations. Translation in solid state of rod-like molecules of POSS bearing reactive functions in their side alkyl chains can be of exceptional synthetic value, for example in POSS-based flexible networks of cooperative structural transformability via entropy-based subnet sliding.

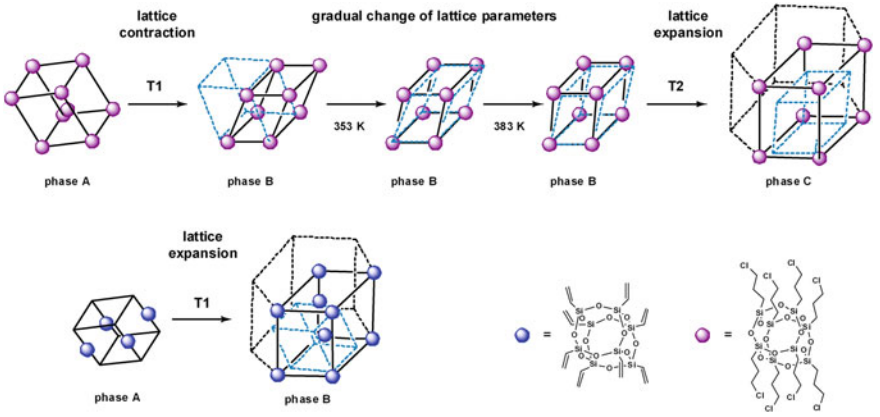

Scheme 5 Crystal lattice rearrangements on thermally induced solid-state phase transitions in $T_8(CH_2CH_2CH_2Cl)_8$ and $T_8(CH{=}CH_2)_8$ ([94]—reproduced by permission of the PCCP Owner Societies)

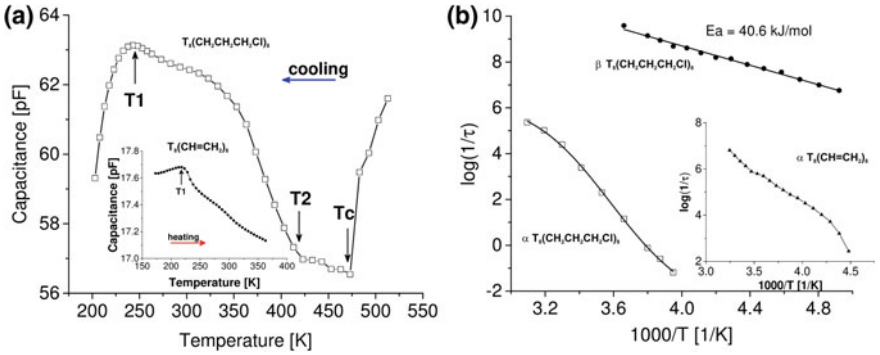

Fig. 3 Dielectric parameters as a function of temperature **a** capacitance plot and **b** temperature dependency of relaxation processes for $T_8(CH_2CH_2CH_2Cl)_8$ [insert $T_8(CH{=}CH_2)_8$] ([94]—reproduced by permission of the PCCP Owner Societies)

4 Advanced Hybrid Materials Based on POSS Self-assembling Phenomena

Single molecules of polyhedral silsesquioxanes can be regarded as organic–inorganic hybrid materials at the molecular level [24]. POSS molecules have been also successfully incorporated into a range of well-defined hybrid nanoarchitectures. The tendency to crystallize and formation of ordered nanostructures make POSS potential supramolecular "recognition elements" and crystalline templates in more complex systems. A wide range of nanotechnologies that were influenced by the phenomenon of the controlled self-assembly of silsesquioxane templates include preparation of nanoparticles of noble metals, quantum dots, complexes with DNA, metal–organic

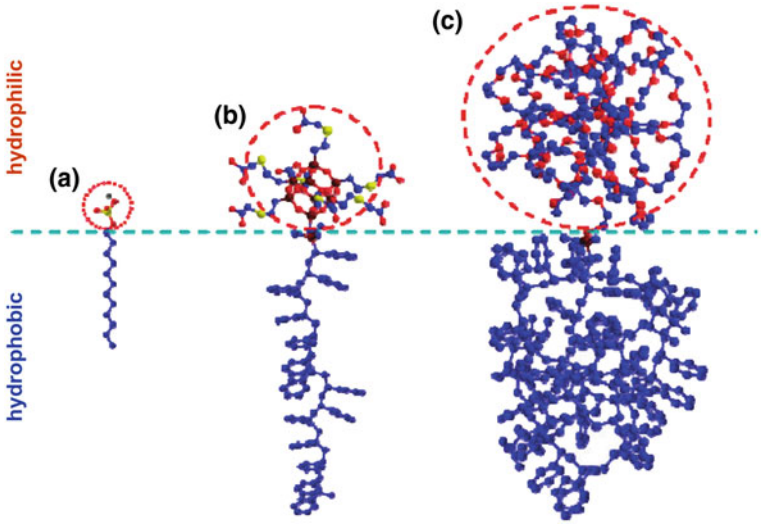

Scheme 6 Structural comparison of **a** typical small-molecule surfactant (sodium dodecyl sulphate); **b** giant hybrid surfactant with POSS head; and **c** typical amphiphilic diblock copolymer. Reprinted with permission from [100]. Copyright 2018 American Chemical Society

frameworks and materials for optoelectronics. They are discussed in the following part of the text.

4.1 Surfactants

Unsymmetrical multifunctional POSS (T_8R_7R') are of exceptional interest for a wide range of supramolecular systems, including amphiphilic moieties and surfactants [23, 97]. POSS of different geometrical and chemical symmetries with inorganic silsesquioxane heads monotethered with organic alkyl tails can form well-defined hierarchical structures. Adjustment of the length and branching of alkyl chains allows to tune intermolecular forces and molecular packing [98, 99]. Nanoscale arrangement of such building blocks in solid state is very important for materials engineering. Surfactants and block copolymers are capable of generating various thermodynamically stable micellar structures (spheres, cylinders and vesicles) in dilute solutions. Packing of such amphiphilic molecules depends on the equilibrium interfacial area of the ionic (hydrophilic) head at the critical micelle concentration (Scheme 6) [100]. Their self-assembly behaviours and the type of micellar structure are also determined by structural parameters (the size and chemical structures of immiscible parts and the overall size of molecule) and physical characteristics of experimental environments (solvent, concentration, pH value, temperature, additives) [22].

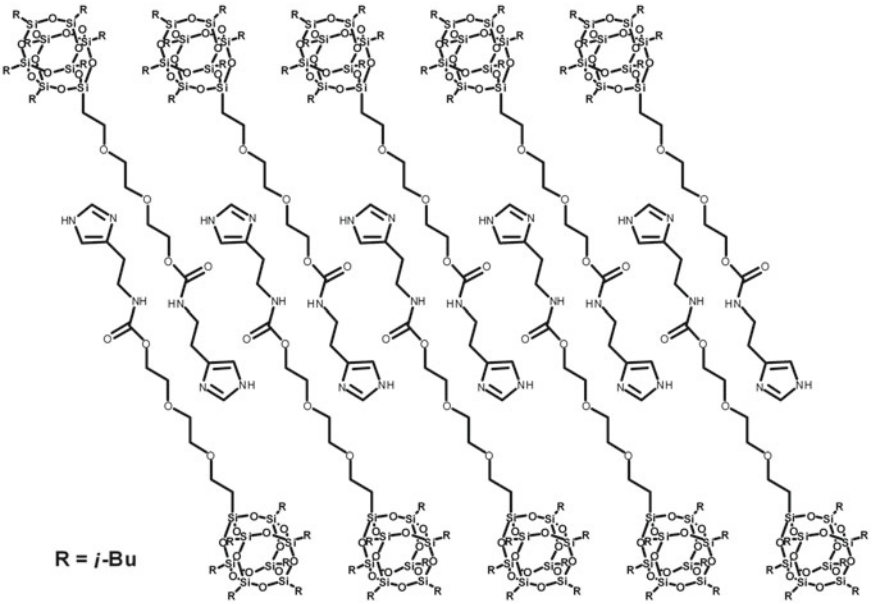

Scheme 7 "Head-to-head" interdigitated bilayer of amphiphilic POSS [102]

Molecular dynamics simulations revealed that attractive electrostatic POSS—POSS interactions in $T_8H_7(n\text{-}C_7H_{15})$ consisting of a silsesquioxane head and a single hydrophobic tail are responsible for association and clustering of inorganic cages [101]. Formation of a bilayer structure with sharp boundaries ("head-to-head", Scheme 7) is the preferred assembly mode for such molecules [98, 99, 101]. Even POSS with a relatively short organic tail at one corner of the cube can act as amphiphilic molecules of uniform molecular weight. To some extent, the order can be preserved even in the molten state since melting starts within the organic domain, prior to the decay of the inorganic lattice. The morphology at the nanometre scale and thermal properties can be changed with the length and number of branching in the side chains due to a minor structural reordering (rotation or translation) [98, 99]. Hydrophobicity of the organic tail is not a prerequisite for the organization of T_8R_7R' in solid state and at the interphase. The structure of such arrays can be controlled also by other factors. $T_8(i\text{-Bu})_7$ tethered with a hydrophilic organic tail terminated with imidazole group formed vesicles in water and well-defined interdigitated bilayer nanosheets in organic solvents due to the amphiphilic nature of the molecules in conjunction with hydrogen bonding from the carbamate groups [102].

Shape has been increasingly recognized as an important factor for the self-assembly of POSS derivatives. Diverse and complex structures can be created by an appropriate manipulation of the shape anisotropy of building blocks. Interesting effects were noted for amphiphilic POSS with long polymeric tails that enable a unique "bottom-up" strategy for the preparation of 2D nanostructures. The molecu-

lar geometry and enthalpy/entropy balance direct the organization of such species. Reduction of free energy guided by geometry (overall molecular shape) and properties (amphiphilic interactions) of those asymmetric molecules are the driving forces. It was observed that the hierarchical structures formed by giant surfactants, composed of various functionalized POSS heads tethered with polystyrene (PS) tails, are highly sensitive to the molecular topology. For example, grafting two PS tails to a POSS head shifted the boundaries between different ordered phases and altered the packing configurations of POSS, compared to the analogue with a single PS chain of equal molecular weight [104]. Two tri-armed organic–inorganic hybrids based on carboxylic acid-functionalized POSS with/without PS linkers self-assembled into hollow spherical nanostructures in water/organic mixed solvents [103].

Two completely different mechanisms and driving forces operate in the self-assembly process depending on the shape of macromolecules (Fig. 4). In the presence of PS linkers, the hybrid species resemble surfactants and form bilayer vesicles in a process driven by hydrophobic interactions. Single-layered, vesicle-like "blackberry"-type structures were obtained without polystyrene linkers. It was found that their formation was mediated by electrostatic interactions, with hybrids behaving like hydrophilic macroions. The alteration of the assembly size in response to the change of the solvent polarity was different for the two species. A remarkable sensitivity of highly ordered self-assembled structures to molecular topology was observed for giant surfactants composed of various functionalized POSS heads tethered with one or two polystyrene tails. It facilitated the engineering of various nanophase-separated structures with sub-10 nm features [104]. The boundaries between different ordered phases could be shifted to adjust the packing of POSS. It led to reduction of the self-assembled nanodomains. Their morphology depended also on the molecular details of functional groups on the silsesquioxane cages.

Asymmetric giant "bolaform-like" surfactants composed of PS chain end-capped with two different POSS [hydrophobic $T_8(i\text{-Bu})_7$ and hydrophilic derivatives of $T_8(CH{=}CH_2)_7$ with added thioglycerol] were able to form a range of structures in solid state, including hexagonally packed cylinders (Hex), double gyroids (DG), lamellae and body-centred cubic spheres (BCC) [105]. The morphology type depended on the compatibility between organic–inorganic segments, the length of PS linkers and the volume fraction of the hydrophilic domain. Hydrophilic POSS were phase-separated from the PS domains, whereas hydrophobic $T_8(i\text{-Bu})_7$ were associated within the polymer matrix. However, favourable interactions between $T_8(i\text{-Bu})_7$ governed their crystallization in the mixed phase if geometry of the confinement was appropriate. The crystalline packing within the self-assembled lamellae resulted in even higher phase separation. However, for other three phases with curved interfaces (DG, Hex and BCC), the polystyrene matrix and $T_8(i\text{-Bu})_7$ were completely miscible and amorphous. Further POSS-PS phase separation took place on flat interfaces. Various highly ordered mesophases were also produced by the self-assembly of other conjugates of hydrophilic POSS tethered with hydrophobic polystyrene tails [106]. The nanophase separation between the heads and tails leads to the formation of Frank–Kasper (F–K) and quasi-crystal phases of ordered spheroids. Increasing the

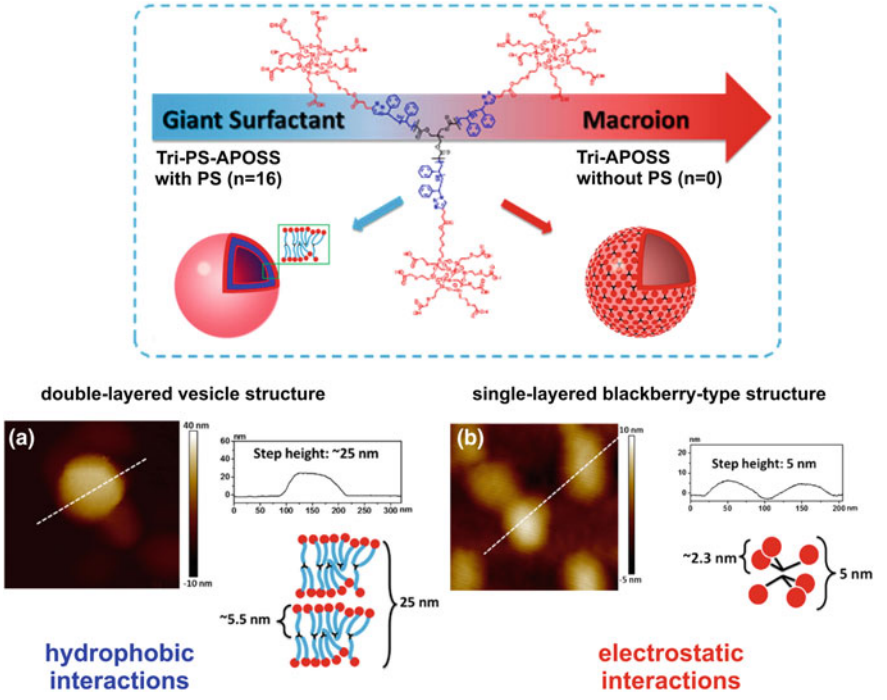

Fig. 4 Structures formed by tri-PS-POSS and tri-POSS hybrids without PS linkers—giant surfactant *vs* macroion; a) AFM images and height profiles of collapsed assemblies after solvent evaporation corresponding to models of the double-layer vesicle and blackberry structure. Adapted with permission from [103]. Copyright 2018 American Chemical Society

number of tails from one to four shifted compositional phase boundaries and stabilized F–K and quasi-crystal phases in regions typical to simple spheroidal micelles.

Polymeric chains of different chemical structure can be used as tails in the POSS-based surfactants. It allows for the formation of novel hybrid materials of specific properties and applicative potential. Giant linear and star-like surfactants with omniphobic perfluorinated POSS heads tethered onto the end point or junction point of diblock polystyrene-*b*-poly(ethylene oxide) (PS-*b*-PEO) copolymer (with fixed length of the PEO block) were capable of forming different ordered phases and phase transitions on changing the molecular weight of the PS block [107]. Varying shape anisotropy of block POSS-PEO copolymers (Scheme 8) was shown to have an effect on the melting (T_m) and recrystallization (T_r) temperatures of both the PEO and POSS layers as well as on the crystallinity of the PEO layer [108]. The crystallization of PEO drives the block copolymers to self-assemble into large nanothick sheets with one PEO crystalline layer sandwiched by two POSS layers. A decrease in T_m and T_r as well as disruption of the crystalline PEO layer and an increase in T_m of the POSS layer were observed with increasing number of POSS. Formation of unique hierarchical assemblies was observed for giant rod-like

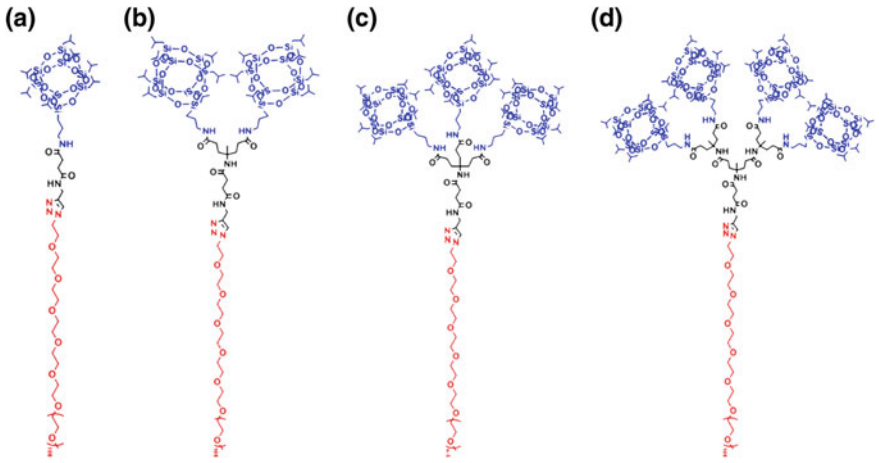

Scheme 8 Chemical structures of shape-anisotropic block copolymers consisting of POSS and PEO chains. Reprinted with permission from [108]. Copyright 2018 American Chemical Society

amphiphiles with perfluorinated $T_8[CH_2CH_2(CF_2)_7CF_3]_7$ heads and PEO or PS tails [109]. Due to the specific molecular geometry, the species did not interdigitate but were hexagonally packed within double-layered lamellae. The lamellae morphology in such systems depends on the structure of polymeric tails. The presence of electronegative fluorine atoms influenced melting properties of T_8R_7R' [$R = (CH_2)_2CF_3$; $R' = CH_3$; $(CH_2)_2C_6H_5$; $(CH_2)_2CF_3$; $(CH_2)_2(CF_2)_nCF_3$ ($n = 5,7,9$); $CH_2CH(CF_3)_2$; $(CH_2)_3OCF(CF_3)_2$] [110]. It can be explained by the strong interactions between fluorine and silicon atoms of neighbouring silsesquioxane cages, which results in a tighter packing. Spontaneous formation of concentric lamellae was observed for self-assembling giant surfactants consisting of $T_8(CH_2CH_2SCH_2CH_2(CF_2)_7CF_3)_7$ heads and flexible polymer tails [111]. Species having a single PS tail (POSS-PS), two different PS and PEO tails (PS-POSS-PEO) and a block copolymer tail (POSS-PS-*b*-PEO) were studied. Owing to the asymmetrical sizes of the head and tail blocks and the rectangular molecular interface between them, the giant surfactants can assume a truncated-wedge-like molecular shape. Their nucleation and growth during phase separation induced smooth morphological curvature during the self-assembly process, which resulted in the formation of curved and concentric lamellae.

Diblock amphiphilic copolymers with $T_8(i\text{-Bu})_7$ side groups grafted on only one block of [PHEMAPOSS-*b*-P(DMAEMA-*co*-CMA)] formed spherical micelles in water. The POSS core was thus surrounded by stimuli-responsive shells sensitive to changes of pH and redox potential [112]. The shells could be cross-linked by photodimerization of coumarin moieties (CMA). The subsequent etching of silsesquioxane structures with hydrofluoric acid left hollow polymeric capsules, suitable for the delivery of active agents in photodynamic therapy.

Evaporation-induced self-assembly of $T_8(OEt)_7(n\text{-alkyl})$ ($n = 16, 18, 20$) resulted in the formation of two-dimensional hexagonal columnar mesophases (p6mm). The

phenomenon was used for the preparation of organic–inorganic hybrids with well-ordered mesostructures and pore diameters governed by the size of *n*-alkyl groups. It was also shown that $T_8(OEt)_6(n\text{-alkyl})_2$ species with two alkyl chains randomly distributed about the silsesquioxane core could generate only lamellar structures [113]. This behaviour was attributed to the increase in space occupied by the head group and to the development of mesophases with higher curvature.

Telechelic macromolecules of two different POSS units symmetrically linked by hydrophilic organic spacers ("dumbbell-shaped") can also form unique structures on self-assembling in bulk. A specific phase separation was observed for amphiphilic $T_8(i\text{-Bu})_7\text{-}(CH_2)_3NHC(O)CH_2S(CH_2)_2\text{-}T_8(CH_2CH_2SCH_2COOH)_7$ [114]. The interlayer hydrogen bonding between carboxyl groups helped to the formation of a specific 3D crystal built of stacked 2D layers. Partial neutralization of –COOH groups with TBAOH broke the interlayer hydrogen bonds that were replaced by competitive electrostatic repulsive interactions. It resulted in the formation of 2D nanoplates. It was also shown that introduction of an excessive number of charges associated with one $T_8(CH_2CH_2SCH_2COOH)_7$ end group prevented completely the lateral growth of crystals. Dumbbell-shaped hybrids, terminated with two POSS molecules and containing poly(tert-butyl acrylate) linkers of three different molecular weights, formed different structures in aqueous solution at pH 8.5 depending on the length of the spacer [115]. The self-assembly of the shorter species resulted in ellipsoidal aggregates with a moderately uniform size, whereas the hybrids with the longest polyacrylate chain self-assembled into aggregates with a broad size distribution. $T_8(i\text{-Bu})_7\text{-}X\text{-}T_8(R'')_7$ (*X*—phthalic anhydride derivative, R''=$CH_2CH_2SCH_2COOH$, $CH_2CH_2SCH_2CH_2OH$ or $CH_2CH_2SCH_2CH_2C_6F_{13}$) formed bilayer head-to-head structures that were organized subsequently into a 3D orthorhombic lattice within a $Pna2_1$ symmetry group [116]. The formation of the ordered structure was associated with an endothermic transition of first order observed at 455 K. It was also demonstrated that the type of highly ordered supramolecular lattices (including a Frank–Kasper A15 phase) in amphiphilic systems built of $T_8(i\text{-Bu})_7$ and polar $T_8(R'')_7$ depended on the number of hydrophobic silsesquioxane ligands [117].

4.2 Hybrid POM–POSS Clusters and Related Structures

Supramolecular phase ordering of asymmetrical dumbbell-shaped nanoparticles of polyoxometalate–organic–POSS (POM–POSS) is quite unique. Such species of Janus-type characteristics (molecular Janus nanoparticles—MJPs) are derivatives of crystalline POSS [typically hydrophobic $T_8(i\text{-Bu})_7$] and polyoxometalates of a Wells–Dawson type $\{[P_2W_{15}V_3O_{62}](n\text{-}Bu_4N)_6\}$ [118, 119] or a Lindqvist type $\{Mo_6O_{18}N(n\text{-}Bu_4N)_2\}$ [114]. Synergistic self-assembly and nanoscale phase separation of POM- and POSS-containing zones is the thermodynamic driving force for the formation of hierarchical nanostructures [118]. POM–POSS self-assemble into 2D nanocrystals with double layers of crystalline POSS sandwiched between

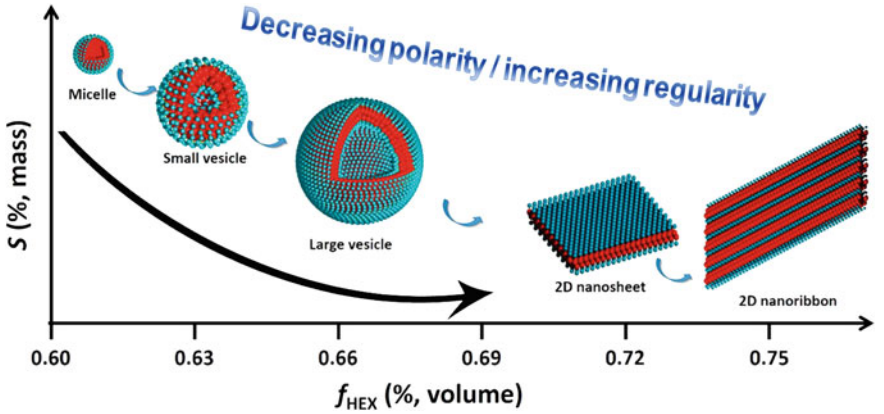

Fig. 5 Sheet-to-ribbon transitions due to the change in packing mode of POM–POSS clusters. Adapted with permission from [120]. Copyright 2018 American Chemical Society

two layers of inorganic species (Fig. 6). The dissimilar rigid clusters at molecule periphery form a brick-like packing in the solid state. The flexible linkers between POSS and POM provide a certain degree of freedom for an appropriate configuration adjustment. The thickness of double layers is controlled by separate crystallization of the nanoparticles. Other factors, such as solvent polarity, number of counterions and size of construction blocks, can change the crystallization mode of clusters of the same type and alter the nanoscale phase separation between incompatible parts [119].

The amphiphilic features of MJPs enable the *co*-clusters to self-assemble into diverse nanoaggregates in the liquid phase (micelles, vesicles, nanosheets and nanoribbons) by tuning the polarity of solvent used [120]. It was found that during the self-assembly process in solution, the increase in packing order causes the vesicle-to-sheet transition, whereas the change in packing mode results in the sheet-to-ribbon transitions (Fig. 5). In media of higher polarity, the *co*-cluster self-assembled into small bilayer vesicles in which a POM layer was sandwiched by the two POSS layers. The vesicle size increased with decreasing polarity of the solvent to break at $\varepsilon \approx 6.1$ and then finally convert into flat bilayer nanosheets at $\varepsilon \approx 5.6$. These changes are due the increasing packing order of the POM clusters that augments the bilayer rigidity. In solvents of low polarity ($\varepsilon \geq 5.3$), long nanoribbons were formed in which the POM–POSS co-clusters were arranged according to a fishbone-shape model with maximized electrostatic interactions between the POM blocks.

MJPs made of covalently linked α-Keggin-type polyoxometalate nanoclusters and $T_8(i\text{-Bu})_7(CH_2CH_2CH_2NH_2)$ self-assembled to form diverse nanostructures driven by secondary interactions among the building blocks and solvents via tuning molecular topology and solvent polarity [121]. Colloidal nanoparticles with nanophase-separated internal lamellar structures were formed initially in highly polar solvents (acetonitrile/water mixtures). Upon ageing, they turned gradually

into 1D nanobelt crystals. Stacked crystalline lamellae were dominant in less polar methanol/chloroform solutions. When $T_8(i\text{-Bu})_7$ heads were replaced with non-crystallizable T_8(cyclohexyl-SCH_2CH_2) groups, then colloidal spheres were also formed, but then failed to evolve further into crystalline nanobelts. Isolated two-dimensional nanosheets were obtained in less polar solvents. The nanosheets were composed of two inner crystalline layers of Keggin POM covered by two monolayers of disordered POSS (amorphous phase). Self-assembly of clusters with two $T_8(i\text{-Bu})_7$ heads was hardly sensitive to solvent polarity and was dominated by the crystallization of silsesquioxane cages that formed the crystalline inner bilayer, sandwiched by two outer layers of Keggin POM clusters (Fig. 6).

Analogous phenomena directed the type of supramolecular structures formed by derivatives of POSS and [60] fullerene (C60) [114]. Proper matching of the size of components at both ends of such dumbbell macromolecules is very important. Two-dimensional layer could be formed only if two $T_8(i\text{-Bu})_7$ residues were attached to one C60. Species having only one $T_8(\text{i-Bu})_7$ molecule tethered to C60 were too imbalanced in their size and did not crystallize [114]. Another asymmetric giant amphiphile composed of one [60] fullerene covalently linked with two $T_8(i\text{-Bu})_7$ moieties formed objects of the so-called one-and-half-layered structure [122]. The compositional asymmetry between C60 and $T_8(i\text{-Bu})_7$ led to a "sandwich-layered" molecular packing, where a single layer of C60 was sandwiched between double $T_8(i\text{-Bu})_7$ layers. Within these layers, the molecules further organized into crystalline arrays. This packing scheme repeated along the c-axis formed a 3D orthorhombic lattice (*P*nnm symmetry group).

4.3 3D Nanonetworks

Highly symmetric structures of octafunctional POSS can be exceptionally useful for the development of 3D hierarchical structures. Octahedral silsesquioxanes can be regarded not only as a platform for blending organic and inorganic modules at the molecular scale but also as building blocks or functional knots for the preparation of well-organized 3D networks. A range of advanced materials can be formed with POSS linked by covalent, supramolecular and coordinative bonds.

4.3.1 Well-Ordered Polymeric Networks

Organic–inorganic meso/macroporous covalent networks were obtained with POSS via a facile template-free strategy exploiting Schiff base chemistry [123]. The materials resulting from the combination of $T_8(CH_2CH_2CH_2NH_2)_8$ with terephthalic aldehyde were used as stabilizing supports for a palladium catalyst due to the presence of N-containing functionalities, large porosities and high BET surface areas. The resulting heterogeneous and recyclable catalyst of high activity and turnover frequency was employed in Suzuki–Miyaura reactions. Schiff base chem-

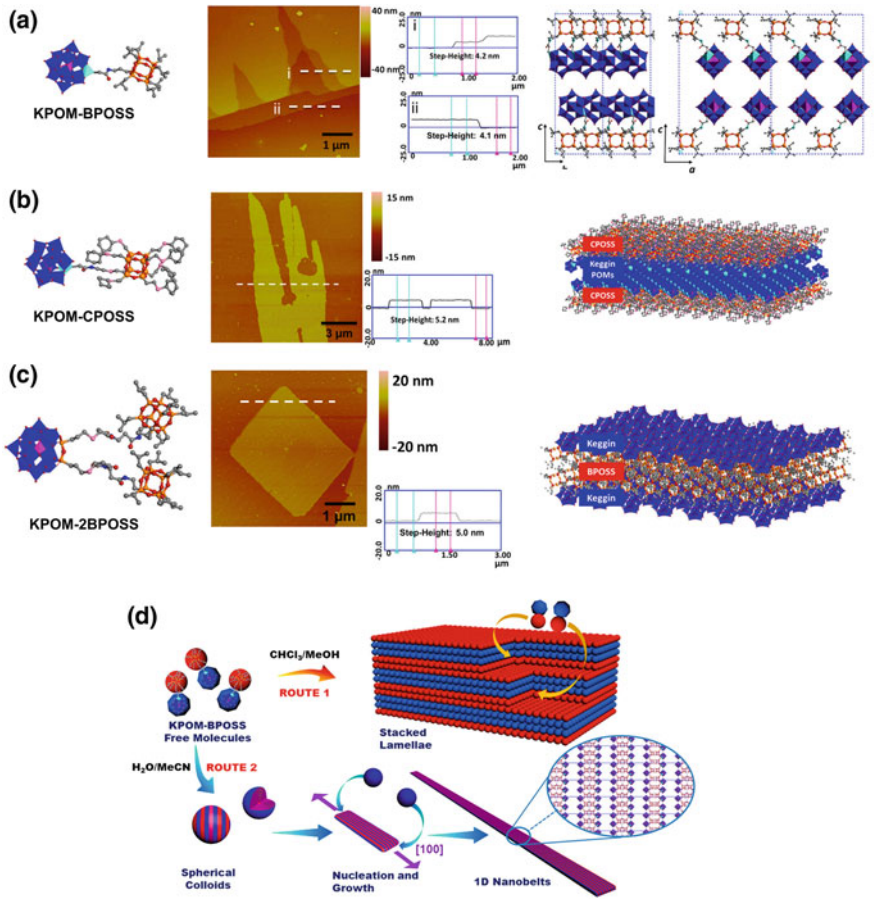

Fig. 6 **a**, **b** AFM height measurements of the flat-on single crystals (2D nanosheet morphology) of POM–POSS of different chemical structure and the respective perspective views of simulated crystal lattices; **d** the proposed mechanism of forming the stacked lamellae in chloroform/methanol and the 1D nanobelts in water/acetonitrile. (Adapted with permission from [121] Copyright 2018 American Chemical Society)

istry was also used for the preparation of a cross-linked silsesquioxane nanohybrid with $T_8(CH_2CH_2CH_2NH_3^+Cl^-)_8$ and glutaraldehyde as a dual cross-linking bridge [124]. Block-like irregular nanoparticles with specific surface area of 42.8 m^2/g were formed. The cross-linked nanohybrid was used as a solid-phase adsorbent for selective adsorption of acidic dyes (such as methyl orange) in aqueous solutions. Electrostatic interactions are the driving force for the adsorption (maximum adsorption capacity of 237.5 mg/g). The process was spontaneous and exothermic. The adsorbed molecules could be efficiently recovered using a methanolic solution of NaOH. The reusable adsorbent can be applied for wastewater treatment in dye industry.

A well-defined covalently linked microporous organic–inorganic nanohybrid framework was obtained with *p*-iodio-octaphenylsilsesquioxane by a Yamamoto-type of Ullmann cross-coupling [125]. This strategy provides an approach for constructing a wide variety of functionalized zeolite-like porous organic frameworks. Formation of well-ordered networks consisting of truncated octahedra [β-cages compared with Linde type A zeolite (LTA)] and truncated cuboctahedra (α-cages compared with LTA) with diameters of about 2 nm was confirmed by NMR spectroscopy and nitrogen adsorption. The inorganic silsesquioxane cubes were linearly linked by biphenyls, which led to the formation of micropores with the narrow pore size distribution and BET surface area of 283 m^2/g. The network was thermally stable up to 670 K in air and efficiently adsorbed benzene and water.

A cross-linked and thermostable fluorinated POSS-based network was prepared by thermal polymerization of trifluorovinyl ether groups (Scheme 9) [126]. The hybrid polymer network shows 5 wt% loss at ~610 K. It is transparent, of low water uptake, of low dielectric constant under both dry and wet conditions (<2.56) and of low dissipation factor ($<3.1 \times 10^{-3}$) in a wide range of frequencies from 40 Hz to 30 MHz. Such high-performance dielectric materials are suitable for microelectronics and fabrication of high-frequency printed circuit boards or integrated circuits.

POSS-based poly(ionic liquid)-like cationic networks of tuneable mesoporosities (surface area > 900 m^2/g) were formed with $T_8(CH_2Cl)_8$ and rigid N-heterocyclic cross-linkers (4,4′-bpy) [127]. When $T_8(CH_2CH_2CH_2Cl)_8$ with more flexible chloropropyl groups was used as the monomer, then the obtained material had a very low surface area (7 m^2/g). It indicates the importance of the rigidity of POSS for the generation of ordered structures. The resulting networks were applied as the supports for loading POM $PMo_{10}V_2O_{40}^{5-}$ (PMoV) as guest species through the anion-exchange process. The POSS–POM hybrid was used as efficient heterogeneous catalysts for H_2O_2-mediated oxidation of cyclohexane and aerobic oxidation of benzene. Hyperbranched polymeric networks of adjustable hydrophilic–hydrophobic properties were also prepared by controlled cross-linking of $T_8(CH{=}CH_2)_7(CH_2CH_2OH)$ followed by grafting PEG chains to residual vinyl groups [128]. The polymers exhibited a characteristic transition from micelle to vesicle in aqueous solutions.

Self-assembly of ordered nanoscale POSS superstructures was evidenced in semicrystalline covalently cross-linked nanocomposites of polyhedral silsesquioxane and poly-(ε-caprolactone) (POSS–PCL) [129]. Asymmetrical triblock copolymers with a single POSS moiety centred between two PCL chains were used for the formation of a shape memory network (Fig. 7). Both crystalline reflections of the PCL orthorhombic phase and POSS rhombohedral phase were shown if PCL was terminated with OH groups. It indicates independent crystallization due to microphase separation. Consequently, two long period spacings—one associated with POSS (long period of 66 Å) and the other associated with PCL lamellar nanophase (long period of 151 Å)—were shown in SAXS diffractograms. The nanostructure was dominated by crystallization of POSS. Coordination via hydrogen bonding between the inert corner isobutyl groups of POSS and the end groups of PCL diols facilitated crystallization of PCL chains. End-capping of PCL with acrylate groups was required for cross-linking but greatly reduced the crystalline order of POSS. End-capping prevented

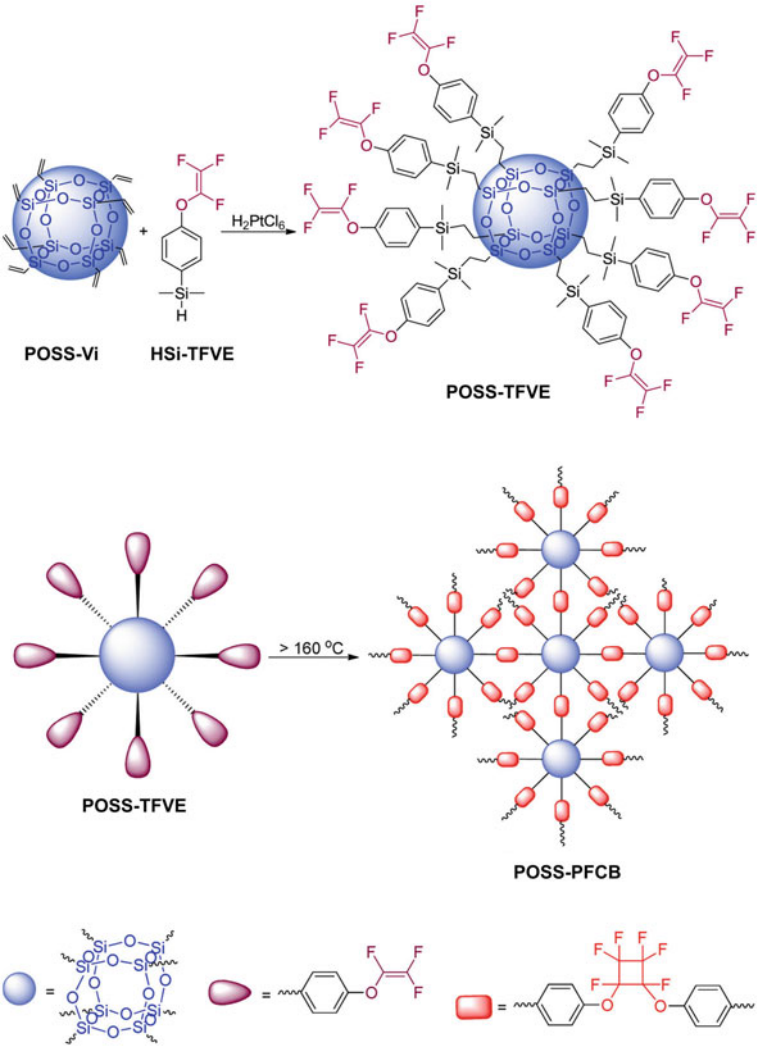

Scheme 9 Synthesis of a POSS-based network by thermal polymerization of trifluorovinyl ether groups. Adapted with permission from [126]. Copyright 2018 American Chemical Society

also the coordination between POSS and PCL, thus freeing the poly-(ε-caprolactone) chains for fold crystallization of the orthorhombic phase. Despite the architectural constraints, cross-linking with tetrathiol molecules supressed the crystallization of PCL, but did not hinder completely the formation of a superstructure in the material. POSS crystals embedded in amorphous PCL matrix were segregated as crystalline clusters organized as a highly ordered cubic phase.

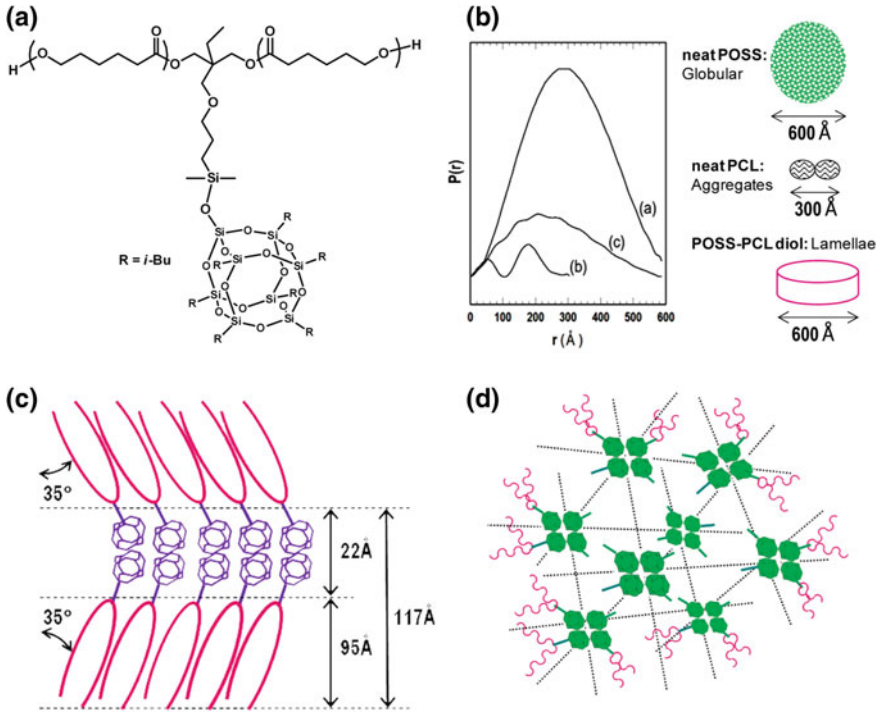

Fig. 7 Formation of hierarchical assemblies in POSS-poly-(ε-caprolactone) networks: **a** the structure of POSS-poly-(ε-caprolactone) hybrid; **b** pair distribution function plots P(r) derived from the SAXS data of (*a*) neat POSS, (*b*) neat PCL homopolymer and (*c*) monomeric POSS-CL diol nanocomposite; **c** the proposed long-range order of POSS-CL acrylate nanocomposites; **d** the model of cubic superstructure for the POSS–PCL network. Adapted with permission from [129]. Copyright 2018 American Chemical Society

Polycarboxyl octaphenylsilsesquioxanes $T_8(C_6H_5COOH)_8$ were used as nanofillers and macromolecular cross-linkers to cure diglycidyl ether of bisphenol A (DGEBA) with formation of ester bonds [130]. The network structures of the obtained inorganic–organic polymer nanocomposites and cross-linking densities were modulated by varying the amount of $T_8(C_6H_5COOH)_8$. The cured samples of POSS/DGEBA were transparent, and a homogeneous dispersion of POSS within the DGEBA matrix was evidenced. The silsesquioxane molecules opened up the organic segments between two cross-linking nodes, leading to an increase in the intersegmental distance. Consequently, the segmental mobility increased, resulting in decreased mechanical modulus and improved toughness of the networks.

4.3.2 Hydrogen-Bonded 3D Networks

Three-dimensional supramolecular assemblies and special type networks can be constructed by controlled assembly of well-defined POSS building blocks via hydrogen bonds. For example, octakis[*N*-(6-aminopyridin-2-yl)-undecanamide-10-dimethylsiloxy]-silsesquioxanes (POSS-C11-Py), self-assembled through hydrogen bonds, formed a physically cross-linked polymer-like structure with good mechanical properties [131]. POSS-C11-Py was transformed into a supramolecular ionomer (HCl-doped POSS-C11-Py) with both quadruple hydrogen-bonding and ionic side arms [132]. The obtained network could be fabricated into films with hierarchical microphase separation. HCl-doped POSS-C11-Py exhibited high proton conductivity and can be used for the preparation of proton-exchange membranes.

POSS bearing residues of carboxylic acids are interesting building blocks due to the propensity of –COOH groups to the formation of stable dimers. A mixture of octa[2-(p-carboxyphenyl)ethyl] and octa[2-(4-carboxy-1,1′-biphenyl)ethyl] silsesquioxanes assembled to form an ordered hybrid two-component network [133]. Networks of complementary hydrogen bonds were also obtained with $Q_8M_8(CH_2CH_2–C_6H_4OH)_8$ bearing side phenol groups by blending with reactive diblock copolymers, such as poly(styrene-*b*-2-vinylpyridine) (PS-*b*-P2VP), poly(styrene-*b*-4-vinylpyridine) (PS-*b*-P4VP) and poly(styrene-*b*-methyl methacrylate) (PS-*b*-PMMA) [134].

The strength of the formed hydrogen bonds was found to be the key feature affecting the morphologies of the hierarchical structures (lamellae, cylinders, body-centred cubic spheres, disordered). Formation of a lamellar phase of thermoreversible characteristics was reported for supramolecular networks with blocks of octakis(vinylbenzylthymine-siloxy)silsesquioxane (OBT-POSS) and octakis[(vinylbenzyltriazolyl)methyladenine-siloxy]silsesquioxane (OBA-POSS) linked by intermolecular complementary hydrogen bonds between adenine and thymine residues [135].

Tetrakis(nicotinoxymethyl)methane (TNMM) and octakis[dimethyl(4-hydroxyphenethyl)siloxy]-silsesquioxane (OP-POSS) were used as tetrahedral and cubic building blocks for the preparation of thermally reversible, 3D hydrogen-bonded transparent network [136]. FTIR spectroscopy provided clear evidence for the formation of intermolecular hydrogen bonds between the OP-POSS and TNMM units. The blend of 40 wt% TNMM in OP-POSS exhibited a single glass transition temperature at 310 K, which is a compromise between Tg of OP-POSS (~293 K) and the melting temperature of TNMM (~340 K), and indicated the low degree of local intermolecular thermal motions.

Self-assembled supramolecular structures were generated in mixtures of multidiamidopyridine-functionalized POSS (MD-POSS) and both mono- and bis-uracil (U)-functionalized poly(ethylene glycols) (U–PEG and U–PEG–U) due to the formation of strong complementary multiple hydrogen bonds between the diaminopyridine groups and uracil moieties [137]. The polymer-like supramolecular materials exhibited improved thermal properties upon increasing the content of MD-POSS. The interactions of uracils with MD-POSS hindered completely crys-

tallization of PEG-U. TEM imaging indicated that the interactions in the symmetric U–PEG–U systems were stronger and their structures were relatively more ordered.

Hydrogen-bonded silsesquioxane networks can be applied as advanced materials in biomedicine. For example, $T_8[CH_2CH_2CH_2N(CH_2CH(OH)CH_2OH)_2]_8$ (POSS-AH) was used for the preparation of pH-responsive aggregates with natural polysacharide hyaluronic acid that can be applied as cell immune barriers, drug and gene delivery systems and chemical sensors [138]. Smart self-healing hydrogels were developed using self-assembled colloidal micelles of POSS-AH and poly(acrylic acid) (PAA) [139]. The micelles could be cross-linked in situ by hydrogen-bonding and ionic interactions between POSS-AH and PAA chains, as well as by covalent bonds linking PAA and bis(*N*,*N*′-methylene-bis-acrylamide). The ratio of reversible physical bonds *vs* chemical cross-links determined the mechanical properties of the hydrogels.

Supramolecular association of molecules bearing silanol (Si-OH) groups is interesting not only because of the formation of hierarchical architectures due to hydrogen bonding. Such systems can be also cross-linked by covalent siloxane linkages generated by the condensation of silanol moieties. The procedure provides a soft-chemical approach to well-defined silica-like materials with molecularly designed structures. Supramolecular lamellar crystals were prepared by hydrogen bond-directed assembly of Q_8MOH_8 with silanol groups [140]. The anisotropic 2D assembly of cubic POSS is different from the 3D assembly of organosilanol-modified cage siloxanes. Drying and thermal treatment induced solid-state polycondensation towards the formation of ordered siloxane networks. Hybrid networks that were synthesized using cage silsesquioxanes bearing diphenylsilanol groups were less ordered due to the steric hindrance provided by bulky diphenylsilyl moieties [141]. A range of hydrogen-bonded 3D crystalline porous materials were also made of POSS with eight organosilanol groups $T_8(CH{=}CHC_6H_4SiR_2OH)_8$ (*R*=*i*-Pr, Ph) [142]. Selective inclusion of hydrocarbons into large cavities of the obtained hydrogen-bonding networks with adjustable porosity was shown, depending on the pore size. Hydrocarbons such as hexane and heptane were included in the open frameworks without interpenetration of one network into another. Perpendicular stacking of the benzene cluster as a guest hydrocarbon in the pores of $T_8(CH{=}CHC_6H_4Si(i\text{-}Pr)_2OH)_8$ and $T_8(CH{=}CHC_6H_4SiPh_2OH)_8$ was also found (Scheme 10).

4.3.3 Metal–Organic Frameworks and Metal Complexes Forming Hierarchical Structures

A range of non-covalent ligand–metal interactions between organic moieties and transition metal centres have been used for the preparation of metal–organic frameworks (MOF) [143–147]. The main advantage of such structures is their dynamic nature. They can be sensitive to various external stimuli (e.g. temperature, pH, light, solvents, concentration, ultrasound), which gives the material an ability to alter its response. Moreover, modification of the metal ion or the structure of ligands can be used to tune the electrochemical, magnetic or optical responses. The formation of

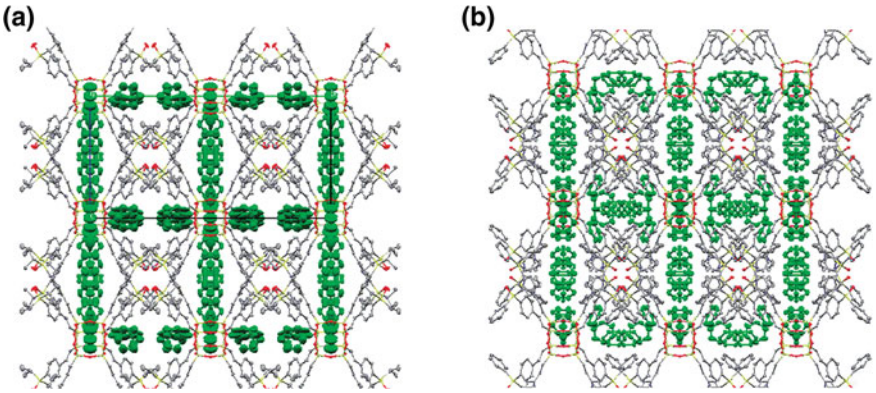

Scheme 10 Supramolecular 3D frameworks made of hydrogen-bonded POSS **a** $T_8(CH{=}CHC_6H_4Si(i\text{-}Pr)_2OH)_8$ and **b** $T_8(CH{=}CHC_6H_4SiPh_2OH)_8$ with included solvent molecules. Reprinted with permission from [142]. Copyright 2018 American Chemical Society

such long-range ordered/crystalline structures and extended networks requires the use of appropriate ligands with shape and functionality suitable for the coordinative ligation.

Octafunctional POSS can be successfully used as 3D ligands for the preparation of MOF. Rigidity of the inorganic cube used as a scaffold, as well as the presence of appropriate reactive groups at each silicon vertex, can increase effectively the symmetry of such hybrid networks and the concentration of doped metal cations. For example, metallo-supramolecular hybrid networks were obtained using $T_8[CH_2CH_2CH_2NHC(O)CH_2CH_2COOH]_8$ coordinated to copper ions [148] or terpyridine-functionalized POSS coordinated to Co(II) or Cu(II) [149]. The latter exhibited electrochromism during the cyclic voltammetry measurements, which makes them good candidates for electronic, optoelectronic and photovoltaic applications. The properties can be adjusted by the type of substituents at pyridine groups. The formed stable terpyridine metal complexes are completely reversible, and addition of a strong competitive ligand (HEDTA-Na_3) led to an efficient decomplexation. POSS decorated with eight terpyridine moieties were also used for the formation of 3D extended supramolecular structures by assembly with two different metal ions (Zn^{2+} and Fe^{2+}) (Fig. 8) [150]. TEM investigations further evidenced the tendency of 4metal@O-POSS to form a 3D organization with an irregular porous structure. The capability of the organic–inorganic hybrid network to trap solvent molecules was verified. Studies carried out with ^{1}H NMR as well as absorption and emission spectroscopy have shown that under selected conditions stable gels could be formed at room temperature. The gels were stable under ambient conditions.

The unique porous structure, large surface area and high pore volume make MOF especially attractive for catalysis, gas storage and separation or drug delivery [151]. They can be tailored for targeted chemical interactions but can also lose their crystallinity and pore ordering upon exposure to chemical compounds. Water can easily

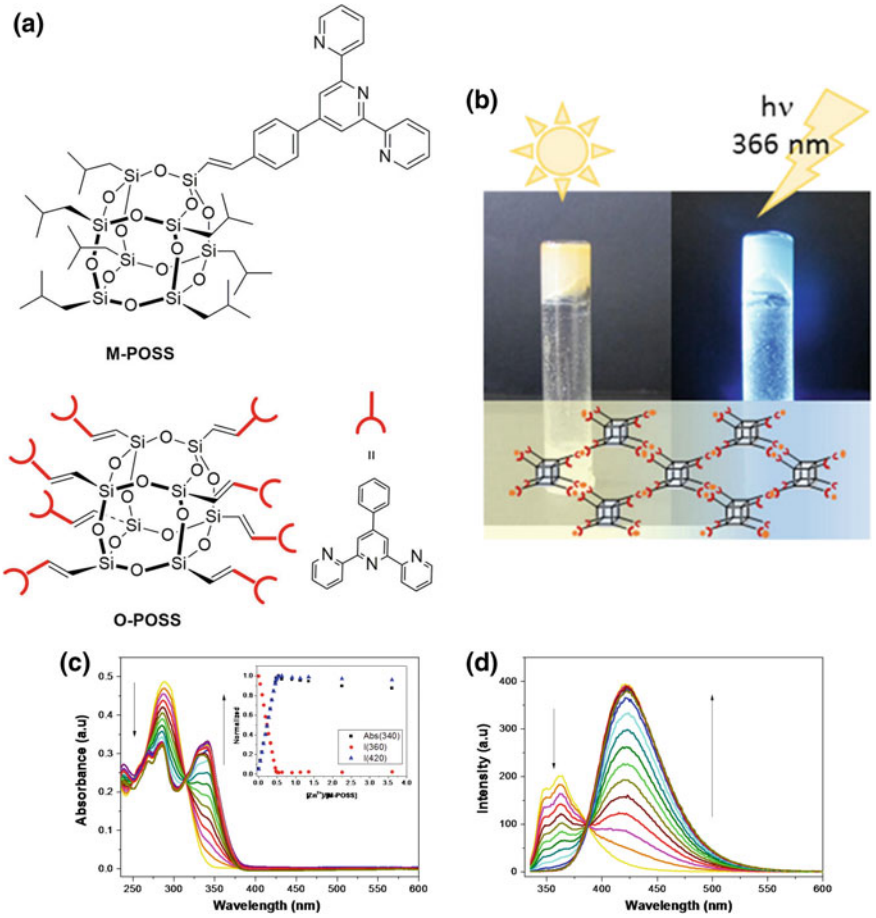

Fig. 8 **a** Structure of POSS bearing a single and eight terpyridine groups; **b** photograph of 4Zn@O-POSS gel without and with UV irradiation at 366 nm; **c** UV–Vis absorption spectra of M-POSS in CH_2Cl_2 (1×10^{-5} M) upon titration with $Zn(OTf)_2$ in EtOH (1.3×10^{-3} M) (the inset: normalized absorption changes at 340 nm (■) and the normalized emission intensity changes at 360 (●) and 420 nm (▲); **d** emission spectra of M-POSS in CH_2Cl_2 upon titration with $Zn(CF_3SO_3)_2$. Adapted with permission from [150] Copyright 2018 American Chemical Society

penetrate the pores and destroy the structure of some MOF by hydrolysis or replacement of ligands coordinated to metal centres. For example, porous MOF of copper trimesate [$Cu_3(BTC)_2$, HKUST-1] had large surface areas, high pore volume, relatively high chemical stability and good lability of coordinated solvents (including molecules of water) in the pores of the framework. The removal of coordinated water molecules from the $Cu_3(BTC)_2$ structure opens coordinatively unsaturated sites which is crucial for catalytic applications but detrimental for the stability of MOF. It is thus important to protect the structure of activated MOF against humidity,

retaining at the same time unhindered access of reagents to the inner parts of the network. Suitable POSS can be used for the purpose. For example, the stability of copper trimesate against moisture was enhanced by selective functionalization of the Cu sites on the outer surface of MOF with $T_8(i\text{-octyl})_7(CH_2CH_2CH_2NH_2)$ [152]. The protection of the surface of activated MOF against moisture was attributed to the hydrophobic nature of the long aliphatic chains. The same POSS were used for modification of other MOFs [low-symmetry rhombohedral MOF-74(Ni and Co) and high-symmetry cubic MIL-100(Fe)] [152]. The crystallinity of the MOF was intact during the modification, and the change of the mesoporous volume of MIL-100 was negligible due to the fact that the windows of MIL-100 are too small to let the POSS into the network. All the modified MOFs were hydrophobic, and $T_8(i\text{-octyl})_7(CH_2CH_2CH_2NH_2)$ successfully protected the outer metal sites on the surface.

In spite of not being formally MOF or MOF-related structures, some metal—POSS complexes can form unique hierarchical architectures. Their appropriate self-assembly can be used for the development of novel materials. For example, platinum(II) polypyridine complexes of d8 square-planar configuration exhibit interesting spectroscopic and luminescent properties due to Pt···Pt and π–π interactions. The characteristics can be changed by altering the molecular association and formation of metallogels or liquid crystals [153–155]. An alkynylplatinum(II) terpyridine complex functionalized with $T_8(CH{=}CH_2)_7$ groups exhibited solvent-induced self-association behaviour [156]. The obtained nanostructures were capable of "rings to rods" morphological transformations in media of different polarity due to the stabilization of Pt···Pt and π–π stacking as well as hydrophobic interactions between POSS moieties. Crystal-packing diagrams suggest a head-to-tail configuration for the dimeric structure. Other alkynylplatinum(II) terpyridine complexes functionalized with POSS exhibited multistage morphological transformations from spheres to nanoplates in response to solvent change through the interplay of hydrophilic, hydrophobic, Pt···Pt and π–π stacking interactions [157]. The intermolecular forces can be adjusted by appropriate structural modifications. If charged moieties were incorporated in the system, then drastic colour changes were observed in response to aggregation–disaggregation induced by changes in solvent polarity. The morphological transformations are associated with changes of spectroscopic characteristics and the complexes can be used as functional materials with sensing or imaging capabilities.

Functionalized POSS can be also complexed with lanthanide ions. Emission intensities of bare lanthanide ions Ln^{3+} are typically weak. Sensitization with organic ligands (the so-called antenna effect) can be a way to solve the problem. The use of POSS ensures uniform distribution of Ln^{3+} and prevents their aggregation at high concentrations. Hybrid luminescent complexes of Eu^{3+} and Tb^{3+} of highly saturated colour and good thermal stability were obtained with POSS dendrimers decorated with β-diketone moieties and incorporated in PMMA matrix [158]. Photo- and thermally stable complexes of Tb^{3+} and POSS bearing eight benzoic acid moieties also exhibited enhanced luminescent properties [159]. High luminescence combined with good stability and processability make those hybrid materials interesting candidates

for luminescent probes in bioassays, UV sensors, flat-panel displays, laser materials, optoelectronic devices as well as for crystal engineering.

4.4 Templating with POSS

Nanosized POSS, substituted on every corner of the inorganic cages with side groups acting as recognition units, are very interesting assembly motives. Formation of a "crystalline template" leading to controlled self-assembly of nanoparticles can be achieved by crystallization of POSS. It can be induced by intermolecular non-covalent interactions (hydrogen bonding, acid/base proton transfer and specific electrostatic forces) and allows for the formation of well-ordered hierarchical structures. Various self-assembling POSS has been applied as stabilizing templates for the preparation of metal nanoparticles, quantum dots and carbon dots. Owing to the presence of siloxane framework, POSS can be also used as sacrificial templates in porous materials.

4.4.1 Stabilizing Templates for Metal Nanoparticles

Nanoparticles (NPs) of noble metals (Au, Ag, Pd) exhibit unique physicochemical and electronic properties, different than those of bulk metal or metal atoms, due to the quantum size effect, high superficial surface areas and confinement of electronic states [160]. That is why, for example, nanocomposites containing Au NPs can act as ferromagnetics at room temperature despite the diamagnetic character of bulk gold [161]. Those peculiar properties make them very attractive for applications in advanced technologies, including optoelectronics, catalysis, sensing and biomedicine [162]. For example, palladium NPs of stable hierarchical structures are attractive for catalysis and hydrogen storage. Well-defined nanoparticles of silver can be applied as plasmonic devices, in photovoltaics, catalysis and for surface-enhanced Raman scattering (SERS) sensors. NPs of gold have high molar absorptivity in the visible region, but their aggregation results in colour changes due to mutually induced dipoles that depend on interparticle distance and aggregate size. The phenomenon can be applied in sensing systems. Bare metal nanoparticles can be prepared by employing various chemical methods (reduction of metal salts in solution) and physical techniques (laser ablation, resistive evaporation in vacuum, mechanic subdivision of metallic aggregates). However, undesired and uncontrolled aggregation and formation of droplets instead of well-dispersed films makes difficult preparation and use of such NPs in the condensed phase. It was found that the size and surface functionality of NPs of noble metals can be finely tuned using POSS as stabilizing templates.

Nanoparticles of gold can be stabilized via electrostatic interactions [163–166]. It was shown that pH-responsive Au NPs can be formed spontaneously on mixing $T_8(CH_2CH_2CH_2NH_3^+Cl^-)_8$ and tetrachloroauric acid under basic conditions [164]. Under the applied conditions, the amino groups reduce cations of Au(III) to Au(0) and

interact with the surface of Au NPs. The size of particle aggregates can be controlled by changing the molar ratio of $T_8(CH_2CH_2CH_2NH_3^+Cl^-)_8$ to Au NPs [165]. The affinity of Au NPs to organic solvents was modified via Michael addition of the aminopropyl groups on POSS to methyl acrylate. $T_8(CH_2CH_2CH_2NH_3^+Cl^-)_8$ was also used for the preparation of nanocomposites containing well-separated Au NPs. Amide bonds were formed in situ between the POSS moieties and COOH groups on the surface of gold primed with 11-mercaptoundecanoic acid [166, 167]. The phenomenon of electrostatic self-assembly allowed for the increase in interparticle spacing upon assembly with POSS. Modulation of the surface plasmon resonance band of Au NPs can be achieved in this way. A shift to higher wavelengths in solution and shift to lower wavelengths in the solid-state were observed as a result of different particle–particle dipolar interactions [167].

Sodium hydroxide was used to hydrolyse partially siloxane bonds of the adsorbed $T_8(CH_2CH_2CH_2NH_3^+Cl^-)_8$ to generate SiO^- species, which additionally stabilized Au NPs via electrostatic interparticle repulsion and hindered their aggregation [164]. The particles were pH-responsive, since addition of hydrochloric acid generated NH_3^+ ions that interacted with SiO^-, inducing reaggregation of NPs. It was also shown that $T_8(CH_2CH_2CH_2NH_3^+Cl^-)_8$ can help to the formation of well-dispersed homogenous NPs of silver, grown in a biphasic system on the interface between graphene oxide (GO) and $AgNO_3$ solution [168]. The obtained Ag NPs–POSS/GO nanocomposite can be used for electrochemical sensing of nitroaromatic compounds.

POSS bearing amine groups were also used as capping agents in the reductive growth of Pd nanocrystallites [169–171]. Studies on primary Pd NPs and their secondary aggregates suggest that the reductive growth of nanocrystallites can depend on the structure of POSS [169]. Uniform secondary Pd aggregates were obtained providing the POSS ligand was functionalized with amine groups in the hydrochloride form [$T_8(CH_2CH_2CH_2NH_3^+Cl^-)_8$]. The morphology of Pd core–shell NPs was determined by the ratio of self-interaction potentials of the ligands to their interaction with solvent. A correlation was found in Pd/POSS systems between sufficiently slow ligand diffusion kinetics of the reactive species and the growth rate of metal crystallites. Rapid diffusion of Pd prenucleating clusters was slowed by relatively slow-moving hydrochloride POSS ligands. It left time for reduction of NPs and their growth into nanocrystals. Pd nucleation does not seem to be preceded by formation of observable self-assembled POSS templates. DFT simulations suggested that the slow diffusion would result in regular spherical morphology of the aggregates, possibly due to the shift of the particle condensation equilibrium towards dissolution. More rapidly diffusing POSS ligands induced random structures and low solubility of nanoparticles after the syntheses.

$T_8(CH_2CH_2CH_2NH_3^+Cl^-)_8$ was used as well for stabilization and cross-linking of bimetallic microporous colloidal NPs made of Pd and Au [172]. The hybrid nanocomposites were generated by electrostatic interactions between Au NPs coated with 11-mercaptoundecanoic acid and aggregates of Pd capped with $T_8(CH_2CH_2CH_2NH_3^+Cl^-)_8$. The procedure resulted in precipitating of NPs of random shape. Stable colloids of spherical aggregates of Pd NPs coated with Au NPs can be obtained in a two-step process by reduction of palladium acetate in the presence of

$T_8(CH_2CH_2CH_2NH_3^+Cl^-)_8$ as a rigid template [171]. Bimetallic platinum–bismuth nanoparticles (Pt-BiNPs, 60% Bi) of blackberry-like morphology were prepared with $T_8(CH_2CH_2CH_2NH_3^+Cl^-)_8$ that played the role of both the morphology control agent and the carrier of electrocatalyst with corrosion resistance [173]. Their electrocatalytic activity (electro-oxidation of formic acid for fuel cell applications), effective CO tolerance and durability were enhanced with respect to commercial catalysts.

It was already mentioned that the surface of noble metals can be easily modified by chemisorption of thiols and sulphur-containing species. Several thiol-functionalized POSS were also used as protective ligands to stabilize NPs of Au, Pd or Ag in solution or as templates for their incorporation into thin films. POSS can also provide a synergistic effect for the surface coverage due to the presence of multianchor sites and hydrophobic interactions between POSS and the surface. For example, molecules of $T_8(i\text{-Bu})_7(CH_2CH_2CH_2SH)$ were applied as protective groups for the preparation of hybrid POSS-coated Au NPs of high stability in solid state [174]. Plate-like morphology of the POSS crystals led to the formation of a unique fern-like microstructure with hybrid POSS–Au NPs on its surface. Removal of the silsesquioxane templates resulted in sintering of nanosized Au islands. Au NPs covered with $T_8(i\text{-Bu})_7(CH_2CH_2CH_2SH)$ were also used for the preparation of polymer nanocomposites [161]. The particles were blended with poly(*n*-butyl methacrylate) randomly decorated with $T_8(i\text{-Bu})_7$ in the side chains. The increased compatibility between both components improved miscibility of Au NPs and the polymer matrix. The distribution of Au NPs was governed by interactions between POSS ligands grafted on the polymer chains and those adsorbed on the surface of gold.

Palladium NPs capped with POSS were prepared by ligand exchange of acetate groups on $Pd(OAc)_2$ with 1-dodecanthiol and $T_8(i\text{-Bu})_7(CH_2CH_2CH_2SH)$, followed by a thermal work-up [175]. High affinity of Pd to thiols led to the formation of cores composed of disordered aggregates. Nanosized storage vessels for Pd(0) atoms with transportation channels in the shell could be formed in this way. The nanoclusters were successfully employed as the catalytic system in a model Mizoroki–Heck coupling reaction.

Cubic silsesquioxanes not only can stabilize nanoclusters of noble metals, but also can provide reactive groups for chemical modification of the formed NPs shells. Diaminopyridine-functionalized octasilsesquioxanes (POSS-DAP) and thymine-functionalized gold nanoparticles (Thy–Au) formed well-defined and well-dispersed spherical aggregates on mixing due to the combined hydrogen-bond recognition and aggregation/crystallization of POSS moieties [176]. DAP units interact with Thy–Au nanoparticles through complementary three-point hydrogen bonds, and POSS nanoparticles were packed uniformly into larger nanocrystals. It was found that side-to-side rather than the face-to-face POSS–POSS packing was preferred. The same three-point hydrogen-bonding recognition motives were used for modification of gold surface covered with thymine-terminated self-assembled monolayers with DAP-functionalized POSS [177]. Hybrid inorganic–organic films were formed in this way showing that both chemical and physical nature of surfaces can be engineered by orthogonal deposition of POSS.

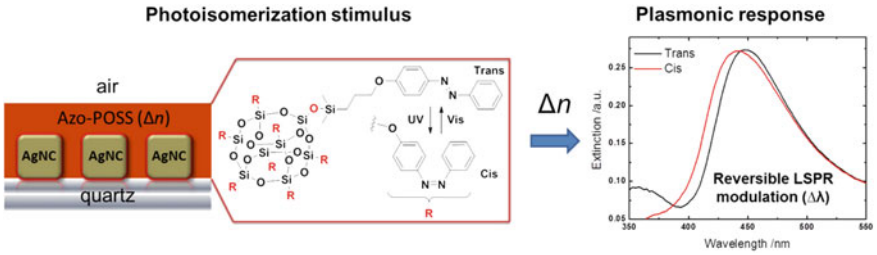

Fig. 9 Plasmonic response of Ag NPs coated with Azo–POSS matrix of adjustable refractive index. Reprinted with permission from [179]. Copyright 2018 American Chemical Society

The self-assembly process controlled by crystallization kinetics of POSS was employed for the preparation of hierarchical Ag NPs/POSS hybrids of branched morphology using $T_8(CH{=}CH_2)_8$ and $T_8(\text{cyclohexyl})_8$ [178]. Well-defined and stable Ag structures, which were left after the treatment on a hot plate at 523 K for 30 min in air, exhibited excellent SERS performance with high enhancement factors.

Hybrid POSS with azobenzene moieties in their side chains (Azo–POSS) were used as a stable photoactive coating for light-induced plasmonic modulations of embedded Ag nanostructures [179]. The refractive index of Azo–POSS conjugate could be altered owing to the *trans–cis* photoisomerization of azobenzene groups on irradiation with UV light (380 nm) (Fig. 9). The reversible changes resulted in 6 nm hypsochromic plasmonic shift in the plasmonic band of the embedded Ag NPs. Moreover, a polarization-dependent variation in reflectance was observed in the total internal refraction (TIR) regime.

POSS with polymeric chains grafted onto silsesquioxane cores were also used for the modification of the surface of noble metals. Hybrid polymer brushes with poly(ethylene glycol) (PEG) chains tethered to POSS via linkers containing thiolate moieties were chemisorbed on the surface of gold [180]. PEG-functionalized POSS were used to coat charged Au NPs of various shapes to aid their transfer into organic solvents [181]. Macromolecules built of thermoresponsive PNIPAM arms grafted to octahedral silsesquioxane core (POSS-*g*-PNIPAM) were explored as stabilizers for colloidal Au NPs [182]. Hybrid thermosensitive Au NPs were obtained. Their lower critical solution temperature (LCST) was decreased compared to POSS-*g*-PNIPAM.

A green solid-state synthetic method was implemented for the fabrication of POSS supported N-heterocyclic carbenes/imidazolium salts of palladium(II) complexes and well-dispersed Pd NPs of a very small size [183]. The prepared homogeneous and recyclable nanocatalyst was highly efficient in Suzuki–Miyaura cross-coupling reactions. The imidazolium moiety on POSS played a key role in the solubility of the catalyst.

Iron oxide nanoparticles can be used for many biological applications, including MRI contrast agents, magnetic separation or localization and thermal ablation. However, the effective use of magnetic nanoparticles depends on their size and composition, physical properties and surface chemistry capable of promot-

ing specific interactions with target biomolecules. Various octafunctional POSS were applied for preparation of well-dispersed metal oxide nanoparticles, biocompatible and transferable into aqueous solutions. For example, magnetic nanoparticles were prepared by exchange of the primary surface monolayer using anionic octa(tetramethylammonium)-POSS $\left(SiO_{4/2}\right)_8{}^{-}NMe_4{}^{+}$ (Fig. 10) [184]. They had excellent stability within biologically relevant pH ranges and salt concentrations and interacted with proteins via surface charge complementarity.

Interesting conjugated structures comprised of γ-Fe_2O_3 nanoparticles and PbSe nanocrystal quantum dots (NQDs) were prepared with the use of 2-aminoethanethiol and $\left(SiO_{4/2}\right)_8{}^{-}NMe_4{}^{+}$ hydrate [185]. Hydrogen bonds that were formed between water-soluble nanoparticles, PbSe NQDs functionalized with amine groups and γ-Fe_2O_3 NPs stabilized with POSS, allowed for hierarchical coupling and the formation of structurally conjugated fluorescing and magnetic nanoparticles. It was found that the hydrogen bonding occurred via the formation of a pseudo-ring, in which the $NH_3{}^{+}$ group was hydrogen bonded to the lone pairs of the siloxane oxygen in POSS and the O^{-} of the hydrate POSS was hydrogen bonded to one of the CH_2 groups in 2-aminoethanethiol (Scheme 11). The unique system can be used for biomedical applications such as biosensing, detection of cancer cells and drug delivery.

An amphiphilic star-shaped hybrid copolymer constructed of POSS core and poly(ε-caprolactone) arms terminated with β-cyclodextrin moieties assembled into hybrid micelles with hydrophobic POSS–PCL chain encapsulating Fe_3O_4 nanoparticles [186]. Good adsorption capacity of the hybrid micelles was shown in removal of bisphenol A from aqueous solutions due to the host–guest interactions with β-CD. The clusters were separated by an external magnetic field, which can be exploited for environmental protection. $T_8[CH_2CH_2CH_2NHCH_2CH_2CH_2Si(OEt)_3]_8$ was anchored on the surface of Fe_3O_4 nanomagnetics [187]. The resulting hybrid was employed as a magnetic nanocatalyst for high-yield synthesis of pyrans.

4.4.2 Stabilizing Templates for Quantum Dots

Colloidal quantum dots (QDs) are nanometric semiconductor particles of specific optical and electronic properties which can change as a function of both size and shape [188]. Because of their high photochemical stability, tuneable bandgap, high molar extinction coefficients, multiple exciton generation and strong light absorption, QDs are of wide interest and applicative potential for the preparation of transistors, LEDs, lasers, solar cells, quantum computing, bioimaging or inkjet printed semiconductors. The ability to control the structure of QDs is critical for the understanding of their collective properties and for the development of new materials and devices. Unfortunately, the undesired surface trap defects on QDs, induced by the dangling bonds of unsaturated atoms, are almost inevitable. They can cause low electron injection efficiency and high charge recombination in both the interior of QDs and at the interface with electrolyte. It limits severely the application of QDs in photovoltaics. Therefore, it is highly desirable to passivate surface defects on QDs. The trapping

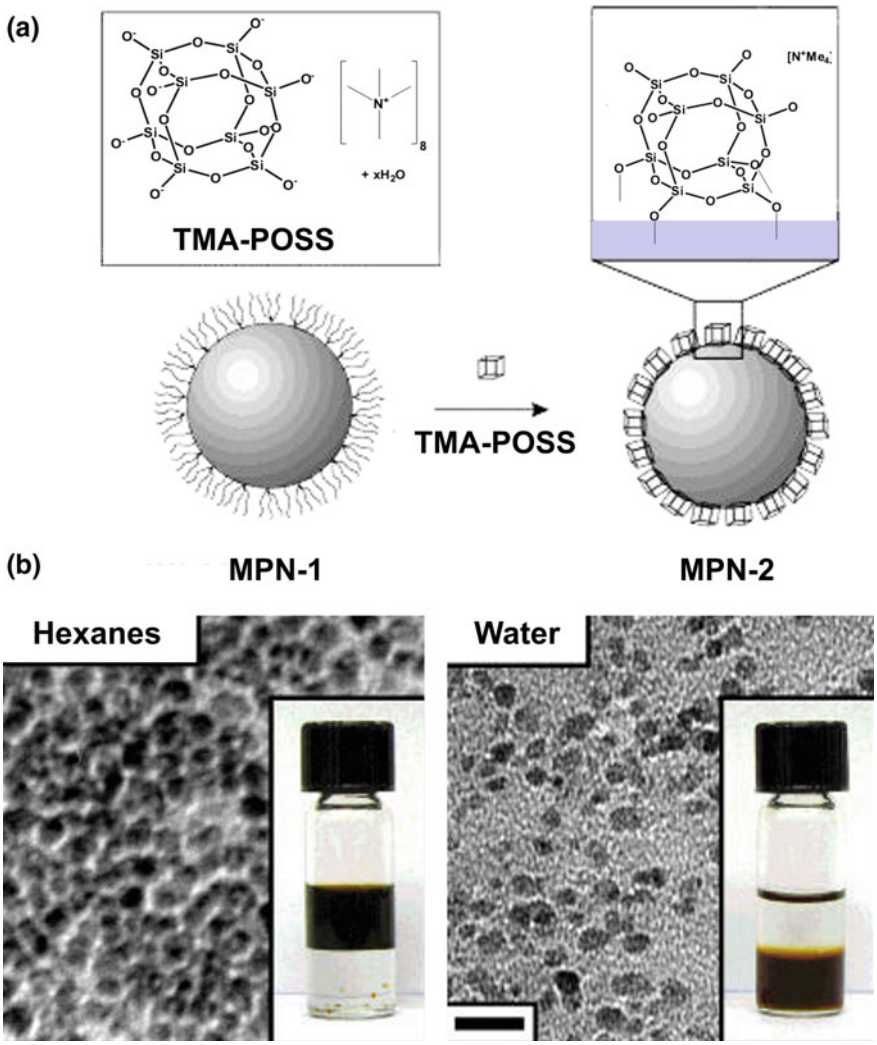

Fig. 10 Magnetic nanoparticles stabilized with $(SiO_{4/2})_8^-NMe_4^+$: **a** passive ligand exchange of the surface monolayer resulting in water-soluble nanoparticles; **b** TEM images of the primary magnetic nanoparticles (in hexanes) and the modified with POSS (in water). The insets show the transfer of particles from non-polar to polar solvent after the exchange (scale bar = 20 nm). Reprinted with permission from [184]. Copyright 2018 American Chemical Society

states can be efficiently suppressed by coating core QDs with small molecular ligands. POSS can also serve for the purpose as high-performance surface modification agents that can play an important role in the spatial stability. The bulky inorganic cage-like core of POSS makes them ideal steric stabilizers. It results in the forma-

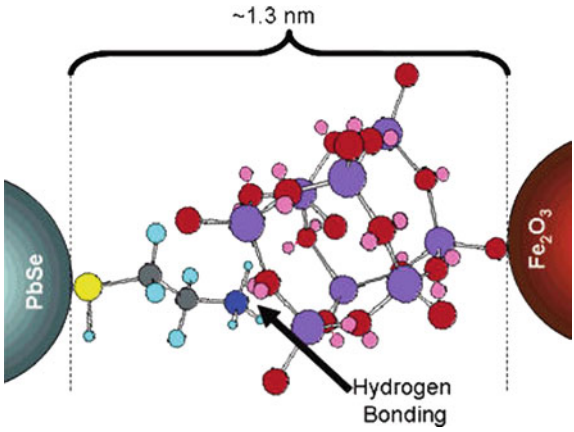

Scheme 11 Structure of a pseudo-ring made of hydrogen bonds between PbSe NQDs with grafted 2-aminoethanethiol and γ-Fe_2O_3 NPs stabilized with POSS. Reprinted with permission from [185]. Copyright 2018 American Chemical Society

tion of an inorganic shell around the core QDs (core/shell structure). POSS can also provide QDs with useful functionalities.

The presence of $T_8(i\text{-Bu})_7(CH_2CH_2CH_2SH)$ on the surface of CdSe QDs improved the photoelectric current, reduced the surface defects and increased the system stability [189]. The modified wurtzite phase QDs of variable sizes capped with POSS (Fig. 11) had desirable light-emission characteristics including photoluminescence quantum efficiencies and fluorescence lifetimes. They were used as efficient photosensitizers for TiO_2 nanotube (TNT) electron acceptor arrays. The silsesquioxane shell allows for the access of small electrolyte ions and electron transport from the surface of QDs. The $T_8(i\text{-Bu})_7(CH_2CH_2CH_2SH)$/CdSe QDs/TNT system exhibited better performance than the conventionally stabilized QDs. The prospective applications of such materials include memory devices, solar cells and semiconductor chalcogenide aerogels. It was also shown that simultaneous use of SH-POSS alongside two other ligands (mercaptosuccinic acid and D-cysteine) favourably reduced the cytotoxicity of CdTe QDs [190].

Well-defined aggregates of QDs with chemical cross-linkers offer desirable collective properties that cannot be found in the individual constituents. The effect depends on the size and nature of the components, the interparticle spacing and their hierarchical organization. Non-covalent assembly is a critical strategy to regulate both spacing and structure. Spherical nanohybrids made of $T_8(CH_2CH_2CH_2NH_3^+Cl^-)_8$ and Mn-doped ZnS QDs capped with 3-mercaptopropionic acid, spontaneously self-assembled in aqueous solutions and were used for quantitative detection of DNA [191]. It was shown that negatively charged phosphate groups in DNA double helix competed with negatively charged QDs in the formation of stable complexes with $T_8(CH_2CH_2CH_2NH_3^+Cl^-)_8$. Molecules of $T_8(CH_2CH_2CH_2NH_3^+Cl^-)_8$ were also used as capping agents to decrease surface defect density of CdTe QDs and to increase their power conversion efficiency (PCE) [192]. The current density and PCE of solar cells made of the POSS modified species was improved with respect to their analogues with bare CdTe QDs.

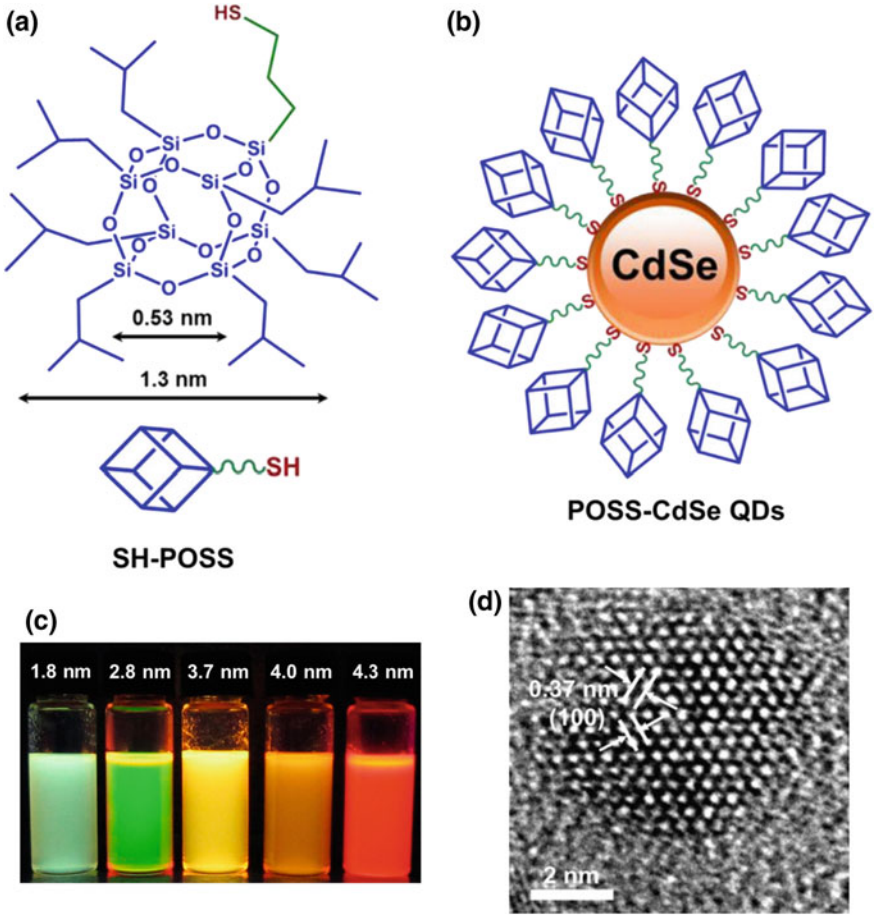

Fig. 11 **a** Chemical structure of $T_8(i\text{-Bu})_7(CH_2CH_2CH_2SH)$ and **b** schematic drawing of a CdSe QD capped with the POSS ligands; **c** the photoluminescence colour change of the POSS-CdSe QDs under a UV lamp during the growth; **d** HRTEM image of POSS-CdSe QDs. Adapted with permission from [189]. Copyright 2018 American Chemical Society

Carbon quantum dots (CDs) are nanosize carbon particles (<10 nm in size) of strong and tuneable fluorescence emission properties [193]. They can be used in biomedicine, optoelectronics, catalysis and sensing. The surface of CDs, characteristically covered with reactive COOH or OH groups, can be chemically modified and passivated with various organic, polymeric, inorganic or biological materials. By surface passivation, the fluorescence properties as well as physical properties of CDs (including dispersibility in various solvents) can be adjusted. CDs were functionalized with $T_8(i\text{-Bu})_7(CH_2CH_2CH_2NH_2)$ to make them superhydrophobic and enhance their photoluminescence and thermal stability [194]. The obtained nanohybrids can be applied as composite fillers, fluorescent liquid marbles and solid-state fluorescent

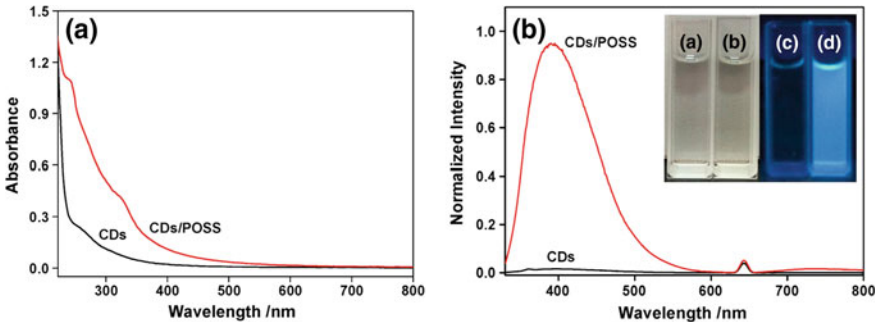

Fig. 12 **a** UV–Vis spectra and **b** fluorescence spectra for the bare CDs and POSS functionalized carbon dots (Cds/POSS) [the inset picture of bare CDs and CDs/POSS under visible (a/c) and UV (b/d) light]. Reprinted with permission from [195]. Copyright 2018 American Chemical Society

sensors. $T_8(CH_2CH_2CH_2NH_3^+Cl^-)_8$ was used as a passivation agent for CDs via formation of amide bonds with carboxylic groups on the surface of CDs [195]. The obtained CDs/POSS were dispersed in aqueous media. In addition to the characteristic features of carbon dots, they exhibited photoluminescence with quantum yield of 24% (Fig. 12), resistance to photobleaching and excellent photoluminescence stability in the presence of biological samples. Both the photoluminescent emission wavelength and the fluorescence intensity depend closely on the size of CDs. The hybrid CDs/POSS can be used for multicolour imaging in biological systems, as it was demonstrated with HeLa cells and MCF-7 cells. Water-soluble molecules of $\left(SiO_{4/2}\right)_8^-NMe_4^+$ were applied as a solid matrix for embedding water-soluble N,S-*co*-doped carbon dots [196]. Highly efficient solid-state luminophores with strong deep blue emission and a very high photoluminescence quantum yield (60%) were obtained.

4.4.3 Sacrifice Templates for Microporous Carbon Supercapacitors

Nanostructured carbon materials, such as graphene, graphene oxide, carbon nanotubes and fullerenes, have been considered promising candidates for a wide range of applications including organic electronics, supercapacitors, semiconductor devices and energy-storage materials [197]. Carbonization of organic precursors in the presence of various templates allows for the replication of the latter in the structure of the final product [198]. The characteristics of templated mesoporous carbons depend both on the employed carbon precursors and the template. The pore size and its distribution are of major importance in determining the performance of porous carbons used as electrode materials of supercapacitors. The maximum electrochemical double-layer (EDL) capacitance is delivered by microporous carbons of monodisperse pore size that matches the size of the desolvated/bare electrolyte ions. The presence of hierarchically interconnected pores or combination of interconnected

micro-/mesopores is an important parameter that can improve the electrochemical efficiency of carbon materials.

The physical and chemical functionalization of the carbon nanomaterials with POSS towards the development of novel hybrid nanostructures was very effective. POSS building blocks can be applied simultaneously as a carbon source and as sacrifice templates for generation of microporous carbons of hierarchical structure. Chemically cross-linked SixOy cage clusters embedded in N-doped carbon were prepared by thermal treatment of $T_8(CH_2CH_2CH_2NH_3^+Cl^-)_8$ in an inert environment [199]. Nanoscale Si-rich clusters distributed in a lighter matrix of N-doped carbon were formed at 1173 K due to chemical cross-linking and carbonization of the side chains of POSS. The material exhibited stable and high cycling, as well as rate capacity when used as a lithium-ion battery anode. The results can be ascribed to the "island–sea" morphology for the "clusters-in-carbon" hybrid structure that enhances interfacial interactions and facilitates charge conduction. Moreover, the small size of clusters with less compact Si–O active sites allow for smooth and complete lithium insertion/extraction. Such electrochemical properties are promising for energy-storage devices.

Molecules of T_8Ph_8 were used for the preparation of well-defined microporous carbon nanospheres [200–202]. The synthetic process included cross-linking of organic components and induced phase separation. It was followed by carbonization and subsequent removal of monodispersed silica domains [200]. The obtained porous material had large specific surface area, as well as excellent adsorption and supercapacitance properties. Ultrasmall Si particles were embedded in carbon matrix with this simple Si-carbon integration strategy. The downsizing of silicon particles in conductive carbon matrix of porous structure enhanced lithium-ion storage performance of Si-based anode [201]. Friedel–Crafts cross-linking of T_8Ph_8 shells resulted in the formation of continuous polymeric nanospheres with inorganic nanosilica wrapped in. The cross-linked nanospheres were converted into porous carbon matrix after high-temperature carbonization treatment and magnesiothermic reduction. Silsesquioxane cages (1.0 nm) were reduced and transformed into ultrasmall Si particles (4–10 nm).

A covalent bond-induced surface-confined cross-linking of T_8Ph_8 was used to construct 1D coaxial microporous carbon composites of the core made of carbon nanotubes (CNT) enveloped by microporous carbon shells ("CNT@micro-C on Fig. 13) [202]. The POSS building blocks were attached to the surface of acylated CNT. A cross-linked layer was formed with the thickness tailored from 6 to 20 nm. It was transformed into a microporous coating after carbonization of T_8Ph_8 and etching of the inorganic cages (BET surface area of about 570–1300 m^2/g). The obtained CNT@micro-C combined the structural advantages of CNT and microporous carbon (large surface area, high electrical conductivity, fast ion transfer speed and short ion transfer distance). CNT serves as electron motion pathway, and the 3D stacked microporous tube accelerates ion transfer rate and shortens ion transfer distance. As a consequence CNT@micro-C revealed superior supercapacitive performance (capacitance retention up to 86%) and can be used as an electrode material.

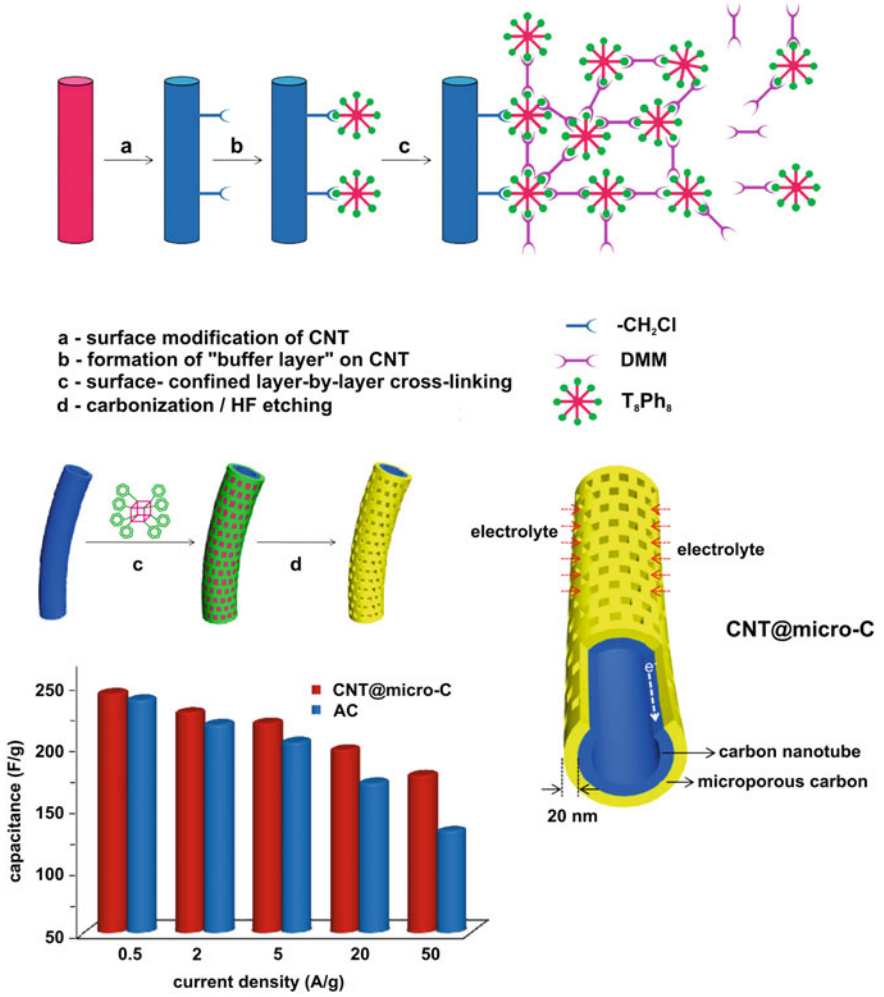

Fig. 13 Preparation and capacitive performance of 1D coaxial microporous carbon composite in the process of surface-confined cross-linking of T_8Ph_8 on the surface of CNT. Adapted with permission from [202]. Copyright 2018 American Chemical Society

Hierarchically porous carbon structures of high specific surface area (>2000 m^2/g), large pore volume and very good power performance were also formed by self-assembling of $T_8(C_6H_5NH_2)_8$ in the presence of block copolymers (Pluronic F127 and Pluronic F108) [203]. The block copolymer-assisted method combined the molecular-scale templating effect of POSS and good compatibility between aminophenyl groups and the block copolymers. Highly ordered mesopores (~4 nm) were formed due to soft templating by Pluronics. Two-dimensional hexagonal (p6 m) or body-centred cubic (Im3 m) mesopore arrangement could be obtained

by adjusting the composition of block copolymers. The presence of POSS template resulted in uniform micropores of ~1 nm diameter in the walls between mesopores. The mesopores facilitated fast transport of ions to fine micropores. Specific capacitance of the porous carbons after ~4 wt% nitrogen doping reached ~160 F/g in an ionic liquid electrolyte and ~ 210 F/g in 1 M H_2SO_4 aq.

4.5 POSS-Containing Hybrid Materials for Optoelectronics

POSS are suitable platforms for the preparation of high-performance materials of unique optoelectronic properties. Incorporation of POSS into organic matrices is of significant interest because of their distinct hybrid nanostructures, confined size effect and physical properties [204, 205]. The inorganic core does not show any significant optical properties and electronic conjugation. The small silica-like cage acts as a nanoparticle filler, and the organic substituents increase their compatibility with organic compounds. The rigid silsesquioxane core not only reinforces the mechanical properties of materials, but also acts as a isolating barrier because of its low thermal conductivity and small dielectric constant. The so-called nanoporous low-j materials of low electric constant are of high demand in microelectronics. They can be prepared by introducing air-filled voids into the bulk. The presence of closed nanopores, homogeneously distributed in the matrix, is required to preserve the electric and mechanical properties. It was found that dielectric constant of polyimide nanocomposites with grafted methacrylate (MA) side chains containing POSS can be tuned by varying the molar ratio of the grafted MA-POSS in the copolymer [206, 207]. POSS molecules formed crystalline nanoaggregates that could act as an isolating barrier. Materials of dielectric constants close to 2.2 were achieved if PI-*g*-PMA-POSS contained 23.5 mol% MA-POSS.

The enhancement of the optoelectronic performance is important for the development of organic light-emitting diodes (OLEDs), liquid crystal displays, AIE-based sensors and biodevices or electrochromic devices. Excessive π–π stacking in many organic luminescent materials causes a significant drop in their quantum yield in the solid state. The undesirable behaviour can be suppressed by generation of 3D structures with POSS scaffolds. The change of the crystal lattice leads to aggregation-induced emission (AIE) effects [208]. Analogously, POSS can disrupt conjugated polymer packing in electrochromic materials. It facilitates free ion movement and creates more accessible sites for the redox reactions.

4.5.1 Luminescent Materials

Derivatives of pyrene (Py) show characteristic large Stokes shift, strong absorbance, high quantum yield and good photochemical stability [209, 210]. The emission of monomeric pyrenes can be found in the ultraviolet part of the electromagnetic spectrum (380 nm), while the excimer emissions are in the range of 450–500 nm. Those

properties can be of advantage in light harvesting systems, especially if the energy is transferred from pyrene excimers to spectrally suitable acceptors. An efficient antenna system should have a very high molar extinction coefficient, excellent photostability and ability to transfer the energy. However, many hydrophobic organic luminophores (especially planar polycyclic aromatics) are efficient light emitters only when molecularly dissolved or dispersed in good solvents. In solid state, they require the presence of separators that would simultaneously prevent the excessive stacking and direct the luminophores in the solid state into their most perfect organization. Pyrene derivatives, due to their high quantum yield and strong affinity with various analytes, are widely used as fluorescent probes to study dynamics and conformational changes of polymers and biomacromolecules [211]. However, it is hard to prepare thin fluorescent Py films that would exhibit strong excimer emission in the solid state. In spite of pure excimer fluorescence of pyrene crystals, the spin-coated thin films of pyrene and its derivatives frequently exhibit weak or no excimer emissions due to the random packing of pyrene rings as a result of rapid evaporation of solvent during the coating process. Moreover, if the films are to be used as sensors, then Py rings should not be aggregated too tightly in order to allow for diffusion of analytes. The use of POSS substituted pyrenes can be a good solution to both problems. Simulation of electronic structures of T_8Ph_8 indicated that the highest occupied molecular orbitals (HOMOs) as well as the lowest unoccupied molecular orbitals (LUMOs) were localized on phenyl side groups [212]. It means that star-shaped organic luminescent dyes grafted on 3D POSS molecules can be less prone to self-quenching and have improved quantum efficiencies in photoluminescence and electroluminescence.

Indeed, the results obtained with several POSS-Py systems show the desired effect. For example, a supramolecular star-like, blue-light electroluminescent material with 4-uracilbutyl-1-methylpyrene units linked to the silsesquioxane core via a triple hydrogen-bonding array (U-Py/ODAP-POSS) exhibits strong and stable fluorescence emission and high quantum efficiency even at high temperatures (423 K) [213]. Good solution processing of U-Py/ODAP-POSS allowed for the preparation of an electroluminescence device of higher maximum brightness and higher luminance efficiency than those of the parent pyrene derivative. An organic–inorganic light-emitting material based on POSS grafted with dipyronecarbazol moieties (POSS–DPCz) is an effective chromophore with substantially improved fluorescence-colour purity and quantum yield compared to control DPCz without incorporated POSS [214]. The introduction of POSS within the chromophore matrix promoted the formation of 3D hierarchical nanostructures. POSS-DPCz exhibited excellent optoelectronic properties and high thermal stability, solution processability, good film-forming ability and efficient control of POSS dispersion. Photoluminescence and electrochemical analyses indicated, both in solution and in the thin films, that POSS cages effectively suppressed aggregation and enhanced the colour stability of DPCz. Spin-coated thin films of ester of 1-pyrenebutyric acid and $T_8(i\text{-Bu})_7$ bearing a single 1-(2,3-propanediol)propoxy chain (PBPOSS) exhibited strong excimer emissions at 475 nm when excited at 350 nm [215]. Spectroscopic studies indicated that the crystallization of silsesquioxane moieties in the films induced the formation

of pyrenyl excimers. A very fast fluorescence quenching was observed upon exposure to the vapours of nitroaromatic compounds. An eight triphenylamino-pyrenyl substituted POSS was designed as a highly sensitive and efficient sensing material of 3D symmetrical spatial conformation, high area-to-volume ratio, high molar extinction coefficient, multiple exciton transfer path and energy level suitable to detection of nitrate ester explosives [216].

Hybrid pyrene–silsesquioxane molecules with two pyrene rings anchored to a single inorganic core via flexible ether bonds (BPy-POSS of "butterfly-like" structure) were designed in order to enrich the fraction of intrinsic intramolecular pyrene dimers on the surface of ordered thin films made of $T_8(i\text{-Bu})_7$ [217]. Silsesquioxane moieties act as crystalline templates through POSS–POSS recognition and direct assembling of Py groups. The emission spectra of BPy-POSS in dichloromethane contained a large share of intramolecular and intermolecular excimers. The result was attributed to the easy rotation of two adjacent ether bonds and the π–π interactions of aromatic rings that facilitate the formation of pyrenyl dimers or aggregates. The fluorescence quenching was observed upon exposure to the vapours of nitrobenzene.

Interesting results were obtained with $T_8(CH{=}CH\text{-}Py)_8$ that exhibits enhanced fluorescence emission from pyrene–pyrene excimers. It was used for the preparation of solution processable emitting materials for OLEDS [218]. It was also shown that such hybrid systems can act as effective fluoride ion sensors in solutions with a π–π^* fluorescence enhancement or quenching, depending on the polarity of the solvent used [219]. The fluorine anion was pulled into the confined space of the silsesquioxane cage owing to electrostatic interactions with electron-deficient silicon atoms. The F^- ion occupies the central position within the cage, which resulted in a slight compression of the silsesquioxane framework [220, 221]. $T_8(CH{=}CH\text{-}Py)_8$ exhibited a significant fluorescence of pyrene–pyrene through space excimers in DMSO, while π–π^* fluorescence emission of monomeric pyrenes was dominant in THF. Fluoride encapsulation in high polarity solvents such as DMSO resulted in increase in the distance between Py groups and diminished the pyrene–pyrene fluorescence but enhanced π–π^* fluorescence emission. In THF, the POSS-F^- complex exhibited a significant excimer emission. The π–π^* effect was quenched and a colour change from light yellow to deep orange was observed as a result of the postulated formation of a charge-transfer (CT) complex among the pyrenyl rings.

Perylene diimide (PDI) is structurally related to pyrene (Fig. 14). Derivatives of PDI have attracted a significant attention as organic semiconductors due to their chemical and photochemical stabilities, as well as high extinction coefficients. The ordered supramolecular structures of perylene derivatives can be also applied as organic electronic devices, such as light-emitting diodes, photovoltaic devices, organic field effect transistors or electron transfer cascades. The self-assembling abilities of PDI and formation of one-dimensional nanostructures due to π–π interactions enable efficient long-range charge migration and increase the electrical conductivity. However, the extended π–π stacking can cause solution-processing problems as well as a significant drop of fluorescence quantum yield in concentrated solutions and in the solid state.

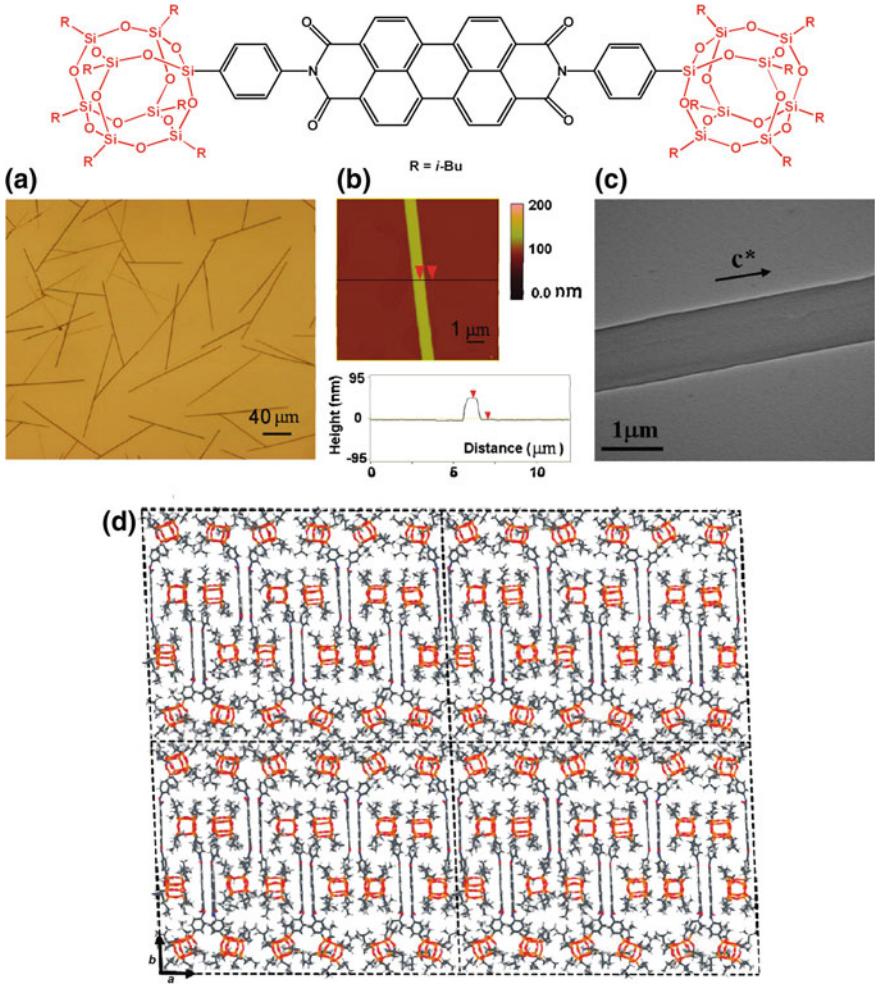

Fig. 14 **a** Optical microscopy image of single-crystalline nanobelts of POSS–PDI–POSS hybrid; **b** AFM image and a line-scan profile of the flat top of single-crystalline nanobelts and **c** TEM bright-field image of a single-crystal nanobelt; **d** molecular packing in the crystal lattice. Adapted with permission from [223]. Copyright 2018 American Chemical Society

Sterically hindered substituents, such as POSS, grafted at imide positions or bay regions of PDI can help to overcome these drawbacks and supress the undesirable effects. Microwave condensation of $T_8(i\text{-Bu})_7(CH_2CH_2CH_2NH_2)$ with a range of mono- and bis-anhydrides yielded the corresponding POSS imide derivatives including bis-phthalic POSS imide, bis-naphthalic POSS imide and bis-perylene POSS imide [222]. The latter displayed particularly strong fluorescence, with quantum yield approaching unity, while the photoluminescence of naphthyl bis/monoimide analogues was only very weak. The X-ray crystal structure of bis-perylene POSS

imide indicated good separation of perylene moieties. PDIs with bulky POSS substituents exhibited a unique supramolecular structure with a discrete dimer packing scheme, which can enhance fluorescence quantum yield in the solid state. Uniform and ultralong crystalline nanobelts with dimensions of 0.2 mm × 1 μm × 50 nm were self-assembled directly by slow evaporation of THF solutions containing symmetric POSS–PDI–POSS hybrids with rigid 1,4-phenylene linkers between the perylene moiety and side $T_8(i\text{-Bu})_7$ groups [223]. The steric hindrance of POSS makes it difficult to achieve a continuous stacking of PDIs. Instead, the molecules dimerized to maximize the π–π interactions and then packed as interdigitating building blocks. Crystal structure consists of six dimers as one supramolecular motif in one triclinic unit cell. It can account for anisotropic crystal growth and the nanobelts formation. Similar phenomena were noted for POSS–PDI–POSS with $T_8(i\text{-Bu})_7$ covalently attached to the PDI linker via flexible spacers [208]. The macromolecules formed ultralong crystalline microbelts with a length of several hundred micrometres. In the first step, the molecules formed dimeric structures (both in solution and in the solid state) that become building blocks of a monoclinic crystal lattice. Quantum yields of 100% (in solution) and 17.5% (in the solid state) were observed. The material was applied as a high-performance colorimetric and ratiometric fluorescent probe for rapid detection of fluoride anions.

However, the presence of bulky groups in PDI molecules does not inevitably promote the improvement of fluorescence quantum yields in the solid state. The self-aggregation behaviour of a series of symmetric PDI bisimide derivatives with bulky $T_8(i\text{-Bu})_7$ groups at imide nitrogens and bearing also side groups at the bay positions of the PDI spacer was studied [224]. The presence of POSS did not have large effects on the spectroscopic properties of PDIs in solution but changed the packing structure of the molecules and their emission in the solid state. It was found that fluorescence quantum yield in the solid state was determined by the type of packing structure. Most of the studied molecules were packed in a "face-to-face" mode, but with different longitudinal displacement. "J"-type interactions between the neighbouring molecules and improved quantum yields were observed if the longitudinal displacement was large. Small positional shifts resulted in "H"-type interactions and poor quantum yields.

Unsymmetrical hybrid PDI–POSS derivatives are well soluble in common organic solvents and show typical absorption and emission features of the perylene diimide fragment in solution, with a quantum efficiency close to unity [225]. The electronic absorption spectra of both, spin-coated films and powders, indicated a reduced fluorophore aggregation and significant quantum yield efficiencies (QY up to 70%) owing to the effect of POSS. Unsymmetrical POSS–PDI derivatives were also used for the preparation of more elaborated macromolecules and sensing systems. An amphiphilic fluorescent polymer of controlled molecular weight and low polydispersity, containing PDI and POSS, was synthesized by grafting perylene anhydride with $T_8(\text{iBu})_7(CH_2CH_2CH_2NH_2)$ and 2-bromoisobutyryl bromide to produce an ATRP macroinitiator for the radical polymerization of N-isopropylacrylamide [226]. Self-assembly of the resulting amphiphilic macromolecules was studied in aqueous solutions. It was found that the hybrid nanoparticles exhibited attractive high red

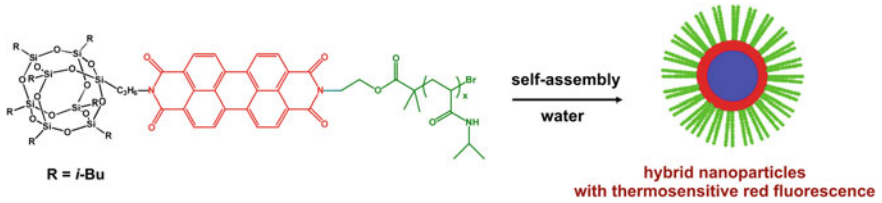

Scheme 12 Thermoresponsive micelles formed by self-assembled POSS–PDI–PNIPAM macromolecules. Reprinted with permission from [226]. Copyright 2018 American Chemical Society

fluorescence at 645 nm due to the incorporation of bulky POSS moieties. The fluorescence intensity of the self-assembled hybrids could be tuned due to the presence of thermoresponsive PNIPAM coronas (Scheme 12).

POSS were also applied as scaffolds for the preparation of other thermally stable solid-state emissive materials [20]. POSS decorated with rigid linear π-conjugated luminophores at each of eight vertices of silsesquioxane core formed intermolecular excimers in dilute solutions. However, the intrinsic luminescent properties of the monomer could be recovered if bulky alkyl chains were introduced to the luminophores. Similar optical properties were observed in the solid state, regardless the increase in steric hindrance. The preservation of electronic states and the lack of non-specific intermolecular interactions in the condensed state were attributed to the presence of rigid 3D inorganic scaffolds and the specific radial distribution of luminophores around the silica cubes. It was also demonstrated that the POSS-based hybrids exhibited bright blue emission beyond 473 K in the open air, which is interesting for advanced electroluminescent devices, displays and sensors. Hard-sphere-like aromatic polyamide dendrimers with POSS cores were synthesized up to the sixth generation using the divergent approach [227]. The intrinsic viscosities of the dendrimers reach the maxima at the fifth generation and have squashed sphere shapes on mica substrates even for the sixth generation. The shells of high-generation dendrimers are rigid owing to the restricted molecular motion of the crowded peripheral units. More intensive fluorescence emission was observed on increasing the generation number of dendrimers terminated with trifluoroacetamide groups, which points to the role of the constrained terminals in the enhancement of photoluminescence.

4.5.2 Liquid Crystals

Polyhedral silsesquioxane cores were also used for the preparation of disc-like or rod-like species of true liquid crystalline (LC) properties. The packing mode and the type of mesophase in such POSS-LC systems depends generally on side mesogens tethered to the inorganic core and their propensity towards formation of mesomorphic phases [228, 229]. However, despite the pseudo-spherical geometry of the core, molecules of POSS bearing long rigid mesogens typically are of cylindrical or rod-like shape and tend to form lamellar enantiotropic smectic A and smectic C phases

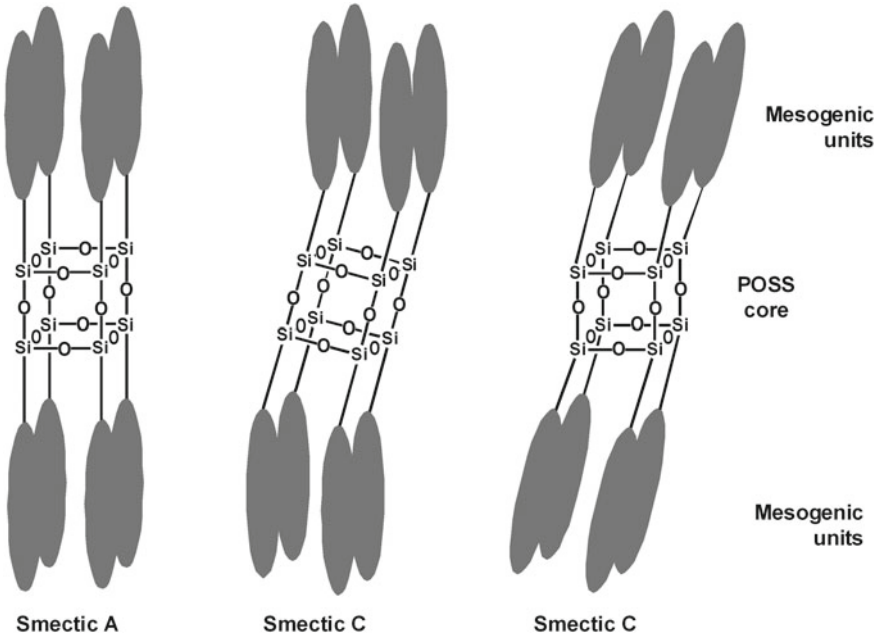

Scheme 13 Distribution of side groups with respect to the inorganic core in lamellar enantiotropic smectic A and smectic C phases formed by POSS grafted with long rigid mesogens [242]

on heating (Scheme 13) [230–233]. The clearing point of the smectic C to smectic A transition and Tg were lowered in the case of dendritic species, compared to the linear mesogens. The specific molecular topology can also play a very important role in the formation of supramolecular LC self-assemblies [234–241].

POSS octasubstituted with 4′-undecyloxybiphenyl-4-yl-4-octyloxy-2-(pent-4-en-1-yloxy)benzoate groups could form both nematic and hexagonal columnar mesophases [243]. Biaxial domains (cybotactic clusters) made of tilted layers, with spacing between layers determined by the length of the rigid part of the mesogenic unit, were observed in each of them in a wide temperature range. Such hybrid molecules can be used in organic optoelectronic devices or employed as sensitive fluorescent probes for detection of metal cations, acids, gases or explosives.

Unfortunately symmetrical silsesquioxanes can easily aggregate in organic LC media, which can result in undesired light scattering by macroscopic particles. Such systems must consist of completely separated phases to be effective. Formation of hierarchically ordered structures by hybrid heterofunctional T_8R_7R' makes them interesting candidates for the application in LC devices with vertical alignment (VA). POSS increase thermal stability of such systems. The required phase separation was obtained with $T_8(i\text{-Bu})_7$ monosubstituted with cyanobiphenyl group [244]. At high temperatures, they form an induced smectic phase and closely packed layered structures on mixing with 4-cyano-4′-heptyloxybiphenyl [245]. The molecules dispersed

in a nematic LC medium gradually diffuse to form a perfectly separated VA layer [244]. It was also found that LC hybrid materials of enhanced nonlinear optical characteristics [246]. and physicochemical properties [247] can be obtained if POSS are grafted with appropriate side groups that help their dispersion in LC media. Mixing POSS functionalized with azobenzene mesogens with a nematic LC matrix resulted in functional hybrid nanocomposites exhibiting reversible dynamic holographic properties [246]. They were capable of rapid, light-induced changes of refractive index due to conformational isomerization of azobenzene units.

Rigid polymers side-jacketed with mesogen groups and POSS can exhibit LC properties due to competitive self-assembling and separation of organic and inorganic phases [248, 249]. For example, rigid poly(terephthalates) with side-grafted POSS can act as rod-like supramolecular mesogens at high temperatures and form hexagonal columnar nanophase (2D Colh) [249]. At low temperatures, the hexagonal order is disrupted by crystallization of POSS. The separate self-assembling of organic and inorganic parts results in the formation of an inclusion complex [coexisting columnar nematic LC phase (Colh) and rhombohedral crystalline (KR) phase]. Interconverting LC phases [crystal (Cr) formed by POSS, coexisting Cr and hexagonal columnar (Colh) phase, and pure Colh phase] were also thermally induced in mesogen-jacketed poly(norbornenes) with side POSS groups [248]. Materials exhibiting chiral nematic phases can be useful in LC displays and electro-optical switches. POSS have been also used as cores for grafting various mesogens including simple molecules [250] and polymeric liquid crystals [251].

Interesting hierarchical structures were obtained with POSS functionalized with discotic side groups. Polyhedral silsesquioxanes bound to discotic triphenylene (TPE) molecules can form unique hierarchical structures owing to the separation of inorganic and organic phases and the tendency of both POSS and TPE to form well-organized mesophases. A unique hierarchical structure was formed by molecules of octafunctional $T_8(TPE)_8$ having peripheral alkyl chain arms of two lengths (C_5 and C_{12}) (Scheme 14). It was ascribed to the incompatibility between POSS and the hydrocarbon parts, favourable interactions among peripheral mesogens and decrease in entropy due to deformation of the silsesquioxane core [252]. The molecular topology was extremely important for the supramolecular self-assembly of the star-shaped supermolecules. It was found that the morphology and thermal characteristics of LC mesophases generated by such molecules depend on the length of spacers between POSS and TPE. Species with C_5 arms were amorphous, but those with C_{12} side chains could self-assemble into hierarchical mesophases. It was a result of the balance between microphase segregation and competition between interactions among peripheral mesogens and decreased entropy owing to the deformation of POSS core. A column-within-column superhexagonal columnar phase was formed by species with C_2 linkers between POSS and TPE. Molecules with C_6 spacers have an alternating POSS-TPE lamellar morphology with a rectangular columnar symmetry. An oblique columnar phase with inverted columnar morphology with four TPE columns arranged into a supercolumn within the POSS/alkyl chain matrix was found for the most separated hybrids with C_{10} linkers.

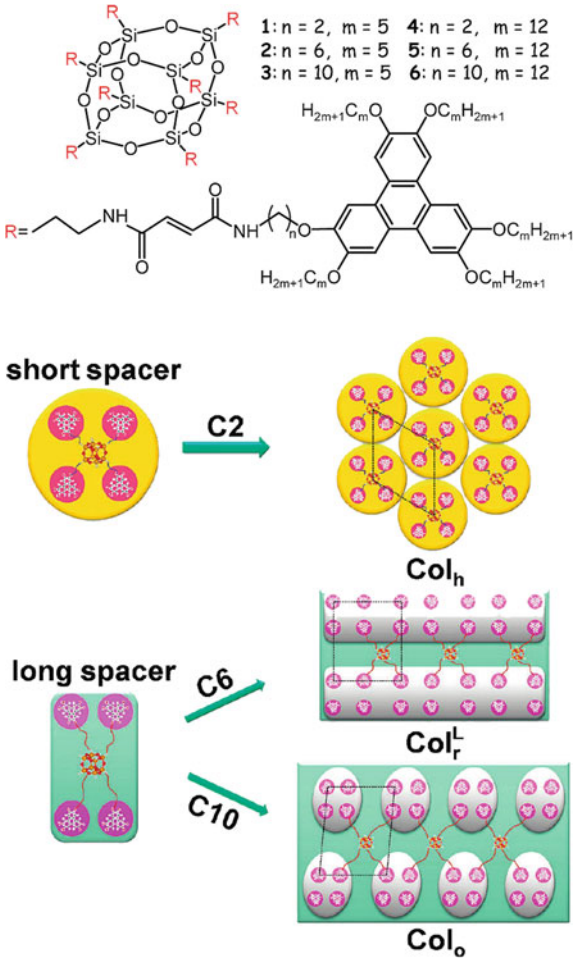

Scheme 14 Chemical structures of hybrid star molecules of $T_8(TPE)_8$ and schematic representation of their supramolecular self-assembly in the solid state (2D unit cells drawn in dotted lines). Adapted with permission from [252]. Copyright 2018 American Chemical Society

Nanophase separation between crystalline lamellae of heterofunctional POSS and liquid crystalline organic moieties was observed both for an asymmetric disc-cube dyad derivative of 2-hydroxy-3,6,7,-10,11-pentakis-(pentyloxy)-triphenylene and $T_8(i\text{-Bu})_7$ linked by a flexible C_{11} organic spacer (Scheme 15) and for 1:1 physical blend of POSS and TPE (Fig. 15) [253]. $T_8(i\text{-Bu})_7$ groups were stacked into an ABCA four-layer lamellar rhombohedral crystal (space group *R*-3*m*) characteristic to the parent POSS. True columnar mesophases were not obtained. The silsesquioxane assemblies were sandwiched between LC bilayers comprised of TPE molecules. In the physical blend, POSS and TPE formed the outer layers with triphenylenes interdigitating in the rhombohedral crystal structure. TPE molecules were oriented parallel to the lamellar normal. The arrangement is similar to homeotropic nematic discotic structures.

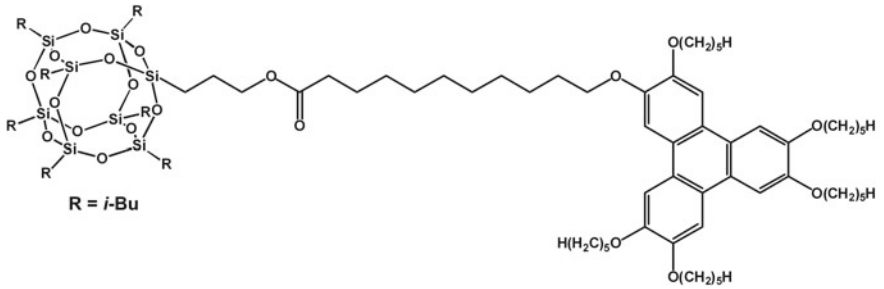

Scheme 15 Polyhedral silsesquioxane $T_8(i\text{-Bu})_7$ bound to the molecule of discotic triphenylene [253]

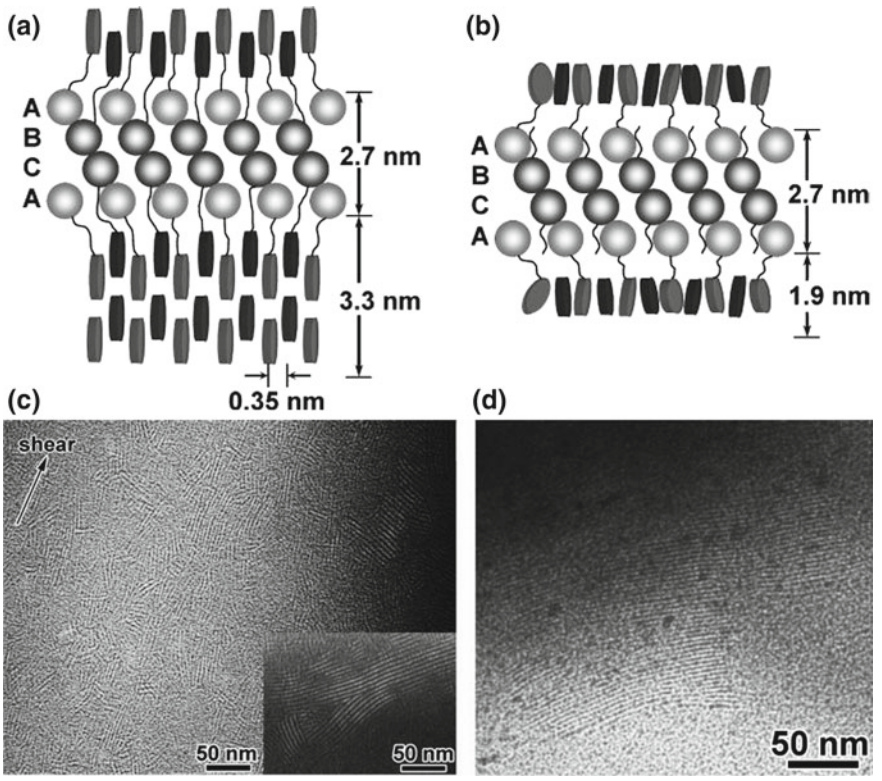

Fig. 15 Schematic representations of self-assembly at room temperature of **a** POSS-TPE (POSS ABCA stacked into a four-layer lamellar crystal and TPE discs formed staggered bilayer) and **b** 1:1 physical blend of POSS and TPE (interdigitating); **c** bright-field TEM micrographs of POSS-TPE; **d** TEM micrograph of 1:1 blend of POSS-TPE:POSS. Adapted with permission from [253]. Copyright 2018 American Chemical Society

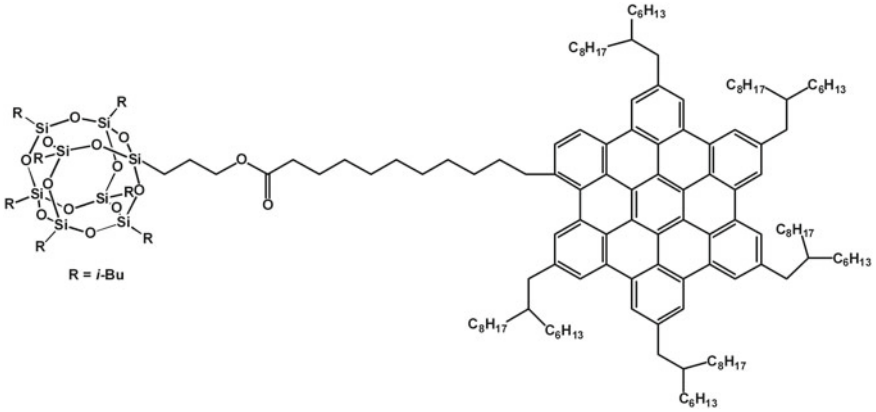

Scheme 16 $T_8(i\text{-Bu})_7$ grafted with hexa-peri-hexabenzocoronene [257]

Tetraphenylethylene can also act as a sensitive fluorescent probe to monitor the self-assembly of POSS molecules. Two nanohybrid dendrimers that were synthesized by grafting tetraphenylethene units onto $Q_8M(CH{=}CH_2)_8$ exhibited aggregation-induced emission (AIE) and high fluorescence quantum efficiencies in both dilute solutions and in the solid state [254]. They were also much more thermally stable than the parent tetraphenylethylene compounds. The emissions of nanoaggregates could be quenched by picric acid or Ru^{3+} ions, which suggests their possible use as highly sensitive chemosensors for explosives and metal ions. Incorporation of Schiff bases furnished the hybrid POSS nanoparticles with pH-responsiveness [255]. Rapid fluorescence quenching was observed under acidic conditions. It was also observed that $T_8(i\text{-Bu})_7$ monomodified with tetraphenylene groups exhibited monomer emission in organic solvents as well as AIE emission in THF/water [256]. Samples prepared separately from THF and THF/water had different hierarchical nanostructures. The flexible spacers between the organic moieties and POSS controlled the lamellar self-assembly and supressed the aggregation of luminophores.

POSS-based derivatives with the silica core grafted with hexa-peri-hexabenzocoronene (HBC) moieties (Scheme 16) are closely related to the POSS-TPE systems. It was found that POSS–HBC hybrids can form various complex self-assembled nanostructures, depending on the POSS content and topology of the molecule [257].

At ambient temperature, structures of low order were observed for molecules of a single $T_8(i\text{-Bu})_7$ linked to HBC, and of long-range hierarchical structures for larger species. The transition temperature increased with the POSS content. Species with two POSS molecules formed a supramolecular structure with a monoclinic unit cell coexisting with KR crystalline phase made of silsesquioxane moieties. HBC core surrounded with six POSS exhibited two order-to-order transitions (Colh coexisting with KR to Colh and Colh-to-BCC) but remained ordered within the experimental temperature range. It should be stressed that the complex BCC phase is quite

unique for a system built of rigid nanoparticles. The effect of the linker on the self-assembling properties of POSS–HBC dyads was investigated [258]. Hierarchically ordered monodisperse structures were obtained with high molecular precision that played an important role in self-assembling. Spacers that were too long or too short could not balance the competition between POSS and HBC moieties, which made them unable to form highly ordered structures at low temperatures. HBC–C_3–POSS dyad with the most suitable spacer consisting of three methylene units generated highly ordered orthorhombic structures. At high temperatures, 2D Colh structure was governed by the length of the flexible spacer between POSS and side HBC groups. All dyads (except the one with the longest spacer) produced hexagonal columnar 2D Colh structures at high temperatures.

4.5.3 POSS-Based Ionic Liquids

Ionic liquids (ILs) are non-volatile salts with unique physicochemical characteristics and melting temperature below 373 K. They have attracted considerable interest due to high ionic conductivity, high polarity, negligible vapour pressure, high thermal stability, non-flammability, high density, high heat capacity and wide electrochemical stability window. Due to the ability to dissolve a wide range of organic and ionic compounds, they can be also used as "green" solvents in conventional and catalytic reactions and separation–purification processes.

Several reports have suggested that POSS-based IL can be used as no-leaking, high-performance electrolytes [259–265]. The observed increased interest in application of POSS as ILs can be attributed to their unique 3D structure that can strengthen ion transportation abilities, high rigidity and thermostability, as well as the presence of functional substituents on the silica cores. The highly symmetric structure of POSS contributes to the suppression of the molecular mobility of ion salts and results in the formation of regular structures, leading to thermally stable, thermotropic IL crystals. It was shown that the temperature range in which hybrid POSS-ILs with various alkyl chain lengths exist in LC phase is enlarged because of the stabilizing effect of the inorganic core [260]. These well-ordered ionic moieties should be able to work as efficient cation carriers and scaffolds for ordering cations, as well as exhibit enhanced optical and magnetic properties. Thermally stable thermotropic IL crystals can be also used in electronic devices. The LC phase of the POSS-tethered ion salts was maintained until decomposition (no clearance point during heating).

The so-called room temperature ionic liquids were obtained with POSS [259, 261]. After tethering to the cubic core, the ion pairs are isolated and distributed in a star shape, which increase the exclusion volume, disrupt the aggregation of ion pairs and lead to decrease in T_m. The products are transparent and colourless, and those of high number of ionic pairs melt below 298 K. It can be attributed to the smaller enthalpy and entropy of fusion of POSS-IL [262]. It was also shown that tethering the ionic arms to the inorganic core led to the enhancement of hydrogen-bonding capability, as indicated by respective chemical shifts in ^{1}H NMR spectra.

The structural features of POSS can contribute more than its rigidity to the enhancement of thermal stabilities of POSS-based ILs. A large number of ion pairs tethered to POSS is essential to increase the temperature of their decomposition, but it is not the only factor that determines the thermostability. Comparative studies on polyanionic POSS with imidazolium cations tethered to the silsesquioxane core (POSS-Im) and the respective counterpart salts of single side chains revealed that the respective values of decomposition temperature (T_d) for POSS derivatives with 6 and 8 ionic pairs were higher than those of single-arm species and the parent POSS core. In contrast, POSS-Im2 and POSS-Im4 showed lower T_d (even than the single chain ion pairs).

Studies on the behaviour of ionic POSS in solution explained the macroion—counterion interactions [263]. Both positively and negatively charged POSS-IL with identical charges and similar sizes self-assembled into blackberry-type supramolecular structures in water/acetone mixtures. The phenomenon was found to be charge-regulated and driven by the counterion-mediated attraction. The size of blackberry structures increased upon increasing the acetone content. Negatively charged POSS self-assembled in polar solvents and formed less ordered supramolecular structures than the positively charged POSS. Those discrepancies were ascribed to different counterions and ionic domains of positively and negatively charged macroions, ionic strength in solution and the water-bridged hydrogen bonding between the monomers.

Ionic liquids of tuneable properties have found numerous applications in materials science (e.g. electrolytes for actuators, lithium batteries and fuel cells). Replacing liquid-state electrolytes with solid-state electrolytes can also improve the durability of dye-sensitized solar cells (DSSCs). Amorphous ionic conductors in the elastomeric state at the operating temperature of solar cells ensure good pore filling and improve the photovoltaic performance due to increased interfacial contact between the electrolyte and the TiO_2 film. Efficient amorphous ionic conductors for solid-state DSSCs were prepared by linking $T_8(CH_2CH_2CH_2Cl)_8$ to imidazolium iodides with propyl and allyl groups (T_g respectively at 278 and 279 K) [264]. Binary solid-state electrolytes were prepared by blending the ionic conductors and appropriate amount of iodine without any other additives. Good power conversion efficiency (6.29%) has been achieved with good long-term stability using an organic dye as the sensitizer. Stronger intermolecular π–π stacking interactions between the allyl groups and imidazolium rings are responsible for the higher conductivity and slower charge recombination than those observed for the propyl counterpart.

Cross-linking and solution extraction of ionic POSS was used for fabrication of inorganic–organic hybrid ionogels and scaffolds with well-defined mesopores (Scheme 17) [265]. High-performance ionogels with superior performance as lithium-ion batteries, excellent electrochemical stability and unique ion conduction behaviour were fabricated through cross-linking of functional groups on silsesquioxane cores and various cationic tertiary amines. The extraction of liquid components left hybrid scaffolds with well-defined, interconnected porous structure and covalently tethered ionic groups in local environment. The products were used as recyclable, heterogeneous catalysts for the CO_2-catalysed cycloaddition of epoxides.

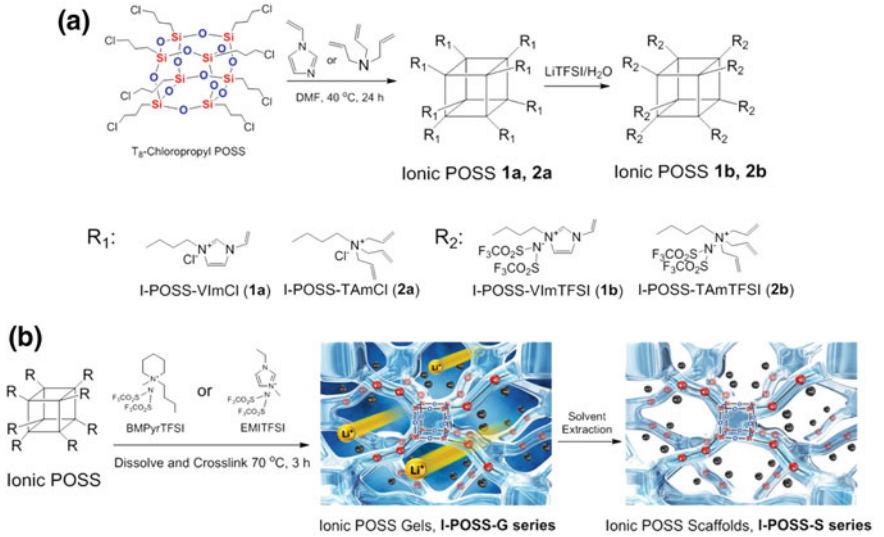

Scheme 17 Cross-linking of ionic POSS for the preparation of hybrid mesoporous ionogels. Adapted with permission from [265]. Copyright 2018 American Chemical Society

Three-dimensional hybrid species having POSS inorganic cores enveloped by coronas made of grafted organic macromolecules can assemble in solution into large-scale structures similar to multidendrimer aggregates with POSS-rich domains surrounded by POSS-poor domains [266]. The flexible chains of polymers attached to POSS tend to adjust their conformation in response to changes of the environment. When dissolved, such systems become more compact and deformed on increasing the concentration of the solution. POSS-poly(*N*-isopropylacrylamide) (PNIPAm)–poly(2-hydroxyethyl methacrylate) (PHEMA) copolymers were found to be dual-responsive to temperature and pH [267]. Similar pH-responsiveness was noted for imidazole-terminated POSS-poly(amidoamine) dendrimers of first and second generation [268]. The effect is structure dependent and the recorded pKa values decreased for larger species owing to electrostatic repulsions between neighbouring polar groups. Such hybrid systems can be used as functional smart materials for, e.g. encapsulation and controlled release of various cargo molecules. Ordered nanonetworks of ionic branched macromolecules, e.g. POSS-poly(amidoamine) (PAMAM) dendrimers of first and second generation terminated with imidazolium bromide residues [269], can be used as solid conductive materials. Formation of well-organized domains combined with segmental mobility of side chains facilitates charge transport in such hybrid polyelectrolytes. Existence of ionic domains for charge transport was confirmed with WAXS for thin films of PAMAM–POSS–PF_6 macromolecules of first and second generation [269].

Maximum ionic conductivity at 324 K was recorded for the POSS-core dendrimer of lower generation and smaller concentration of lithium ions. The observed VFT-

type behaviour indicated that segmental motions may contribute to long-range charge transport.

Hybrid amphiphilic POSS-IL of low T_g and good thermal stability were also prepared from $T_8(CH_2CH_2CH_2SH)_8$ and 1-allyl-3-methylimidazolium salts through the photochemical thiol–ene reaction. They self-assembled into perfect vesicles with "yolk–shell" structures, in which the anions formed the "shell" and POSS cages aggregated to form the "yolk" [270]. Water-soluble ionic dendrimers were prepared with $T_8(CH{=}CH_2)_8$ via subsequent thiol–ene addition and Menschutkin reaction [271]. The products can be modified via click chemistry and were also used for host–guest encapsulation of dyes, exhibiting an ultrahigh loading capability due to the regular structure and relatively big cavities.

4.6 Supramolecular Bioactive POSS Nanoassemblies

Molecular self-assembly plays an important role in biology and underlies the formation of a wide variety of natural biological structures with high level of precision and complexity. Nanotechnology aspires to create artificial materials, with hierarchical structures and tailored properties, exploiting principles that can be found in nature. Polyhedral silsesquioxanes have found application in biomedicine, drug delivery and diagnostics [272, 273]. Moreover, a broad range of bioinspired POSS-based hybrid systems was developed, including molecular recognition techniques based on peptides and DNA. POSS-based cargo peptide delivery system can be used for drug targeting and labelling in human cells [274]. Organic–inorganic hybrids, able to interact with poly(amino acids) via hydrogen bonds and exhibit smart pH-responsive and thermoresponsive properties, were made of water-soluble silsesquioxane nanoparticles with side tertiary amine moieties [275, 276]. It was also suggested that structures formed by POSS–polypeptide and POSS–DNA hybrids can be used in organic microelectronics (integrated circuit materials) [277, 278].

4.6.1 Polypeptides

Polypeptides are short chain macromolecules built of several amino acid monomers linked by amide bonds. They are closely related to proteins and can form hierarchically ordered structures (α-helices and β-sheets) stabilized by intra and intermolecular hydrogen bonds both in the solid state and in solutions [279]. The importance of peptides as self-assembling building blocks for the construction of nanobiomaterials is well known [280–282]. They offer a great diversity of biochemical properties (specificity, intrinsic bioactivity, biodegradability) and physical features (small size, conformation) and can be used as excellent structural units for the bottom-up fabrication of complex nanobiomaterials. Synthesis of poly(peptide-*b*-non-peptide) (rod/coil) block copolymers containing well-defined and rigid polypeptide segments has received a considerable attention due to their unique self-assembly behaviour and

well-designed 3D architectures that can mimic biological activity of more complex proteins.

POSS can be used for the preparation of block polypeptides of various molecular architectures (linear block, side grafted or of star shape). The hybrid silsesquioxane moieties attached to polypeptides can prevent uncontrolled aggregation of peptide nanoribbons and enhance α-helical conformation of the biomolecules in the solid state [273, 283, 284]. The hierarchical self-assembly via intramolecular hydrogen bonding between siloxane bonds and polypeptides or π–π interactions can play a significant role in the process. POSS–polypeptide copolymers exhibit a significant stability of α-helical conformation and superior thermal properties.

Various nanostructures featuring aggregated POSS and polypeptides in α-helical or β-sheet conformations can be obtained on adjusting the structure of macromolecules. Linear chains of poly(γ-propargyl-L-glutamate)-*g*-POSS copolymers (PPLG-*g*-POSS) were packed in the solid state as hexagonal cylinders featuring α-helical conformations and POSS aggregates [285]. Their block analogues with γ-benzyl-L-glutamate segments (PBLG-*b*-POSS) tend to form bilayer-like nanostructures (Fig. 16) [286, 287]. Incorporation of cube silsesquioxanes at the core of well-defined star PBLG-*b*-POSS copolymers also enhanced formation of α-helical structures [283]. The star-shaped macromolecules exhibited larger conformational stability than linear PBLG, which resulted in the change of liquid crystal ordering and alignment of PBLG chains in the solid state.

Hierarchical self-assembly of the organic–inorganic hybrid triblock copolymers polystyrene-*b*-poly(γ-propargyl-L-glutamate-*g*-POSS) [PS-*b*-(PPLG-g-POSS)] also resulted in the formation of cylindrical structures due to microphase separation in the diblock part of copolymers [277]. Grafting of POSS units onto side chains of PPLG enhanced the α-helical conformation in the solid state, induced hexagonal lattice packing and increased the thermal stability of α-helical secondary structures of polypeptide segments. Combination of PBLG segments with amyloidogenic short peptide (LVF) tethered to $T_8(i\text{-Bu})_7$ yielded a wide variety of hierarchical nanostructures [288]. Owing to π–π aromatic interactions between side chain phenyl groups in PBLG, the hybrid conjugate formed 2D hexagonal cylinders comprised of 18/5 α-helices. Removal of the side chain benzyl groups from the conjugate produced a pH-sensitive amphiphilic anionic homopolymers. The conjugate assembled into various spherical to square-shaped morphologies in aqueous media, depending on the ratio of hydrophobic/hydrophilic segments as well as the content of POSS.

4.6.2 DNA Complexes

Negatively charged double-stranded DNA is a unique biomacromolecule of helical conformation and long persistent length, capable of genetic information storage. It can be also used in catalysis, bioinformatics and for gene transfection. Efficient transfer to the cell and into the cell nuclei is the main challenge for transfection agents in gene therapy, in particular for plasmid DNA (pDNA) delivery. Understanding the structure–function relationship of cationic lipid-based gene transfection and mor-

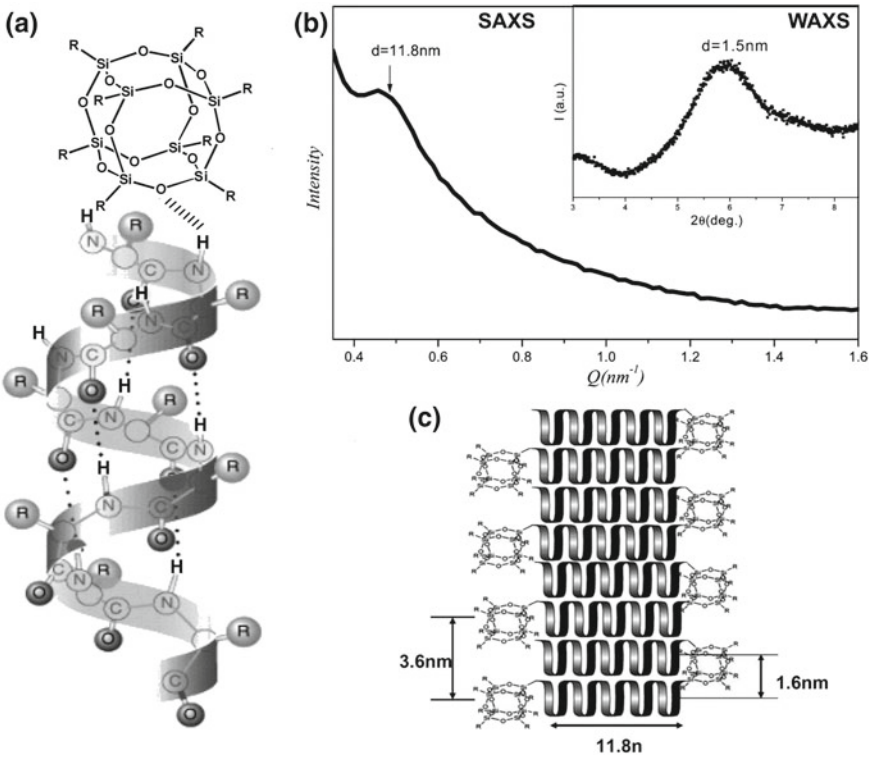

Fig. 16 **a** Intramolecular hydrogen-bonding interaction in POSS-b-PBLG copolymer, **b** schematic presentation of the nanoribbon formed in the network structure of the toluene gel of POSS-*b*-PBLG and its **c** SAXS and WAXS (inset) profiles. Adapted with permission from [287]. Copyright 2018 American Chemical Society

phology of the formed mesophase is crucial for the preparation of efficient carriers. The equilibrium morphology of lipoplexes is determined by the free energy balance among surface charge density, spontaneous curvature of the lipids and elastic properties of the lipid bilayers. Thermodynamically, the complexation is driven by the electrostatic interaction between negatively charged DNA and positively charged cationic lipids and the release of small-molecule counterions. Moreover, the transfection mechanism based on the polyplex interaction with the cellular membrane depends on the polymer architecture. Various cationic polymers show promising features as transfection vesicles that are able to enter cells by endocytosis and can be dissociated to release DNA for gene expression [289]. The polyplex dissociation is governed by the polymer chemistry and biodegradability. Several important reports have been published on superior gene transfection abilities of POSS–DNA polyplexes [290–292]. They can be also used as carriers of drugs into malfunctioning cells [293].

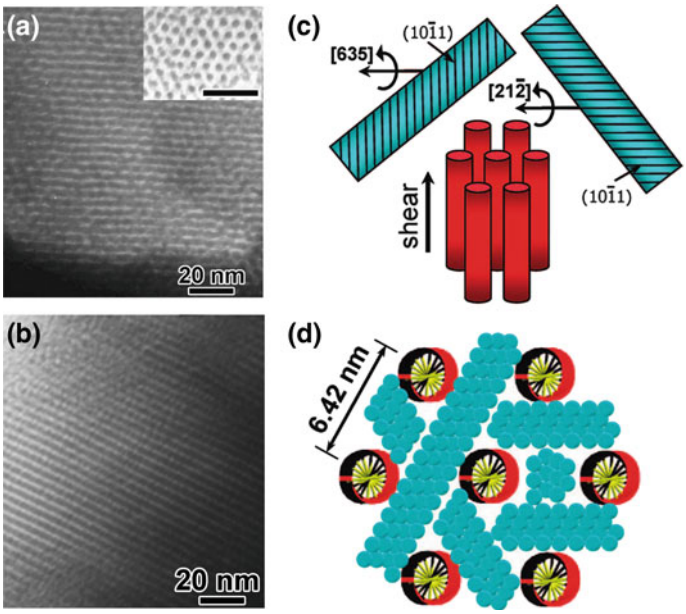

Fig. 17 Bright-field TEM micrographs of the DNA–imidazolium POSS complex having **a** the inverted hexagonal and **b** the lamellar phases; **c** representation of the DNA inverted hexagonal phase (red cylinders) and POSS crystal orientations (top bars) and **d** parallel and hexagonally aligned DNA cylinders and ABCA four-layer POSS lamellar crystals in the interstitials. Adopted with permission from [294]. Copyright 2018 American Chemical Society

POSS-based imidazolium salt was used as a cubic cationic lipid complexed with double-stranded DNA, and the mesophase self-assembly behaviour of the hybrid was studied [278]. Formation of an inverted hexagonal columnar (H_{II}^{C}) phase for the DNA–POSS-imidazolium salt complex above the melting point of POSS crystals was observed. The effect is a consequence of the induced negative spontaneous curvature of species made of bulky hydrophobic POSS tails and hydrophilic imidazolium head. Various self-assembled phase morphologies were obtained depending on the competition between the lamellar crystallization and the negative spontaneous curvature of cationic POSS-imidazolium lipids [294]. A lamellar phase was generated when the crystallization was relatively slow (e.g. isothermal crystallization at 403 K predominated by crystallization of POSS molecules), but if it was rapid (e.g. sample quenched to 273 K), then an inverted hexagonal phase was obtained with POSS lamellar crystals grown in the interstitials of DNA cylinders. In the latter case, the lipid negative curvature predominated the self-assembly process (Fig. 17). The double-stranded DNA retained the β-form helical conformation in the inverted hexagonal phase, whereas in the lamellar phase the helical conformation was largely destroyed, possibly due to the ionic complexation of POSS crystals at both sides of the DNA double strand.

POSS can be used for preparation of biosensors due to the formation of specific supramolecular assemblies. Cationic POSS were successfully applied as very sensitive probes for the detection of DNA by resonance light scattering [295]. It was shown that the electrostatic interactions of cationic POSS and DNA enhance the RLS signal.

Nucleoside triphosphates play crucial roles in a wide variety of biological events such as nucleic acid synthesis (building blocks for DNA and RNA), signal transduction, metabolism and enzymatic reactions. Precise POSS-based recognition system for triphosphates can be used for the construction of biosensors and biotechnological tools for monitoring biorelated reactions. Selective molecular recognition for nucleoside triphosphates, adenosine triphosphate (ATP), uridine triphosphate (UTP) and cytidine triphosphate (CTP), was observed inside the ligand-modified water-soluble hybrid gels composed of POSS [296]. It was found that the ligands inside the gels could form a stable complex only with the target nucleoside triphosphate that was able to participate in the complementary pattern of hydrogen bonds. A similar procedure with the affinity enhancement and the precise recognition of the hydrogen bond patterns was applied for the selective encapsulation of guanosine triphosphate (GTP) into POSS-based water-soluble polymers via the complex formation with the naphthyridine derivatives.

4.7 Self-assembly of POSS at the Interface

The investigation of silsesquioxane molecules contained at interfaces can be critical for the advancement in materials science and development of surface-based technologies. The results obtained in solution are not always useful for practical applications that often require immobilization of functional molecules at surfaces or interfaces (fabrication of sensors or functionalization of high-surface area materials). Solid and liquid surfaces are fundamentally different in many aspects including energy state, motional freedoms and adsorption of molecules. Consequently, they allow for the investigation of different properties of molecules. The lower dynamicity of the solid surface is advantageous for high-resolution observations. Motions of molecules on solid surfaces are often restricted. On the other hand, liquid surfaces (such as the air–water interface) are flexible and dynamic, with rapid diffusion of molecular components leading to mixing and rearrangements. The dynamic nature of liquid interfaces enables flexible control of nanostructures and molecular functions.

The surface behaviour of functionalized POSS is interesting from the point of view of the interfacial assembly process. It is also of importance regarding ultrathin film technologies and fast and sensitive signal transmission over short-time intervals. Very little is known about the morphologies that develop within 2D monolayers of POSS molecules. The comparative discussion of the properties of POSS positioned at solid or liquid surfaces included in the following sections.

4.7.1 Langmuir–Blodgett Films

General tendency of POSS for aggregation can be an obstacle for the preparation of well-organized thin films using typical methods such as spin coating. Deposition of POSS-based coatings as a result of specific interactions with the substrates [161, 170, 297] or by layer-by-layer deposition [298] is an exception. Langmuir–Blodgett (LB) technique can be at least a partial solution to the problem. The method exploits the phenomenon of particle self-assembly upon compression at the air–water interface and is a unique tool for inducing highly ordered layered structures with well-defined, molecular-level precision [299]. Molecules in such thin films are ordered in a quasi-smectic way. LB technique made a significant contribution to physical chemistry, nanotechnology and surface science. The general observations concerning Langmuir films can be applied to other coating technologies. Thin-film formation at the air–water interface by silicon containing polymeric materials is well known [300]. Polyhedral silsesquioxanes is another class of surface-active materials that can be used alone for the preparation of LB films or embedded as nanofillers in polysiloxane monolayers [300]. The rigid structure of POSS derivatives results in a more traditional Langmuir film behaviour.

Symmetrical T_8R_8 with short hydrophobic alkyl chains [e.g. $T_8(i\text{-Bu})_8$] do not form thin films at the air–water interface, despite their ability for crystallization due to interactions between side groups. Such POSS can be assembled into uniform Langmuir–Blodgett or Langmuir–Schaefer films only after cleaving one of siloxane bonds, which transform the molecules into amphiphilic species [301–304]. The open-cage $T_7(i\text{-Bu})_7OH_3$ is amphiphilic and formed Langmuir films, whereas its closed-cage analogue—$T_8(i\text{-Bu})_8$—formed only heterogeneous films at all surface concentrations. It was also shown that in contrast to trisilanolisobutyl-POSS, trisilanolcyclohexyl-POSS formed intricate structures in the collapse state, including rod-like domains at very high Π. These phenomena were attributed to dimerization of trisilanol POSS. It was also shown that molecules of amphiphilic open-cage $T_7(i\text{-Bu})_7OH_3$ form a 2D rugged monolayers on the surface of water, which undergo a counter-intuitive reversible crystallization [305]. The in-plane interparticle correlation peaks, characteristic of a 2D system, were replaced during the transition by intense localized spots. The finding was explained with a model that assumed crystalline periodic stacking of the $T_7(i\text{-Bu})_7OH_3$ dimers, relaxing upon decompression to retain the initial monolayer state.

Amphiphilic POSS can be also obtained by modification of the open-cage trisilanol POSS precursors. The effect of the kind of functional groups (polyether and fluoroalkyl) bound to two different open-cage POSS molecules not bearing silanol groups was studied regarding the formation of Langmuir monolayers [306]. Both derivatives were able to form insoluble Langmuir films at the air–water interface. They could be transferred onto quartz plates and changed wetting properties of the substrates. It was shown that structure and properties of the prepared monolayers (i.e. packing density, orientation of the molecules, stability, electric surface potential) depended on the chemical structure of the side groups grafted onto POSS core. The behaviour of T_8R_8 at the interface can change on increase in the length of side

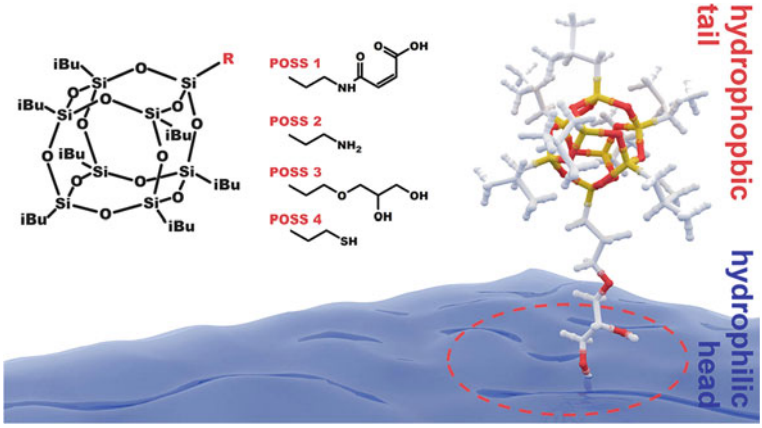

Scheme 18 Arrangement of $T_8(i\text{-Bu})_7R'$ at the air–water interface. Reprinted with permission from [308]. Copyright 2018 American Chemical Society

chains. All fluorocarbon POSS admixed with silica nanoparticles were able to form a hydrophobic LB film (condensed and rigid due to the incorporation of silica) [307]. It was observed that fluorinated POSS dispersed silica nanoparticles and prevented their aggregation. It was also found that the character of only one out of eight functional groups can have a great influence on the behaviour of POSS at the air–water interface. The Langmuir–Blodgett technique was applied for $T_8(i\text{-Bu})_7R'$ with hydrophilic heterorganic functional group R' (Scheme 18) [308]. Bifunctional amphiphilic POSS formed more easily well-organized films at the air–water interface.

However, it is not always the case and $T(i\text{-Bu})_7(CH_2CH_2CH_2SH)$ could form only 2D aggregates and multilayer films [308]. Analogously, amphiphilic POSS bearing two hetero-organic groups: $T(i\text{-Oct})_6(CH_2CH_2CH_2SH)_2$ and $T(i\text{-Oct})_4[CH_2CH_2(CF_2)_6CF_3]_2(CH_2CH_2CH_2SH)_2$ aggregated at the air–water interface [309]. Quite surprisingly, symmetric T_8R_8 with side groups containing heteroatoms easily formed Langmuir–Blodgett films. For example, a permeable but highly stable and reproducible Langmuir layer was obtained with $T_8(CH_2CH_2CH_2SH)_8$ [309]. The film could be transferred to a range of solid supports. Octakis[{2-(3,4-epoxycyclohexyl)ethyl}-dimethylsilyloxy]-octasilsesquioxanes of Q_8MR_8 type were assembled into a homogeneous monolayer that underwent a stepwise collapse with time [310]. It was found that the monolayer behaviour is totally different from that of typical amphiphiles. The $\Pi - A$ isotherm and equilibrium elasticity suggested formation of a liquid expanded monolayer. After the collapse, films of multilayer morphology were formed. Stepwise transitions from flake-like domains, then star-like structures, and finally aggregation into a ring network were observed. The formed unusual multilayer morphology is a consequence of side group reorganization, followed by a progressive decrease in the distance between the inorganic cores.

The importance of the balance between hydrophilic and hydrophobic parts for the stability of a Langmuir film was shown for two series of organic-functionalized

core–shell silsesquioxane derivatives (POSS-M)*p*-(*x*/*y*) with various compositions of hydrophobic and hydrophilic terminal groups. The studies were carried out in the bulk state and within mono- and multilayered Langmuir films at the air–water interface as well as on solid surfaces [311]. A mixture of silsesquioxanes (POSS-M) composed of polyhedra, incompletely condensed POSS species, ladder-type structures, linear structures, and all other possible combinations, was used. The two series of $(POSS\text{-}M)_{p\text{-}(x/y)}$ molecules were different in the hydrophobic–hydrophilic balance of their peripheral groups (*x* and *y* referring to the molar per cent of –OCONH–$C_{18}H_{37}$ tails and –OH for $(POSS\text{-}M)_{1-(x/y)}$ and the ratio of –OCONH–$C_{18}H_{37}$ tails and –OC-C_6H_4COOH terminal groups for $(POSS\text{-}M)_{2-(x/y)}$. The unit cell dimensions of the crystalline phase suggested the molecular packing with interdigitated peripheral tails of POSS cores. However, in the bulk state the presence of aromatic rings in $(POSS\text{-}M)_{2-(x/y)}$ series resulted in the crystal structure of lower symmetry than that of the $(POSS\text{-}M)_{1\text{-}(x/y)}$. The molecules that contained a sufficient amount of –OCONH-$C_{18}H_{37}$ tails exhibited double endothermic transition that was attributed to independent melting of alkyl chains, followed by the disassembly of the unit cells of (POSS-M) cores. The surface morphologies for the various hydrophobic–hydrophilic combinations at low surface pressure (0.5 mN/m) were found to be similar to those observed for the classical amphiphilic star polymers. However, at higher surface pressure (5 mN/m), a uniform monolayer was formed for POSS-M compounds with lower content of hydrophilic groups. The variation of terminal group composition led to diverse morphologies that ranged from one-dimensional and curved domains for low hydrophobic content to planar aggregates with increasing amount of hydrophobic alkyl chains. The surface morphologies resembled the two-phase solid–liquid state, typically observed for alkyl-containing hyperbranched systems. All hydrophilic–hydrophobic $(POSS\text{-}M)_{p-(x/y)}$ aggregated into uniform monolayer films at high surface pressure. The formation of multilayered structures was observed for $(POSS\text{-}M)_{p-(50/50)}$ with equal content of hydrophilic and hydrophobic groups (Fig. 18). The absence of hydrophobic segments in a fully hydroxylated $(POSS\text{-}M)_{1-(0/100)}$ compromised the ability to form a stable monolayer.

POSS have been also used as components of more elaborated systems aggregated at the air–water interface. Binary mixtures of cholesterol and octakis[{2-(3,4-epoxycyclohexyl) etyl}dimethylsilyloxy]octasilsesquioxane (OE-POSS) were compressed into Langmuir films [312]. The presence of two collapse points on the obtained isotherms was their most characteristic feature. The first point occured at similar surface pressures for all compositions, and it was attributed to the collapse of less-stable OE-POSS. The second one corresponded to the collapse of the cholesterol part. True mixed and homogenous films were not obtained, but phase separation and formation of microdomains of each component in the matrix of the other one was observed due to the differences in the molecular structure. Squeezing out less-stable OE-POSS molecules *co*-spread with cholesterol from the monolayer was noted after exceeding the collapse surface pressure of pure silsesquioxane. The system can be regarded as a simplified biomembrane model. The lack of the interactions between OE-POSS and biomembrane components represented by cholesterol suggests that

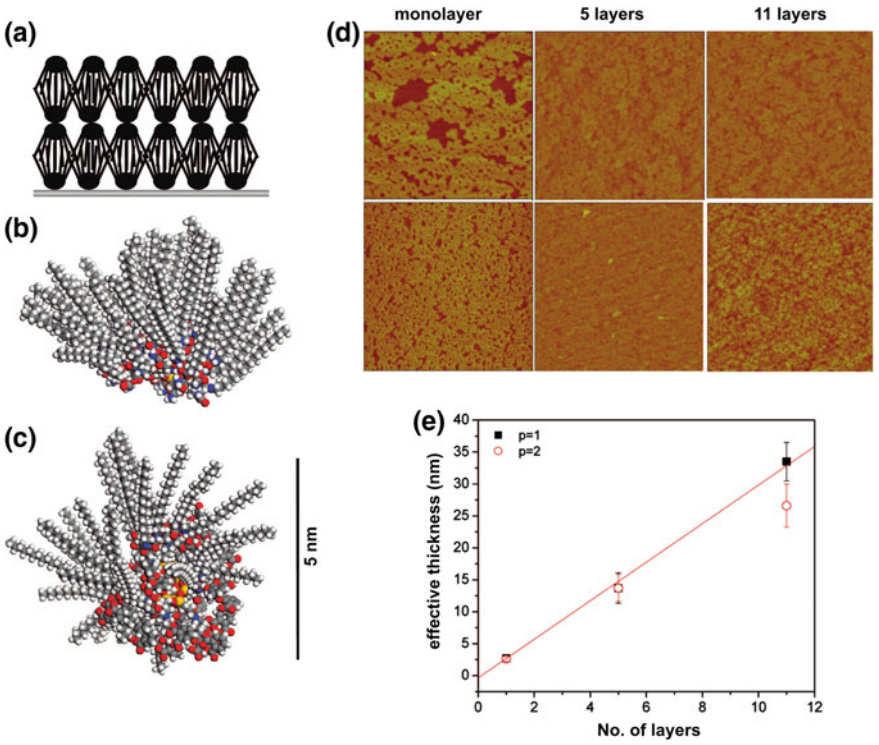

Fig. 18 **a** Multilayered LB film composed of amphiphilic silsesquioxane cores with alternating hydrophilic and hydrophobic peripheral groups; **b** $(POSS\text{-}M)_{1\text{-}(50/50)}$ and **c** $(POSS\text{-}M)_{2\text{-}(50/50)}$ with the alkyl chains stretched vertically, away from the hydrophilic surface; **d** AFM images of LB multilayers deposited at surface pressure of 10 mN/m; **e** plot of effective thickness *vs* number of layers for LB films of $(POSS\text{-}M)_{1\text{-}(50/50)}$ and $(POSS\text{-}M)_{2\text{-}(50/50)}$. Adapted with permission from [311]. Copyright 2018 American Chemical Society

such membranes would fluidize in the presence of functionalized POSS, which can be important for biomedical applications.

Aggregation behaviour of three star-shaped fluoropolymers containing POSS cores and grafted with side chains [POSS-(PMMA-*b*-PTFEMA)$_8$, POSS-(PTFEMA-*b*-PMMA)$_8$ and POSS-(PTFEMA-*b*-PMPEGMA)$_8$] was investigated at the air–water interface [313]. It was found that the surface pressure–mean molecular area isotherms exhibited four different regions. A pseudo-plateau corresponding to a "pancake-to-brush" transition was observed. The process of the relaxation of the monolayer was found to be related to the fast adsorption–desorption exchange of molecules and polymer segments on the surface and slow reconformation of the adsorbed macromolecules inside the adsorption layer. A variety of morphologies were observed for the LB films prepared at the air–water interface at different surface pressures, depending on the structure of the star-shaped copolymers.

4.7.2 Exfoliation of Silicate Clays

The well-defined structural features and tailor-made physicochemical properties, that can be tuned to enhance interfacial interactions, make POSS ideal nanofillers for polymer composites. Self-assembling phenomena strongly influence the behaviour of both small silsesquioxane molecules blended into polymers as well as tethered to polymer chains that can form crystalline domains in the organic matrix [5, 6, 314–316]. The aggregation or crystallization of POSS moieties used as nanofillers in polymeric systems as well as the interphase interactions can play a prominent role determining viscosity, melt elasticity and flammability of polymer nanocomposites.

However, POSS can be used not only as specialty nanofillers in polymer matrices, but they can also modify other materials used as additives in polymer composites. The self-assembling ability of POSS was used for intercalation of natural mineral clays, such as montmorillonite (MMT) [317]. Due to the special layered structure, adhesion, ion-exchange capacity and organic adsorption behaviour, MMT is frequently used in polymer composites to improve their chemical, physical, mechanical and thermal properties. Such polymer/clay nanocomposites have a wide range of applications as structural, coating and packaging materials. MMT is expandable and allows for intercalation the interlayer space with surfactant molecules up to the saturation limit. The surfactant concentration, dimensions as well as packing density determine the morphology of modified clays. POSS of T_8R_7R' type, because of their large molecular dimension, high thermal stability, biocompatibility, recyclability and poor flammability, were found to be good substitutes for alkyl ammonium tallow salts and 'onium ions in clay modification [318–321]. The rigid and cubic-shaped POSS can be absorbed into the clay galleries, but they cannot be arranged as flexibly as chain surfactants in the interlayer space. Once a double layer of POSS is assembled, then the *d*-spacing in expanded MMT is defined. The incorporation into the clay interlayer spacing results in the formation of "silicate clay" with a sandwich structure (Scheme 19). The interlayer spacing in composites with POSS intercalated into clay galleries is increased, and their thermo-oxidative stability is enhanced.

The chemistry and texture of POSS intercalated clays have been investigated for POSS bearing different functional groups that could interact with MMT. Amine-functionalized POSS can be intercalated into the layered clay via the onium exchange reaction. High concentration of POSS is not a prerequisite for the increase in the interlayer spacing. It was found that interlayer space of MMT modified with T_8(*i*-Oct)($CH_2CH_2CH_2NH_2$) was strongly dependent on the arrangement of POSS surfactant but less dependent on the POSS concentration [322, 323]. However, it is not always the case. Other reports on MMT-T_8(*i*-Oct)($CH_2CH_2CH_2NH_2$) complexes with a large interlayer distance and specific surface area were synthesized via ion-exchange reaction followed by freeze-drying treatment [324]. It was observed that the morphology of the POSS–MMT can depend on the POSS concentration, but also on pH of the suspension and the drying procedure. The tensile properties of the composites of POSS–MMT and poly(butylene terephthalate) were extensively improved as compared to the pristine PBT, due to the homogeneous dispersion of POSS–MMT in the polymer matrix (formation of a clay network).

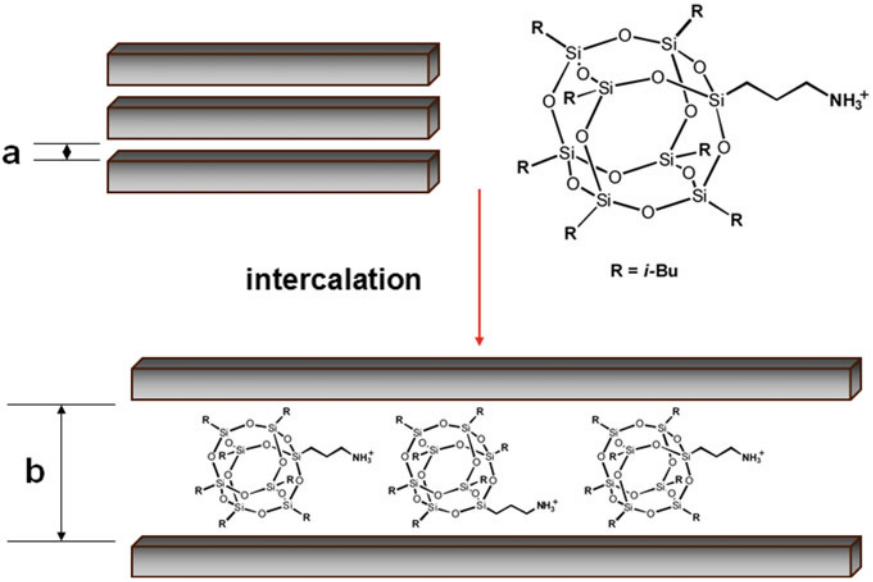

Scheme 19 Intercalation of mineral clays with POSS surfactants [5]

Clays modified with imidazolium-based surfactants are more thermally stable than those intercalated with their ammonium-based analogues. POSS-imidazolium derivatives were used as an organic modifier for MMT [325]. It was found that the self-assembled crystalline POSS domains are present in the clay interlayers but the solvent can change the efficiency of the ion-exchange reaction. The *d*-spacing of the exchanged clay is large (3.6 nm), accommodating a bilayer structure of the POSS-imidazolium molecules, even at low surfactant loading levels. It was observed that the structure and rigidity of the linker between the POSS and the cationic part interacting with MMT can be of significant importance. The packing structures of two types of POSS-imidazolium surfactants with different molecular rigidity intercalated in the intergalleries of MMT results in a bilayer packing structure with long axes of molecules largely tilted with respect to the basal plane [326]. The more flexible POSS-imidazolium cation formed a 2D ordered structure in the clay intergalleries, while the structure of layers formed by the rigid one were disordered (Scheme 20). Furthermore, the clay modified with the rigid surfactant exhibited increased interlayer *d*-spacings on reducing the surfactant loading. Formation of a more extended conformation of the POSS surfactant was postulated. The clay modified with the rigid POSS, despite the low organic content and disordered packing structure, has better thermal and thermo-oxidative stability than the more flexible one.

A range of interesting nanocomposites can be obtained using POSS–MMT hybrids. For example, nanocomposites of polylactide (PLA) reinforced with MMT modified with T_8(*i*-Bu)($CH_2CH_2CH_2NH_2$) were manufactured through melt-compounding [327]. It was found that the melt crystallization rates of the nanocom-

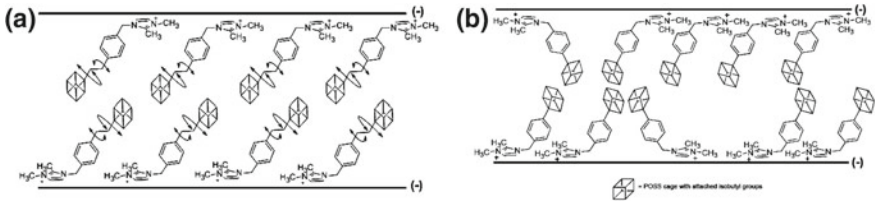

Scheme 20 Organization of rigid and flexible POSS in the interlayer galleries of MMT [326]

posite were enhanced remarkably in comparison with the neat PLA. The overall melt crystallization of PLA/POSS–MMT nanocomposites was found to be dominated by the heterogeneous nucleation and 3D spherulite growth. The isothermal crystallization analysis based on the Avrami model indicated higher spherulite nucleation density of PLA/POSS–MMT nanocomposites but identical spherulite growth rates (regardless of POSS–MMT content). It was also found that the crystalline morphological features of PLA were not influenced by the presence of POSS–MMT.

Poly(ethylene terephthalate) (PET)/montmorillonite nanocomposites were prepared on addition of a very small amount of $T_7Ph_7(OH)_3$ as a functional molecular spacer enhancing the degree of clay dispersion [328]. The trisilanol POSS was able to draw molecules of monomeric bis(2-hydroxyethyl) terephthalate into clay intergalleries, which allowed for their in situ polymerization between platelets of MMT. Moreover, $T_7Ph_7(OH)_3$ reacted with PET, further facilitating clay delamination and reinforcing the mechanical properties of the polymer due to the higher degree of flow-induced clay orientation.

MMT pretreated with a propargyl-containing primary intercalator was exfoliated into layers or sheets of nanoparticles through Huisgen [2 + 3] cycloaddition of singly or multiply azido-functionalized POSS to the propargyl derivative [329].

5 Conclusions and Perspectives

Polyhedral silsesquioxanes are nanoscale hybrid building blocks that can be used in template-free processes leading to the formation of nano- and micro-objects via "bottom-up" strategies. Formation of hierarchical superstructures by those unique self-assembling molecules plays an increasingly important role in materials science. Specific molecular packing and aggregation in the solid state are efficient tools enabling the control of morphology of POSS-derived hybrid materials, modulation of their physicochemical characteristics and performance.

Hierarchical structures formed by POSS can be used in applications related to energy, adsorption, separation and catalysis. Nanotechnologies exploiting self-organization of polyhedral silsesquioxanes and their crystallization patterns afford for the preparation of metal nanoparticles and quantum dots that can be used for high-resolution printing of defect-free microcircuits. Supramolecular materials based on

POSS can be also applied as surfactants, cargo vessels and templates. Understanding the cooperation and complementarity in POSS-based materials is essential for the design of such advanced systems. Precise control of the self-assembling process is the key factor for tailored organization of POSS.

References

1. Wang L, Du W, Wu Y, Xu R, Yu D (2012) Synthesis and characterizations of a latent polyhedral oligomeric silsesquioxane-containing catalyst and its application in polybenzoxazine resin. J Appl Polym Sci 126:150–155
2. Lee YJ, Huang JM, Kuo SW, Chang FC (2005) Low-dielectric, nanoporous polyimide films prepared from PEO–POSS nanoparticles. Polymer 46:10056–10065
3. Eon D, Raballand V, Cartry G, Cardinaud C, Vourdas N, Argitis P, Gogolides E (2006) Plasma oxidation of polyhedral oligomeric silsesquioxane polymers. J Vac Sci Technol B 24:2678–2688
4. Hirai T, Leolukman M, Liu CC, Han E, Kim YJ, Ishida Y, Hayakawa T, Kakimoto MA, Nealey PF, Gopalan P (2009) One-step direct-patterning template utilizing self-assembly of POSS-containing block copolymers. Adv Mater 21:4334–4338
5. Kuo S-W, Chang F-C (2011) POSS related polymer nanocomposites. Progr Polym Sci 36:1649–1696
6. Zhang W, Müller AHE (2013) Architecture, self-assembly and properties of well-defined hybrid polymers based on polyhedral oligomeric silsequioxane (POSS). Progr Polym Sci 38:1121–1162
7. Lim S-K, Lee JY, Choi HJ, Chin I-J (2015) On interaction characteristics of polyhedral oligomeric silsesquioxane containing polymer nanohybrids. Polym Bull 72:2331–2352
8. Mammeri F, Bonhomme C, Ribot F, Babonneau F, Dirè S (2009) New monofunctional POSS and its utilization as dewetting additive in methacrylate based free-standing films. Chem Mater 21:4163–4171
9. Żubrowska A, Piórkowska E, Kowalewska A, Cichorek M (2015) Novel blends of polylactide with ethylene glycol derivatives of POSS. Colloid Polym Sci 293:23–33
10. Kowalewska A, Fortuniak W, Chojnowski J, Pawlak A, Gadzinowska K, Zaród M (2012) Polymer nano-materials through self-assembly of polymeric POSS systems. Silicon 4:95–107
11. Grala M, Bartczak Z (2015) Morphology and mechanical properties of high density polyethylene-POSS hybrid nanocomposites obtained by reactive blending. Polym Eng Sci 55:2058–2072
12. Frone AN, Perrin FX, Radovici C, Panaitescu DM (2013) Influence of branched or unbranched alkyl substitutes of POSS on morphology, thermal and mechanical properties of polyethylene. Composites Part B 50:98–106
13. Sarkar B, Ayandele E, Venugopal V, Alexandridis P (2013) Polyhedral oligosilsesquioxane (POSS) nanoparticle localization in ordered structures formed by solvated block copolymers. Macromol Chem Phys 214:2716–2724
14. Martins JN, Bianchi O, Wanke CH, Dal Castel C, Oliveira RVB (2015) Effects of POSS addition on non-isothermal crystallization and morphology of PVDF. J Polym Res 22:224
15. Zhang D, Shi Y, Liu Y, Huang G (2014) Influences of polyhedral oligomeric silsesquioxanes (POSSs) containing different functional groups on crystallization and melting behaviors of POSS/polydimethylsiloxane rubber composites. RSC Adv 4:41364–41370
16. Jeon J-H, Tanaka K, Chujo Y (2014) Light-driven artificial enzymes for selective oxidation of guanosine triphosphate using water-soluble POSS network polymers. Org Biomol Chem 12:6500–6506

17. Teng CP, Mya KY, Win KY, Yeo CC, Low M, He C, Han M-Y (2014) Star-shaped polyhedral oligomeric silsesquioxane-polycaprolactone-polyurethane as biomaterials for tissue engineering application. NPG Asia Mater 6:e142
18. Wysokowski M, Materna K, Walter J, Petrenko I, Stelling AL, Bazhenov VV, Klapiszewski Ł, Szatkowski T, Lewandowska O, Stawski D, Molodtsov SL, Maciejewski H, Ehrlich H, Jesionowski T (2015) Solvothermal synthesis of hydrophobic chitin–polyhedral oligomeric silsesquioxane (POSS) nanocomposites. Int J Biol Macromol 78:224–229
19. Kakuta T, Tanaka K, Chujo Y (2015) Synthesis of emissive water-soluble network polymers based on polyhedral oligomeric silsesquioxane and their application as optical sensors for discriminating the particle size. J Mater Chem C 3:12539–12545
20. Gon M, Sato K, Tanaka K, Chujo Y (2016) Controllable intramolecular interaction of 3D arranged π-conjugated luminophores based on a POSS scaffold, leading to highly thermally-stable and emissive materials. RSC Adv 6:78652–78660
21. Asad U, Shakir U, Gul SK, Syed MS, Zakir H, Saz M, Muhammad S, Hazrat H (2016) Water soluble polyhedral oligomeric silsesquioxane based amphiphilic hybrid polymers: synthesis, self-assembly, and applications. Eur Polym J 75:67–92
22. Yu X, Li Y, Dong X-H, Yue K, Lin Z, Feng X, Huang M, Zhang W-B, Cheng SZD (2014) Giant surfactants based on molecular nanoparticles: precise synthesis and solution self-assembly. J Polym Sci Part B Polym Phys 52:1309–1325
23. Ullah A, Ullah S, Khan GS, Shah SM, Hussain Z, Muhammada S, Siddiq M, Hussain H (2016) Water soluble polyhedral oligomeric silsesquioxane based amphiphilic hybrid polymers: synthesis, self-assembly, and applications. Eur Polym J 75:67–92
24. Tanaka K, Chujo Y (2012) Advanced functional materials based on polyhedral oligomeric silsesquioxane (POSS). J Mater Chem 22:1733–1746
25. Lickiss PD, Rataboul F (2088) Fully condensed polyhedral oligosilsesquioxanes (POSS): from synthesis to application. In: West R (ed) Advances in organometallic chemistry, vol 57. Elsevier Inc., The Netherlands, pp 1–116
26. Cordes DB, Lickiss PD, Rataboul F (2010) Recent developments in the chemistry of cubic polyhedral oligosilsesquioxanes. Chem Rev 110:2081–2173
27. Cordes DB, Lickiss PD (2011) Preparation and characterization of polyhedral oligosilsesquioxanes. In: Hartmann-Thompson C (ed) Advances in silicon science, vol 3. Springer Science B. V., Berlin, pp 47–113
28. Laine RM (2005) Nanobuilding blocks based on the $[OSiO_{1.5}]_x$ ($x = 6, 8, 10$) octasilsesquioxanes. J Mater Chem 15:3725–3744
29. Marcolli C, Calzaferri G (1999) Monosubstituted octasilasesquioxanes. Appl Organomet Chem 13:213–226
30. Feher FJ, Wyndham KD, Baldwin RK, Soulivong D, Lichtenhan JD, Ziller JW (1999) Methods for effecting monofunctionalization of $(CH_2{=}CH)_8Si_8O_{12}$. Chem Commun 1289–1290
31. Li Y, Guo K, Su H, Li X, Feng X, Wang Z, Zhang W, Zhu S, Wesdemiotis C, Cheng SZD, Zhang W-B (2014) Tuning, "thiol-ene" reactions toward controlled symmetry breaking in polyhedral oligomeric silsesquioxanes. Chem Sci 5:1046–1053
32. Ye Q, Zhou H, Xu J (2016) Cubic polyhedral oligomeric silsesquioxane based functional materials: synthesis, assembly, and applications. Chem Asian J 11:1322–1337
33. Kowalewska A (2017) Self-assembling polyhedral silsesquioxanes—structure and properties. Curr Org Chem 21:1234–1264
34. Barry AJ, Daudt WH, Domicone JJ, Gilkey JW (1955) Crystalline organosilsesquioxanes. J Am Chem Soc 77:4248–4252
35. Auner N, Ziemer B, Herrschaft B, Ziche W, John P, Weis J (1999) Structural studies of novel siloxysilsesquioxanes. Eur J Inorg Chem 7:1087–1094
36. Bolln C, Tsuchida A, Frey H, Mülhaupt R (1997) Thermal properties of the homologous series of 8-fold alkyl-substituted octasilsesquioxanes. Chem Mater 9:1475–1479
37. Perrin FX, Nguyen TBV, Margaillan A (2011) Linear and branched alkyl substituted octakis(dimethylsiloxy)-octasilsesquioxanes: WAXS and thermal properties. Eur. Polym. J. 47:1370–1382

38. Waddon AJ, Coughlin EB (2003) Crystal structure of polyhedral oligomeric silsequioxane (POSS) nano-materials: a study by X-ray diffraction and electron microscopy. Chem Mater 15:4555–4561
39. Bassindale AR, Chen H, Liu Z, MacKinnon IA, Parker DJ, Taylor PG, Yang Y, Light ME, Horton PN, Hursthouse MB (2004) A higher yielding route to octasilsesquioxane cages using tetrabutylammonium fluoride, Part 2: further synthetic advances, mechanistic investigations and X-ray crystal structure studies into the factors that determine cage geometry in the solid state. J Organomet Chem 689:3287–3300
40. Larsson K (1960) Crystal structure of $(HSiO_{1.5})_8$. Arkiv foer Kemi 16:215–219
41. Larsson K (1960) Crystal structure of octa(methylsilsesquioxane), $(CH_3SiO_{1.5})_8$. Arkiv foer Kemi 16:203–208
42. Larsson, K (1960)Crystal structure of substituted octa(silsesquioxanes), $(RSiO_{1.5})_8$ and $(ArSiO_{1.5})_8$. Arkiv foer Kemi 16:209–214
43. Handke B, Jastrzębski W, Kwaśny M (2012) Klita, Structural studies of octahydridooctasilsesquioxane—$H_8Si_8O_{12}$. J Mol Struct 1028:68–72
44. Törnroos KW (1994) Octahydridosilasesquioxane determined by neutron diffraction. Acta Cryst C50:1646–1648
45. Cordes DB, Lickiss PD (2011) Preparation and characterization of polyhedral oligosilsesquioxanes. In: Hartmann-Thompson C (ed) Applications of polyhedral oligomeric silsesquioxanes, vol 3. Advances in silicon science. Springer Science B.V., The Netherlands, pp 47–113
46. Podberezskaya NV, Baidina IA, Alekseev VI, Borisov SV, Martynova TN (1982) X-ray structural study of silasesquioxanes. The crystal structure of octa(allylsilasesquioxane). J Struct Chem 22:737–740
47. El Aziz Y, Bassindale AR, Taylor PG, Stephenson RA, Hursthouse MB, Harrington RW, Clegg W (2013) X-ray crystal structures, packing behavior, and thermal stability studies of a homologous series of *n*-alkyl-substituted polyhedral oligomeric silsesquioxanes. Macromolecules 46:988–1001
48. Chinnam PR, Gau MR, Schwab J, Zdilla MJ, Wunder SL (2014) The polyoctahedral silsesquioxane (POSS) 1,3,5,7,9,11,13,15-octaphenylpentacyclo[9,5,1,13,9,15,15,17,13]-octasiloxane (octaphenyl-POSS). Acta Cryst C70:971–974
49. Morimoto S, Imoto H, Naka K (2017) POSS solid solutions exhibiting orientationally disordered phase transitions. Chem Commun 53:9273–9276
50. Zakharov AV, Masters SL, Wann DA, Shlykov SA, Girichev GV, Arrowsmith S, Cordes DB, Lickiss PD, White AJP (2010) The gas-phase structure of octaphenyloctasilsesquioxane $Si_8O_{12}Ph_8$ and the crystal structures of Si_8O_{12}(p-tolyl)$_8$ and Si_8O_{12}(p-$ClCH_2C_6H_4$)$_8$. Dalton Trans 39:6960–6966
51. Heeley EL, Hughes DJ, El Aziz Y, Williamson I, Taylor PG, Bassindale AR (2013) Properties and self-assembled packing morphology of long alkyl-chained substituted polyhedral oligomeric silsesquioxanes (POSS) cages. Phys Chem Chem Phys 15:5518–5529
52. Bassindale AR, Gentle TE (1993) Siloxane and hydrocarbon octopus molecules with silsesquioxane cores. J Mater Chem 12:1319–1325
53. Heeley EL, Hughes DJ, El Aziz Y, Taylor PG, Bassindale AR (2013) Linear long alkyl chain substituted POSS cages: the effect of alkyl chain length on the self-assembled packing morphology. Macromolecules 46:4944–4954
54. Boese R, Weiss H-C, Bläser D (1999) The melting point alternation in the short-chain n-alkanes: single-crystal X-ray analyses of propane at 30 K and of *n*-butane to *n*-nonane at 90 K. Angew Chem Int Ed 38:988–992
55. Dumitriu AMC, Cazacu M, Bargan A, Balan M, Vornicu N, Varganici C-D, Shova S (2015) Full functionalized silica nanostructure with well-defined size and functionality: Octakis(3-mercaptopropyl)octasilsesquioxane. J Organomet Chem 799–800:195–200
56. Kowalewska A, Nowacka M, Maniukiewicz W (2016) Octa(3-mercaptopropyl)octasilsesquioxane—a reactive nanocube of unique self-assembled packing morphology. J Organomet Chem 810:15–24

57. Marciniec B, Dutkiewicz M, Maciejewski H, Kubicki M (2008) New, effective method of synthesis and structural characterization of octakis(3-chloropropyl)octasilsesquioxane. Organometallics 27:793–794
58. Dumitriu A-M-C, Balan M, Bargan A, Shova S, Varganici C-D, Cazacu M (2016) Synthesis of functionalized silica nanostructure: unexpected conversion of cyanopropyl group in chloropropyl one during HCl-catalysed hydrolysis of the corresponding triethoxysilane. J Molec Struct 1110:150–155
59. Handke B, Jastrzębski W, Mozgawa W, Kowalewska A (2008) Structural studies of crystalline octamethylsilsesquioxane $(CH_3)_8Si_8O_{12}$. J Molec Str 887:159–164
60. Day VW, Klemperer WG, Mainz VV, Millari DM (1985) Molecular building blocks for the synthesis of ceramic materials: $[Si_8O_{12}](OCH_3)_8$. J Am Chem Soc 107:8262–8264
61. Provatas A, Luft M, Mu JC, White AH, Matisons JG, Skelton BW (1998) Silsesquioxanes: part I: a key intermediate in the building of molecular composite materials. J Organomet Chem 565:159–164
62. Xu J, Li X, Cho CM, Toh CL, Shen L, Mya KY, Lu X, He C (2009) Polyhedral oligomeric silsesquioxanes tethered with perfluoroalkylthioether corner groups: facile synthesis and enhancement of hydrophobicity of their polymer blends. J Mater Chem 19:4740–4745
63. Janeta M, John Ł, Ejfler J, Szafert S (2015) Novel organic-inorganic hybrids based on T_8 and T_{10} silsesquioxanes: synthesis, cage-rearrangement and properties. RSC Adv 5:72340–72351
64. Li G, Wang L, Ni H, Pittman CU (2001) Polyhedral oligomeric silsesquioxane (POSS) polymers and copolymers: a review. J Inorg Organomet Polym 11:123–154
65. Liu H, Puchberger M, Schubert U (2011) A facile route to difunctionalized monosubstituted octasilsesquioxanes. Chem Eur J 17:5019–5023
66. Li Y, Dong X-H, Zou Y, Wang Z, Yue K, Huang M, Liu H, Feng X, Lin Z, Zhang W, Zhang W-B, Cheng SZD (2017) Polyhedral oligomeric silsesquioxane meets "click" chemistry: rational design and facile preparation of functional hybrid materials. Polymer 125:303–329
67. Yue K, Liu C, Guo K, Yu X, Huang M, Li H, Wesdemiotis C, Chang SZD, Zhang W-B (2012) Sequential, "click" approach to polyhedral oligomeric silsesquioxane-based shape amphiphiles. Macromolecules 45:8126–8134
68. Li Y, Dong X-H, Guo K, Wang Z, Chen Z, Wesdemiotis C, Quirk RP, Zhang W-B, Chang SZD (2012) Synthesis of shape amphiphiles based on POSS tethered with two symmetric/asymmetric polymer tails via sequential "grafting-from" and thiol–ene "click" chemistry. ACS Macro Lett 1:834–839
69. Li Y, Wang Z, Zheng J, Su H, Lin F, Guo K, Feng X, Wesdemiotis C, Becker ML, Cheng SZD, Zhang W-B (2013) Cascading one-pot synthesis of single-tailed and asymmetric multitailed giant surfactants. ACS Macro Lett 2:1026–1032
70. Wang Z, Li Y, Dong X-H, Yu X, Guo K, Su H, Wesdemiotis C, Cheng SZD, Zhang W-B (2013) Giant gemini surfactants based on polystyrene–hydrophilic polyhedral oligomeric silsesquioxane shape amphiphiles: sequential "click" chemistry and solution self-assembly. Chem Sci 4:1345–1352
71. Su H, Li Y, Yue K, Wang Z, Lu P, Feng X, Dong X-H, Zhang S, Cheng SZD, Zhang W-B (2014) Macromolecular structure evolution toward giant molecules of complex structure: tandem synthesis of asymmetric giant gemini surfactants. Polym Chem 5:3697–3706
72. Li Y, Su H, Feng X, Yue K, Wang Z, Lin Z, Zhu X, Fu Q, Zhang Z, Cheng SZD, Zhang W-B (2015) Precision synthesis of macrocyclic giant surfactants tethered with two different polyhedral oligomeric silsesquioxanes at distinct ring locations via four consecutive "click" reactions. Polym Chem 6:827–837
73. Li Y, Su H, Feng X, Wang Z, Guo K, Wesdemiotis C, Fu Q, Cheng SZD, Zhang W-B (2014) Thiol-Michael "click" chemistry: another efficient tool for head functionalization of giant surfactants. Polym Chem 5:6151–6162
74. Guo S, Sasaki J, Tsujiuchi S, Hara S, Wada H, Kuroda K, Shimojima A (2017) Role of cubic siloxane cages in mesostructure formation and photoisomerization of azobenzene siloxane hybrid. Chem Lett 46:1237–1239

75. Shao Y, Yin H, Wang X-M, Han S-Y, Yan X, Xu J, He J, Ni P, Zhang W-B (2016) Mixed [2:6] hetero-arm star polymers based on Janus POSS with precisely defined arm distribution. Polym Chem 7:2381–2388
76. Han S-Y, Wang X-M, Shao Y, Guo Q-Y, Li Y, Zhang W-B (2016) Janus POSS Based on Mixed [2:6] Octakis-Adduct Regioisomers. Chem Eur J 22:6397–6403
77. Wang X-M, Shao Y, Xu J, Jin X, Shen R-H, Shen D-W, Wang J, Li W, Ni P, Zhang W-B (2017) Precision synthesis and distinct assembly of double-chain giant surfactant regioisomers. Macromolecules 50:3943–3953
78. De Gennes PG (1992) Soft matter (Nobel lecture). Angew Chem 104:856–859
79. Walther A, Müller AHE (2013) Janus particles: synthesis, self-assembly, physical properties, and applications. Chem Rev 113:5194–5261
80. Andrianov KA, Tikhonov VS, Makhneva GP, Chernov GS (1973) Synthesis of polycyclic tetramethyl-tetraphenylcyclooctasilsesquioxane. Bull Acad Sci USSR Div Chem Sci 22:928–928
81. Asuncion MZ, Ronchi M, Abu-Seir H, Laine RM (2010) Synthesis, functionalization and properties of incompletely condensed "half cube" silsesquioxanes as a potential route to nanoscale Janus particles. C R Chim 13:270–281
82. Tateyama S, Kakihana Y, Kawakami Y (2010) Cage octaphenylsilsesquioxane from cyclic tetrasiloxanetetraol and its sodium salt. J Organomet Chem 695:898–902
83. Blázquez-Moraleja A, Pérez-Ojeda ME, Suárez JR, Jimeno ML, Chiara JL (2016) Efficient multi-click approach to well-defined two-faced octasilsesquioxanes: the first perfect Janus nanocube. Chem Commun 52:5792–5795
84. Oguri N, Egawa Y, Takeda N, Unno M (2016) Janus-cube octasilsesquioxane: facile synthesis and structure elucidation. Angew Chem Int Ed 55:9336–9339
85. Yandek GR, Moore BM, Ramirez SM, Mabry JM (2012) Effects of peripheral architecture on the properties of aryl polyhedral oligomeric silsesquioxanes. J Phys Chem C 116:16755–16765
86. Brand R, Lunkenheimer P, Loidl A (2002) Relaxation dynamics in plastic crystals. J Chem Phys 116:10386–10401
87. Folmer JCW, Withers RL, Welberry TR, Martin JD (2008) Coupled orientational and displacive degrees of freedom in the high-temperature plastic phase of the carbon tetrabromide α–CBr 4. Phys. Rev. B 77:144205–144214
88. Kopesky ET, McKinely GH, Cohen RE (2004) Thermomechanical properties of poly(methyl methacrylate)s containing tethered and untethered polyhedral oligomeric silsesquioxanes. Macromolecules 37:8992–9004
89. Croce G, Carniato F, Milanesio M, Boccaleri E, Paul G, van Beek W, Marchese L (2009) Understanding the physico-chemical properties of polyhedral oligomeric silsesquioxanes: a variable temperature multidisciplinary study. Phys Chem Chem Phys 11:10087–10094
90. Bonhomme C, Tolédano P, Maquet J, Livage J, Bonhomme-Coury L (1997) Studies of octameric vinylsilasesquioxane by carbon-13 and silicon-29 cross polarization magic angle spinning and inversion recovery cross polarization nuclear magnetic resonance spectroscopy. J Chem Soc Dalton Trans 1617–1626
91. Taylor PG, Gelbrich T, Hursthouse MB University of Southampton, Crystal structure report archive 2000. http://ecrystals.chem.soton.ac.uk/838/
92. Baidina IA, Podberezskaya NV, Alekseev VI, Martynova TN, Borisov SV, Kanev AN (1980) The crystal structure of vinylsilasesquioxane $[C_2H_3SiO_{3/2}]_8$. J Struct Chem 20:550–554
93. Wu J, Wu ZL, Yang H, Zheng Q (2014) Crosslinking of low density polyethylene with octavinyl polyhedral oligomeric silsesquioxane as the crosslinker. RSC Adv 4:44030–44038
94. Kowalewska A, Nowacka M, Włodarska M, Zgardzińska B, Zaleski R, Oszajca M, Krajenta J, Kaźmierski S (2017) Solid-state dynamics and single-crystal to single-crystal structural transformations in octakis(3-chloropropyl)octasilsesquioxane and octavinyloctasilsesquioxane. Phys Chem Chem Phys 19:27516–27529
95. Poliskie GM, Haddad TS, Blanski RL, Gleason KK (2005) Characterization of the phase transitions of ethyl substituted polyhedral oligomeric silsesquioxane. Thermochim Acta 438:116–125

96. Jalarvo N, Gourdon O, Ehlers G, Tyagi M, Kumar SK, Dobbs KD, Smalley RJ, Guise WE, Ramirez-Cuesta A, Wildgruber C, Crawford MK (2014) Structure and dynamics of octamethyl-POSS nanoparticles. J Phys Chem C 118:5579–5592
97. Tanaka K, Chujo Y (2013) Unique properties of amphiphilic POSS and their applications. Polymer J 45:247–254
98. Wang L, Ishida Y, Maeda R, Tokita M, Hayakawa T (2014) Alkylated cage silsesquioxanes: a comprehensive study of thermal properties and self-assembled structure. RSC Adv 4:34981–34986
99. Wang L, Ishida Y, Maeda R, Tokita M, Horiuchi S, Hayakawa T (2014) Alkylated cage silsesquioxane forming a long-range straight ordered hierarchical lamellar nanostructure. Langmuir 30:9797–9803
100. Yu X, Zhong S, Li X, Tu Y, Yang S, Van Horn R, Ni CY, Pochan DJ, Quirk RP, Wesdemiotis C, Zhang W-B, Cheng SZD (2010) A giant surfactant of polystyrene-(carboxylic acid-functionalized polyhedral oligomeric silsesquioxane) amphiphile with highly stretched polystyrene tails in micellar assemblies. J Am Chem Soc 132:16741–16744
101. Zhou J, Kieffer J (2008) Molecular dynamics simulations of monofunctionalized polyhedral oligomeric silsesquioxane $C_6H_{13}(H_7Si_8O_{12})$. J Phys Chem C 112:3473–3481
102. Takeda M, Kuroiwa K, Mitsuishi M, Matsui J (2015) Self-assembly of amphiphilic POSS anchoring a short organic tail with uniform structure. Chem Lett 44:1560–1562
103. Zhang W, Chu Y, Mu G, Eghtesadi SA, Liu Y, Zhou Z, Lu X, Kashfipour MA, Lillard RS, Yue K, Liu T, Cheng SZD (2017) Rationally controlling the self-assembly behavior of triarmed POSS–organic hybrid macromolecules: from giant surfactants to macroions. Macromolecules 50:5042–5050
104. Yue K, Liu C, Huang M, Huang J, Zhou Z, Wu K, Liu H, Lin Z, Shi A-C, Zhang W-B, Cheng SZD (2017) Self-assembled structures of giant surfactants exhibit a remarkable sensitivity on chemical compositions and topologies for tailoring sub-10 nm nanostructures. Macromolecules 50:303–314
105. Wu K, Huang M, Yue K, Liu C, Lin Z, Liu H, Zhang W, Hsu C-H, Shi A-C, Zhang W-B, Stephen ZD, Cheng SZD (2014) Asymmetric giant "bolaform-like" surfactants: precise synthesis, phase diagram, and crystallization-induced phase separation. Macromolecules 47:4622–4633
106. Yue K, Huang M, Marson RL, He J, Huang J, Zhou Z, Wang J, Liu C, Yan X, Wu K, Guo Z, Liu H, Zhang W, Ni P, Wesdemiotis C, Zhang W-B, Glotzer SC, Cheng SZD (2016) Geometry induced sequence of nanoscale Frank-Kasper and quasicrystal mesophases in giant surfactants. PNAS 113:14195–14200
107. Hsu C-H, Dong X-H, Lin Z, Ni B, Lu P, Jiang Z, Tian D, Shi A-C, Thomas EL, Cheng SZD (2016) Tunable affinity and molecular architecture lead to diverse self-assembled supramolecular structures in thin films. ACS Nano 10:919–929
108. Yu C-B, Ren L-J, Wang W (2017) Synthesis and self-assembly of a series of nPOSS-b-PEO block copolymers with varying shape anisotropy. Macromolecules 50:3273–3284
109. Dong X-H, Ni B, Huang M, Hsu C-H, Chen Z, Lin Z, Zhang W-B, Shi A-C, Cheng SZD (2015) Chain overcrowding induced phase separation and hierarchical structure formation in fluorinated polyhedral oligomeric silsesquioxane (FPOSS)-based giant surfactants. Macromolecules 48:7172–7179
110. Kettwich SC, Pierson SN, Peloquin AJ, Mabry JM, Iacono ST (2012) Anomalous macromolecular assembly of partially fluorinated polyhedral oligomeric silsesquioxanes. New J Chem 36:941–946
111. Dong X-H, Ni B, Huang M, Hsu C-H, Bai R, Zhang W-B, Shi A-C, Cheng SZD (2016) Molecular-curvature-induced spontaneous formation of curved and concentric lamellae through nucleation. Angew Chem Int Ed 55:2459–2463
112. Zhang Z, Xue Y, Zhang P, Müller AHE, Zhang W (2016) Hollow polymeric capsules from POSS-based block copolymer for photodynamic therapy. Macromolecules 49:8440–8448
113. Shimojima A, Goto R, Atsumi N, Kuroda K (2008) Self-assembly of alkyl-substituted cubic siloxane cages into ordered hybrid materials. Chem Eur J 14:8500–8506

114. Liu H, Hsu C-H, Lin Z, Shan W, Wang J, Jiang J, Huang M, Lotz B, Yu X, Zhang W-B, Yue K, Cheng SZD (2014) Two-dimensional nanocrystals of molecular Janus particles. J Am Chem Soc 136:10691–10699
115. Zhang W, Yuan J, Weiss S, Ye X, Li C, Müller AHE (2011) Telechelic hybrid poly(acrylic acid)s containing polyhedral oligomeric silsesquioxane (POSS) and their self-assembly in water. Macromolecules 44:6891–6898
116. Li Y, Zhang W-B, Hsieh I-F, Zhang G, Cao Y, Li X, Wesdemiotis C, Lotz B, Xiong H, Cheng SZD (2011) Breaking symmetry toward nonspherical Janus particles based on polyhedral oligomeric silsesquioxanes: molecular design, "click" synthesis, and hierarchical structure. J Am Chem Soc 133:10712–10715
117. Huang M, Hsu C-H, Wang J, Mei S, Dong X, Li Y, Li M, Liu H, Zhang W, Aida T, Zhang W-B, Yue K, Cheng SZD (2015) Selective assemblies of giant tetrahedra via precisely controlled positional interactions. Science 348:424–428
118. Hu M-B, Hou Z-Y, Hao W-Q, Xiao Y, Yu W, Ma C, Ren L-J, Zheng P, Wang W (2013) POM–organic–POSS cocluster: creating a dumbbell-shaped hybrid molecule for programming hierarchical supramolecular nanostructures. Langmuir 29:5714–5722
119. Ma C, Wu H, Huang Z-H, Guo R-H, Hu M-B, Kĩbel C, Yan L-T, Wang W (2015) A filled-honeycomb-structured crystal formed by self-assembly of a Janus polyoxometalate–silsesquioxane (POM–POSS) co-cluster. Angew Chem Int Ed 54:15699–15704
120. Wu H, Zhang Y-Q, Hu M-B, Ren L-J, Lin Y, Wang W (2017) Creating quasi two-dimensional cluster-assembled materials through self-assembly of a Janus polyoxometalate-silsesquioxane co-cluster. Langmuir 33:5283–5290
121. Liu H, Luo J, Shan W, Guo D, Wang J, Hsu C-H, Huang M, Zhang W, Lotz B, Zhang W-B, Liu T, Yue K, Cheng SZD (2016) Manipulation of self-assembled nanostructure dimensions in molecular janus particles. ACS Nano 10:6585–6596
122. Lin M-C, Hsu C-H, Sun H-J, Wang C-L, Zhang W-B, Li Y, Chen H-L, Cheng SZD (2014) Crystal structure and molecular packing of an asymmetric giant amphiphile constructed by one C60 and two POSSs. Polymer 55:4514–4520
123. Zhang C, Leng Y, Jiang P, Lu D (2016) POSS-based meso-/macroporous covalent networks: supporting and stabilizing Pd for Suzuki-Miyaura reaction at room temperature. RSC Adv 6:57183–57189
124. Liu J, Yu H, Liang Q, Liu Y, Shen J, Bai Q (2017) Preparation of polyhedral oligomeric silsesquioxane based cross-linked inorganic-organic nanohybrid as adsorbent for selective removal of acidic dyes from aqueous solution. J Colloid Interface Sci 497:402–412
125. Peng Y, Ben T, Xu J, Xue M, Jing X, Deng F, Qiu S, Zhu G (2011) A covalently-linked microporous organic-inorganic hybrid framework containing polyhedral oligomeric silsesquioxane moieties. Dalton Trans 40:2720–2724
126. Wang J, Sun J, Zhou J, Jin K, Fang Q (2017) Fluorinated and thermo-cross-linked polyhedral oligomeric silsesquioxanes: new organic–inorganic hybrid materials for high-performance dielectric application. ACS Appl Mater Interfaces 9:12782–12790
127. Chen G, Zhou Y, Wang X, Li J, Xue S, Liu Y, Wang Q, Wang J (2015) Construction of porous cationic frameworks by crosslinking polyhedral oligomeric silsesquioxane units with N-heterocyclic linkers. Scientific Reports 5:11236
128. Li D, Niu Y, Yang Y, Wang X, Yang F, Shen H, Wu D (2015) Synthesis and self-assembly behavior of POSS-embedded hyperbranched polymers. Chem Commun 51:8296–8299
129. Alvarado-Tenorio B, Romo-Uribe A, Mather PT (2011) Microstructure and phase behavior of POSS/PCL shape memory nanocomposites. Macromolecules 44:5682–5692
130. Wang Z, Wang Z, Yu H, Zhao L, Qu J (2012) Controlled network structure and its correlations with physical properties of polycarboxyl octaphenylsilsesquioxanes-based inorganic–organic polymer nanocomposites. RSC Adv 2:2759–2767
131. Cheng C-C, Yen Y-C, Chang F-C (2011) Self-supporting polymer from a POSS derivative. Macromol Rapid Commun 32:927–932
132. Cheng C-C, Yen Y-C, Ko F-H, Chu C-W, Fan S-K, Chang F-C (2012) A new supramolecular film formed from a silsesquioxane derivative for application in proton exchange membranes. J Mater Chem 22:731–734

133. Voisin D, Flot D, Van der Lee A, Dautel OJ, Moreau JJE (2017) Hydrogen bond-directed assembly of silsesquioxanes cubes: synthesis of carboxylic acid POSS derivatives and the solid state structure of octa[2-(p-carboxyphenyl)ethyl] silsesquioxane. CrystEngComm 19:492–502
134. Lu Y-S, Yu C-Y, Lin Y-C, Kuo S-W (2016) Hydrogen bonding strength of diblock copolymers affects the self-assembled structures with octa-functionalized phenol POSS nanoparticles. Soft Matter 12:2288–2300
135. Wu Y-C, Shiao-Wei Kuo S-W (2012) Self-assembly supramolecular structure through complementary multiple hydrogen bonding of heteronucleobase-multifunctionalized polyhedral oligomeric silsesquioxane (POSS) complexes. J Mater Chem 22:2982–2991
136. Shih R-S, Lu C-H, Kuo S-W, Chang F-C (2010) Hydrogen bond-mediated self-assembly of polyhedral oligomeric silsesquioxane-based supramolecules. J Phys Chem C 114:12855–12862
137. Wang J-H, Altukhov O, Cheng C-C, Chang F-C, Kuo S-W (2013) Supramolecular structures of uracil-functionalized PEG with multi-diamidopyridine POSS through complementary hydrogen bonding interactions. Soft Matter 9:5196–5206
138. Lu L, Zhang C, Li L, Zhou C (2013) Reversible pH-responsive aggregates based on the self-assembly of functionalized POSS and hyaluronic acid. Carbohydrate Polym 94:444–448
139. Yang L, Lu L, Zhang C-W, Zhou C-R (2016) Highly stretchable and self-healing hydrogels based on poly(acrylic acid) and functional POSS. Chin J Polym Sci 34:185–194
140. Sato N, Kuroda Y, Abe T, Wada H, Shimojima A, Kuroda K (2015) Regular assembly of cage siloxanes by hydrogen bonding of dimethylsilanol groups. Chem Commun 51:11034–11037
141. Kawahara K, Tachibana H, Hagiwara Y, Kuroda K (2012) A spherosilicate oligomer with eight stable silanol groups as a building block of hybrid materials. New J Chem 36:1210–1217
142. Kawakami Y, Sakuma Y, Wakuda T, Nakai T, Shirasaka M, Kabe Y (2010) Hydrogen-bonding 3D networks by polyhedral organosilanols: selective inclusion of hydrocarbons in open frameworks. Organometallics 29:3281–3288
143. Farha OK, Hupp JT (2010) Rational design, synthesis, purification, and activation of metal–organic framework materials. Acc Chem Res 43:1166–1175
144. Stock N, Biswas S (2012) Synthesis of metal-organic frameworks (MOFs): routes to various MOF topologies, morphologies, and composites. Chem Rev 112:933–969
145. Meek ST, Greathouse JA, Allendorf MD (2011) Metal-organic frameworks: a rapidly growing class of versatile nanoporous materials. Adv Mater 23:249–267
146. Liu J, Chen L, Cui H, Zhang J, Zhang L, Su C-Y (2014) Applications of metal-organic frameworks in heterogeneous supramolecular catalysis. Chem Soc Rev 43:6011–6061
147. Cui YJ, Li B, He HJ, Zhou W, Chen BL, Qian GD (2016) Metal-organic frameworks as platforms for functional materials. Acc Chem Res 49:483–493
148. Banerjee S, Kataoka S, Takahashi T, Kamimura Y, Suzuki K, Sato K, Endo A (2016) Controlled formation of ordered coordination polymeric networks using silsesquioxane building blocks. Dalton Trans 45:17082–17086
149. Köytepe S, Demirel MH, Gültek A, Seçkin T (2014) Metallo-supramolecular materials based on terpyridine-functionalized polyhedral silsesquioxane. Polym Int 63:778–787
150. Carbonell E, Bivona LA, Fusaro L, Aprile C (2017) Silsesquioxane–terpyridine nano building blocks for the design of three-dimensional polymeric networks. Inorg Chem 56:6393–6403
151. Dang S, Zhu QL, Xu Q (2017) Nanomaterials derived from metal–organic frameworks. Nat Rev Mater 3, Article no. 17075
152. Sanil ES, Cho K-H, Hong D-Y, Lee JS, Lee S-K, Ryu SG, Lee HW, Chang J-S, Hwang YK (2015) A polyhedral oligomeric silsesquioxane functionalized copper trimesate. Chem Commun 51:8418–8420
153. Chan MHY, Ng M, Leung SYL, Lam WH, Yam VWW (2017) Synthesis of luminescent platinum(II) 2,6-bis-(N-dodecylbenzimidazol-2 '-yl)pyridine foldamers and their supramolecular assembly and metallogel formation. J Am Chem Soc 139:8639–8645
154. Zhang SL, Luo KJ, Geng H, Ni HL, Wang HF, Li Q (2017) New phosphorescent platinum(II) complexes with tetradentate CNNC ligands: liquid crystallinity and polarized emission. Dalton Trans 46:899–906

155. Chico R, de Domingo E, Dominguez C, Donnio B, Heinrich B, Termine R, Golemme A, Coco S, Espinet P (2017) High one-dimensional charge mobility in semiconducting columnar mesophases of isocyano-triphenylene metal complexes. Chem Mater 29:7587–7595
156. Au-Yeung H-L, Leung SY-L, Tam AYY, Yam VW-W (2014) Transformable nanostructures of platinum-containing organosilane hybrids: non-covalent self-assembly of polyhedral oligomeric silsesquioxanes assisted by Pt···Pt and π–π stacking interactions of alkynylplatinum(II) terpyridine moieties. J Am Chem Soc 136:17910–17913
157. Au-Yeung H-L, Tam AYY, Leung SY-L, Yam VW-W (2017) Supramolecular assembly of platinum-containing polyhedral oligomeric silsesquioxanes: an interplay of intermolecular interactions and a correlation between structural modifications and morphological transformations. Chem Sci 8:2267–2276
158. Li L, Feng S, Liu H (2014) Hybrid lanthanide complexes based on a novel β-diketone functionalized polyhedral oligomeric silsesquioxane (POSS) and their nanocomposites with PMMA via in situ polymerization. RSC Adv 4:39132–39139
159. Xu Q, Li Z, Chen M, Li H (2016) Synthesis and luminescence of octacarboxy cubic polyhedral oligosilsesquioxanes coordinated with terbium. CrystEngComm 18:177–182
160. Naka K, Chujo Y (2009) Nanohybridized synthesis of metal nanoparticles and their organization. In: Muramatsu A, Miyashita T (eds) Nanohybridization of organic-inorganic materials, vol XVI. Springer, Berlin, p 191
161. Kuo S-W, Wu Y-C, Lu C-H., Chang F-C (2009) Surface modification of gold nanoparticles with polyhedral oligomeric silsesquioxane and incorporation within polymer matrices. J Polym Sci Part B Poly Phys 47:811–819
162. Daniel M-C, Astruc D (2004) Gold nanoparticles: assembly, supramolecular chemistry, quantum-size-related properties, and applications toward biology, catalysis, and nanotechnology. Chem Rev 104:293–346
163. Naka K, Itoh H, Chujo Y (2004) Preparation of gold nanoparticles protected by a cubic silsesquioxane and their monolayer formation on a glass substrate. Bull Chem Soc Jpn 77:1767–1771
164. Imoto H, Ishida K, Sasaki A, Irie Y, Ito H, Naka K, Chujo Y (2015) Spontaneous formation of gold nanoparticles with octa(3-aminopropyl) polyhedral oligomeric silsesquioxane. Bull Chem Soc Jpn 88:653–656
165. Imoto H, Shigeyoshi S, Naka K (2015) Surface modification and aggregation control of gold nanoparticles via multifunctional stabilizer based on polyhedral oligomeric silsesquioxane. Bull Chem Sci Jpn 88:693–697
166. Wang X, Naka K, Itoh H, Chujo Y (2004) Self-organized nanocomposites of functionalized gold nanoparticles with octa(3-aminopropyl)octasilsesquioxane. Chem Lett 33:216–217
167. Carroll JB, Frankamp BL, Srivastava S, Rotello VM (2004) Electrostatic self-assembly of structured gold nanoparticle/polyhedral oligomeric silsesquioxane (POSS) nanocomposites. J Mater Chem 14:690–694
168. Bai W, Sheng Q, Ma X, Zheng J (2015) Synthesis of silver nanoparticles based on hydrophobic interface regulation and its application of electrochemical catalysis. ACS Sustain Chem Eng 3:1600–1609
169. Létant SE, Maiti A, Jones TV, Herberg JL, Maxwell RS, Saab AP (2009) Polyhedral oligomeric silsesquioxane (POSS)-stabilized Pd nanoparticles: factors governing crystallite morphology and secondary aggregate structure. J Phys Chem C 113:19424–19431
170. Naka K, Itoh H, Chujo Y (2002) Self-organization of spherical aggregates of palladium nanoparticles with a cubic silsesquioxane. Nano Lett 2:1183–1186
171. Naka K, Sato M, Chujo Y (2008) Stabilized spherical aggregate of palladium nanoparticles prepared by reduction of palladium acetate in octa(3-aminopropyl)octasilsesquioxane as a rigid template. Langmuir 24:2719–2726
172. Wang X, Naka K, Zhu M, Itoh H, Chujo Y (2005) Microporous nanocomposites of Pd and Au nanoparticles via hierarchical self-assembly. Langmuir 21:12395–12398
173. Chen T, Ge C, Zhang Y, Zhao Q, Hao F, Bao N (2015) Bimetallic platinum-bismuth nanoparticles prepared with silsesquioxane for enhanced electrooxidation of formic acid. Int J Hydrogen Energy 40:4548–4557

174. Lu C-H, Kuo S-W, Huang C-F, Chang F-C (2009) Self-assembled fernlike microstructures of polyhedral oligomeric silsesquioxane/gold nanoparticle hybrids. J Phys Chem C 113:3517–3524
175. Lu C-H, Chang F-C (2011) Polyhedral oligomeric silsesquioxane-encapsulating amorphous palladium nanoclusters as catalysts for Heck reactions. ACS Catal 1:481–488
176. Carroll JB, Frankamp BL, Rotello VM (2002) Self-assembly of gold nanoparticles through tandem hydrogen bonding and polyoligosilsequioxane (POSS)–POSS recognition processes. Chem Commun 1892–1893
177. Jeoung E, Carroll JB, Rotello VM (2002) Surface modification via 'lock and key' specific self-assembly of polyhedral oligomeric silsequioxane (POSS) derivatives to modified gold surfaces. Chem Commun, 1510–1511
178. Cai J, Chao L, Watanabe, A (2015) Facile preparation of hierarchical structures using crystallization-kinetics driven self-assembly. ACS Appl Mater Interfaces 18697–18706
179. Ledin PA, Russell M, Geldmeier JA, Tkachenko IM, Mahmoud MA, Shevchenko V, El-Sayed MA, Tsukruk VV (2015) Light-responsive plasmonic arrays consisting of silver nanocubes and a photoisomerizable matrix. ACS Appl Mater Interfaces 7:4902–4912
180. Ye X, Gong J, Wang Z, Zhang Z, Han S, Jiang X (2013) Hybrid POSS-containing brush on gold surfaces for protein resistance. Macromol Biosci 13:921–926
181. Wang F, Phonthammachai N, Mya KY, Tjiu WW, He C (2011) PEG-POSS Assisted facile preparation of amphiphilic gold nanoparticles and interface formation of Janus nanoparticles. Chem Commun 47:767–769
182. Zhang X, Hu Y, Liu R, Sun J, Fang S (2015) Thermosensitive gold nanoparticles based on star-shaped poly(N-isopropylacrylamide) with a cubic silsesquioxane core. Macromol Res 23:227–230
183. Mohapatra S, Chaiprasert T, Sodkhomkhum R, Kunthom R, Hanprasit S, Sangtrirutnugul P, Ervithayasuporn V (2016) Solid–state synthesis of polyhedral oligomeric silsesquioxane-supported N-heterocyclic carbenes/imidazolium salts on palladium nanoparticles: highly active and recyclable catalyst. ChemistrySelect 1:5353–5357
184. Frankamp BL, Fischer NO, Hong R, Srivastava S, Rotello VM (2006) Surface modification using cubic silsesquioxane ligands. Facile synthesis of water-soluble metal oxide nanoparticles. Chem Mater 18:956–959
185. Etgar L, Lifshitz E, Tannenbaum R (2007) Hierarchical conjugate structure of γ-Fe_2O_3 nanoparticles and PbSe quantum dots for biological applications. J Phys Chem C 111:6238–6244
186. Yuan W, Shen J, Lia L, Liu X, Zou H (2014) Preparation of POSS-poly(ε-caprolactone)-β-cyclodextrin/Fe_3O_4 hybrid magnetic micelles for removal of bisphenol A from water. Carbohyd Polym 113:353–361
187. Safaei-Ghomi J, Nazemzadeh SH, Shahbazi-Alavi H (2016) Novel magnetic nanoparticles-supported inorganic-organic hybrids based on POSS as an efficient nanomagnetic catalyst for the synthesis of pyran derivatives. Catalysis Comm 86:14–18
188. Evans CM, Cass LC, Knowles KE, Tice DB, Chang RPH, Weiss EA (2012) Review of the synthesis and properties of colloidal quantum dots: the evolving role of coordinating surface ligands. J Coordination Chem 65:2391–2414
189. Wang Y, Vaneski A, Yang H, Gupta S, Hetsch F, Kershaw SV, Teoh WY, Li H, Rogach AL (2013) Polyhedral oligomeric silsesquioxane as a ligand for CdSe quantum dots. J Phys Chem C 117:1857–1862
190. Rizvi SB, Yildirimer L, Ghaderi S, Ramesh B, Seifalian AM, Keshtgar M (2012) A novel POSS-coated quantum dot for biological application. Int J Nanomed 7:3915–3927
191. He Y, Wang H-F, Yan X-P (2009) Self-assembly of Mn-doped ZnS quantum dots/octa(3-aminopropyl)octasilsequioxane octahydrochloride nanohybrids for optosensing DNA. Chem Eur J 15:5436–5440
192. Zhao X, Ma R, Yang M, Yang H, Jin P, Li Z, Fan Y, Du A, Cao X (2017) Fabrication of POSS-coated CdTe quantum dots sensitized solar cells with enhanced photovoltaic properties. J Alloys Comp 726:593–600

193. Park Y, Yoo J, Lim B, Kwon W, Rhee S-W (2016) Improving the functionality of carbon nanodots: doping and surface functionalization. J Mater Chem A 4:11582–11603
194. Wang D, Liu J, Chen J-F, Dai L (2015) Surface functionalization of carbon dots with polyhedral oligomeric silsesquioxane (POSS) for multifunctional applications. Adv Mater Interfaces 3:1500439
195. Wang W-J, Hai X, Mao Q-X, Chen M-L, Wang J-H (2015) Polyhedral oligomeric silsesquioxane functionalized carbon dots for cell imaging. ACS Appl Mater Interfaces 7:16609–16616
196. Wang Y, Kalytchuk S, Wang L, Zhovtiuk O, Cepe K, Zboril R, Rogach AL (2015) Carbon dot hybrids with oligomeric silsesquioxane: solid-state luminophores with high photoluminescence quantum yield and applicability in white light emitting devices. Chem Commun 51:2950–2953
197. Potsi G, Rossos A, Kouloumpis A, Antoniou MK, Spyrou K, Karakassides MA, Gournis D, Rudolf P (2016) Carbon nanostructures containing polyhedral oligomeric silsesquioxanes (POSS). Curr Org Chem 20:662–673
198. Inagaki M, Toyoda M, Soneda Y, Tsujimura S, Morishita T (2016) Templated mesoporous carbons: synthesis and applications. Carbon 107:448–473
199. Kong J, Wei Y, Lu X, He C (2017) Cross-linking Si_xO_y cages with carbon by thermally annealing polyhedral oligomeric silsesquioxane: structures, morphology, and electrochemical properties as lithium-ion battery anodes. ChemElectroChem 4:49–55
200. Li Z, Wu D, Liang Y, Fu R, Matyjaszewski K (2014) Synthesis of well-defined microporous carbons by molecular-scale templating with polyhedral oligomeric silsesquioxane moieties. J Am Chem Soc 136:4805–4808
201. Li Z, Li Z, Zhong W, Li C, Li L, Zhang H (2017) Facile synthesis of ultra-small Si particles embedded in carbon framework using Si-carbon integration strategy with superior lithium ion storage performance. Chem Eng J 319:1–8
202. Li Z, Li Z, Li L, Li C, Zhong W, Zhang H (2017) Construction of hierarchically one-dimensional core–shell CNT@microporous carbon by covalent bond-induced surface-confined cross-linking for high-performance supercapacitor. ACS Appl Mater Interfaces 9:15557–15565
203. Liu D, Cheng G, Zhao H, Zeng C, Qu D, Xiao L, Tang H, Deng Z, Li Y, Su B-L (2016) Self-assembly of polyhedral oligosilsesquioxane (POSS) into hierarchically ordered mesoporous carbons with uniform microporosity and nitrogen-doping for high performance supercapacitors. Nano Energy 22:255–268
204. Ren Z, Yan S (2016) Polysiloxanes for optoelectronic applications. Progr Mater Sci 83:383–416
205. Li Z, Kong J, Wang F, He C (2017) Polyhedral oligomeric silsesquioxanes (POSSs): an important building block for organic optoelectronic materials. J Mater Chem C 5:5283–5298
206. Leu C-M, Chang Y-T, Wei K-H (2003) Polyimide-side-chain tethered polyhedral oligomeric silsesquioxane nanocomposites for low-dielectric film applications. Chem Mater 15:3721–3727
207. Chen Y, Kang E-T (2014) New approach to nanocomposites of polyimides containing polyhedral oligomeric silsesquioxane for dielectric applications. Mater Lett 58:3716–3719
208. Ben H-J, Ren X-K, Song B, Li X, Feng Y, Jiang W, Chen E-C, Wang Z, Jiang S (2017) Synthesis, crystal structure, enhanced photoluminescence properties and fluoride detection ability of S-heterocyclic annulated perylene diimide-polyhedral oligosilsesquioxane dye. J Mater Chem C 5:2566–2576
209. Vinnik FM (1993) Photophysics of preassociated pyrenes in aqueous polymer solutions and in other organized media. Chem Rev 93:587–614
210. Figueira-Duarte TM, Müllen K (2011) Chem Rev 111:7260–7314
211. Bains G, Patel AB, Narayanaswami V (2011) Molecules 16:7909–7935
212. Lin TT, He C, Xiao Y (2003) Theoretical studies of monosubstituted and higher phenyl-substituted octahydrosilsesquioxanes. J Phys Chem B 107:13788–13792
213. Chu Y-L, Cheng C-C, Chen Y-P, Yen Y-C, Chang F-C (2012) A new supramolecular POSS electroluminescent material. J Mater Chem 22:9285–9292

214. Cheng C-C, Chu Y-L, Chu C-W, Lee D-J (2016) Highly efficient organic–inorganic electroluminescence materials for solution processed blue organic light-emitting diodes. J Mater Chem C 4:6461–6465
215. Bai H, Li C, Shi G (2008) Pyrenyl excimers induced by the crystallization of POSS moieties: spectroscopic studies and sensing applications. ChemPhysChem 9:1908–1913
216. Gao Y, Xu W, Zhu D, Chen L, Fu Y, He Q, Cao H, Cheng J (2015) Highly efficient nitrate ester explosive vapor probe based on multiple triphenylaminopyrenyl substituted POSS. J Mater Chem A 3:4820–4826
217. Lu C-H, Tsai C-H, Chang F-C, Jeong K-U, Kuo S-W (2011) Self-assembly behavior and photoluminescence property of bispyrenyl-POSS nanoparticle hybrid. J Colloid Interf Sci 358:93–101
218. Yang XH, Giovenzana T, Feild B, Jabbour GE (2012) Sellinger, A Solution processeable organic–inorganic hybrids based on pyrene functionalized mixed cubic silsesquioxanes as emitters in OLEDs. J Mater Chem 22:12689–12694
219. Chanmungkalakul S, Ervithayasuporn V, Hanprasit S, Masik M, Prigyai N, Kiatkamjornwong S (2017) Silsesquioxane cages as fluoride sensors. Chem Commun 53:12108–12111
220. Bassindale AR, Pourny M, Taylor PG, Hursthouse MB, Light ME (2003) Fluoride-Ion encapsulation within a silsesquioxane cage. Angew Chem Int Ed 42:3488–3490
221. Pappalardo RR, Marcos ES, Lopez-Ruiz MF (1993) Solvent effects on molecular geometries and isomerization processes: a study of push-pull ethylenes in solution. J Am Chem Soc 115:3722–3730
222. Clarke D, Mathew S, Matisons J, Simon G, Skelton BW (2011) Synthesis and characterization of a range of POSS imides. Dyes Pigm 92:659–667
223. Ren X, Sun B, Tsai C-C, Tu Y, Leng S, Li K, Kang Z, Van Horn RM, Li X, Zhu M, Wesdemiotis C, Zhang W-B, Cheng SZD (2010) Synthesis, self-assembly, and crystal structure of a shape-persistent polyhedral-oligosilsesquioxane-nanoparticle-tethered perylene diimide. J Phys Chem B 114:4802–4810
224. Zhang Y, Zhang L, Liu H, Sun D, Li X (2015) Synthesis and aggregation properties of a series of dumbbell polyhedral oligosilsesquioxane-perylene diimide triads. CrystEngComm 17:1453–1463
225. Lucenti E, Botta C, Cariati E, Righetto S, Scarpellini M, Tordin E, Ugo R (2013) New organic-inorganic hybrid materials based on perylene diimide-polyhedral oligomeric silsesquioxane dyes with reduced quenching of the emission in the solid state. Dyes Pigm 96:748–755
226. Du F, Tian J, Wang H, Liu B, Jin B, Bai R (2012) Synthesis and luminescence of POSS-containing perylene bisimide-bridged amphiphilic polymers. Macromolecules 45:3086–3093
227. Matsumoto K, Nishi K, Ando K, Jikei M (2015) Synthesis and properties of aromatic polyamide dendrimers with polyhedral oligomeric silsesquioxane cores. Polym Chem 6:4758–4765
228. Mehl GH, Saez IM (1999) Polyhedral liquid crystal silsesquioxanes. Appl Organometal Chem 13:261–272
229. Saez IM, Goodby JW (2001) Chiral nematic octasilsesquioxanes. J Mater Chem 11:2845–2851
230. Haxton KJ, Morris RE (2009) Polyhedral oligomeric silsesquioxane dendrimers in silicon-containing dendritic polymers. In: Dvornic PR, Owen MJ (eds) Advances in silicon science. Springer Science + Business Media B.V., Berlin, pp 121–139
231. Saez IM, Goodby JW (2008) Supermolecular liquid crystals. In: Kato T (ed) Structure and bonding (Series Editor: Mingos DMP) liquid crystalline functional assemblies and their supramolecular structures, vol 128. Springer, Berlin, pp 1–62
232. Zhang C, Bunning TJ, Laine RM (2001) Synthesis and characterization of liquid crystalline silsesquioxanes. Chem Mater 13:3653–3662
233. Shibaev V, Boiko N (2009) Liquid crystalline silicon-containing dendrimers with terminal mesogenic groups. In: Dvornic PR, Owen MJ (eds) Advances in silicon science. Springer Science + Business Media B.V., Berlin, pp 237–283

234. Mehl GH, Goodby JW (1996) Liquid-crystalline, substituted octakis-(dimethylsiloxy)octasilsesquioxanes: oligomeric supermolecular materials with defined topology. Angew Chem Int Ed Eng 35:2641–2643
235. Saez IM, Goodby JW, Richardson RM (2001) A liquid-crystalline silsesquioxane dendrimer exhibiting chiral nematic and columnar mesophases. Chem Eur J 7:2758–2764
236. Keith C, Dantlgraber G, Reddy RA, Baumeister U, Prehm M, Hahn H, Lang H, Tschierske C (2007) The influence of shape and size of silyl units on the properties of bent-core liquid crystals—from dimers via oligomers and dendrimers to polymers. J Mater Chem 17:3796–3805
237. Pan Q, Chen X, Fan X, Shen Z, Zhou Q (2008) Organic–inorganic hybrid bent-core liquid crystals with cubic silsesquioxane cores. J Mater Chem 18:3481–3488
238. Białecka-Florjańczyk E, Sołtysiak JT (2010) Liquid crystalline silicon-containing oligomers. J Organomet Chem 695:1911–1917
239. Chiang I-H, Chuang W-T, Lu C-L, Lee M-T, Lin H-C (2015) Shape and confinement effects of various terminal siloxane groups on supramolecular interactions of hydrogen-bonded bent-core liquid crystals. Chem Mater 27:4525–4537
240. Pan Q, Gao L, Chen X, Fan X, Zhou Q (2007) Star mesogen-jacketed liquid crystalline polymers with silsesquioxane core: synthesis and characterization. Macromolecules 40:4887–4894
241. Wang X, Cho CM, Say WY, Tan AYX, He C, Chan HSO, Xu J (2011) Organic–inorganic hybrid liquid crystals derived from octameric silsesquioxanes. Effect of the peripheral groups in mesogens on the formation of liquid crystals. J Mater Chem 21:5248–5257
242. Saez IM, Goodby JW (1999) Supermolecular liquid crystal dendrimers based on the octasilsesquioxane core. Liq Cryst 26:1101–1105
243. Karahaliou PK, Kouwer PHJ, Meyer T, Mehl GH, Photinos DJ (2008) Long- and short-range order in the mesophases of laterally substituted calamitic mesogens and their radial octapodes. J Phys Chem B 112:6550–6556
244. Kim D-Y, Kim S, Lee S-A, Choi Y-E, Yoon W-J, Kuo S-W, Hsu C-H, Huang M, Lee SH, Jeong K-U (2014) Asymmetric organic–inorganic hybrid giant molecule: cyanobiphenyl monosubstituted polyhedral oligomeric silsesquioxane nanoparticles for vertical alignment of liquid crystals. J Phys Chem C 118:6300–6306
245. Kim N, Kim D-Y, Park M, Choi Y-J, Kim S, Lee SH, Jeong K-U (2015) Asymmetric organic–inorganic hybrid giant molecule: hierarchical smectic phase induced from POSS nanoparticles by addition of nematic liquid crystals. J Phys Chem C 119:766–774
246. Miniewicz A, Girones J, Karpinski P, Mossety-Leszczak B, Galina H, Dutkiewicz M (2014) Photochromic and nonlinear optical properties of azo-functionalized POSS nanoparticles dispersed in nematic liquid crystals. J Mater Chem C 2:432–440
247. Liu H-S, Jeng S-C (2013) Liquid crystal alignment by polyhedral oligomeric silsesquioxane (POSS)–polyimide nanocomposites. Opt Mater 35:1418–1421
248. Hou P-P, Gu K-H, Zhu Y-F, Zhang Z-Y, Wang Q, Pan H-B, Yang S, Shen Z, Fan X-H (2015) Synthesis and sub-10 nm supramolecular selfassembly of a nanohybrid with a polynorbornene main chain and side-chain POSS moieties. RSC Adv 5:70163–70171
249. Zhu Y-F, Liu W, Zhang M-Y, Zhou Y, Zhang Y-D, Hou P-P, Pan Y, Shen Z, Fan X-H, Zhou Q-F (2015) POSS-containing jacketed polymer: hybrid inclusion complex with hierarchically ordered structures at sub-10 nm and Angstrom length scales. Macromolecules 48:2358–2366
250. Mehl GH, Thornton AJ, Goodby JW (1999) Oligomers and dendrimers based on siloxane and silsesquioxane cores: does the structure of the central core affect the liquid-crystalline properties? Mol Cryst Liquid Cryst Sci Technol Sect A. Mol Cryst Liquid Cryst 332:455–461
251. Wang G, Xiong Y, Tang H (2015) Synthesis and characterisation of star-shaped liquid crystalline polymer with a POSS core. Liquid Cryst 42:1280–1289
252. Miao J, Zhu L (2010) Topology controlled supramolecular self-assembly of octa triphenylene-substituted polyhedral oligomeric silsesquioxane hybrid supermolecules. J Phys Chem B 114:1879–1887
253. Cui L, Collet JP, Xu G, Zhu L (2006) Supramolecular self-assembly in a disk-cube dyad molecule based on triphenylene and polyhedral oligomeric silsesquioxane (POSS). Chem Mater 18:3503–3512

254. Xiang K, He L, Li Y, Xu C, Li S (2015) Dendritic AIE-active luminogens with a POSS core: synthesis, characterization, and application as chemosensors. RSC Adv 5:97224–97230
255. Zuo Y, Wang X, Yang Y, Huang D, Yang F, Shen H, Wu D (2016) Facile preparation of pH-responsive AIE-active POSS dendrimers for the detection of trivalent metal cations and acid gases. Polym Chem 7:6432–6436
256. Zhou H, Li J, Chua MH, Yan H, Ye Q, Song J, Lin TT, Tang BZ, Xu J (2016) Tetraphenylethene (TPE) modified polyhedral oligomeric silsesquioxanes (POSS): unadulterated monomer emission, aggregation-induced emission and nanostructural self-assembly modulated by the flexible spacer between POSS and TPE. Chem Commun 52:12478–12481
257. Zhang M-Y, Zhou S, Pan H-B, Ping J, Zhang W, Fan X-H, Shen Z (2017) Structural complexity induced by topology change in hybrids consisting of hexa-perihexabenzocoronene and polyhedral oligomeric silsesquioxane. Chem Commun 53:8679–8682
258. Zhang M-Y, Gu K-H, Zhou Y, Zhou S, Fan X-H, Shen Z (2016) The synthesis and self-assembly of disc-cube dyads with spacers of different lengths. Chem Commun 52:3923–3926
259. Tan J, Ma D, Sun X, Feng S, Zhang C (2013) Synthesis and characterization of an octaimidazolium based polyhedral oligomeric silsesquioxanes ionic liquid by an ion-exchange reaction. Dalton Trans 42:4337–4339
260. Tanaka K, Ishiguro F, Jeon J-H, Hiraoka T, Chujo Y (2015) POSS ionic liquid crystals. NPG Asia Mater 7:e174
261. Tanaka K, Ishiguro F, Chujo Y (2010) POSS ionic liquid. J Am Chem Soc 132:17649–17651
262. Gon M, Tanaka K, Chujo Y (2017) Creative synthesis of organic-inorganic molecular hybrid materials. Bull Chem Soc Jpn 90:463–474
263. Zhou J, Yin P, Hu L, Haso F, Liu T (2014) Self-assembly of subnanometer-scaled polyhedral oligomeric silsesquioxane (POSS) macroions in ddilute solution. Eur J Inorg Chem 4593–4599
264. Zhang W, Wang Z-S (2014) Synthesis of POSS-based ionic conductors with low glass transition temperatures for efficient solid-state dye-sensitized solar cells. ACS Appl Mater Interfaces 6:10714–10721
265. Lee JH, Lee AS, Lee J-C, Hong SM, Hwang SS, Koo CM (2017) Multifunctional mesoporous ionic gels and scaffolds derived from polyhedral oligomeric silsesquioxanes. ACS Appl Mater Interfaces 9:3616–3623
266. Yuan G, Wang X, Wu D, Hammouda B (2016) Structural analysis of dendrimers based on polyhedral oligomeric silsesquioxane and their assemblies in solution by small-angle neutron scattering: fits to a modified two correlation lengths model. Polymer 100:119–125
267. Bai Y, Yang L, Toh CL, He C, Lu X (2013) Temperature and pH dual-responsive behavior of dendritic poly(*N*-isopropylacrylamide) with a polyoligomeric silsesquioxane core and poly(2-hydroxyethyl methacrylate) shell. Macromol Chem Phys 214:396–404
268. Naka K, Masuoka S, Shinke R, Yamada M (2012) Synthesis of first- and second-generation imidazole terminated POSS-core dendrimers and their pH responsive and coordination properties. Polym J 44:353–359
269. Naka K, Shinke R, Yamada M, Belkada FD, Aijo Y, Irie Y, Shankar SR, Smaran KS, Matsumi N, Tomita S, Sakurai S (2014) Synthesis of imidazolium salt-terminated poly(amidoamine)-typed POSS-core dendrimers and their solution and bulk properties. Polym J 46:42–51
270. Li L, Liu H (2016) Rapid preparation of silsesquioxane-based ionic liquids. Chem Eur J 22:4713–4716
271. Han J, Zheng Y, Zheng S, Li S, Hu T, Tang A, Gao C (2014) Water soluble octa-functionalized POSS: all-click chemistry synthesis and efficient host–guest encapsulation. Chem Commun 50:8712–8714
272. Ghanbari H, Cousins BG, Seifalian AM (2011) A nanocage for nanomedicine: polyhedral oligomeric silsesquioxane (POSS). Macromol Rapid Commun 32:1032–1046
273. Fabritz S, Hörner S, Avrutina O, Kolmar H (2013) Bioconjugation on cube-octameric silsesquioxanes. Org Biomol Chem 11:2224–2236
274. Hörner S, Fabritz S, Herce HD, Avrutina O, Dietz C, Stark RW, Cardosoc M, Kolmar H (2013) Cube-octameric silsesquioxane-mediated cargo peptide delivery into living cancer cells. Org Biomol Chem 11:2258–2265

275. Mori H, Saito S (2011) Smart organic–inorganic hybrids based on the complexation of amino acid-based polymers and water-soluble silsesquioxane nanoparticles. React Funct Polym 71:1023–1032
276. Mori H, Saito S, Shoji K (2011) Complexation of amino-acid-based block copolymers with dual thermoresponsive properties and water-soluble silsesquioxane nanoparticles. Macromol Chem Phys 212:2558–2572
277. Lin Y-C, Kuo S-W (2012) Hierarchical self-assembly structures of POSS-containing polypeptide block copolymers synthesized using a combination of ATRP, ROP and click chemistry. Polym Chem 3:882–891
278. Cui L, Zhu L (2006) Lamellar to inverted hexagonal mesophase transition in DNA complexes with calamitic, discotic, and cubic shaped cationic lipids. Langmuir 22:5982–5985
279. Mendes AC, Baran ET, Reis RL, Azevedo HS (2013) Self-assembly in nature: using the principles of nature to create complex nanobiomaterials. WIREs Nanomed Nanobiotechnol 5:582–612
280. Kricheldorf HR (2006) Polypeptides and 100 years of chemistry of a-amino acid *N*-carboxyanhydrides. Angew Chem Int Ed 45:5752–5784
281. Byrne M, Murphy R, Kapetanakis A, Ramsey J, Cryan S-A, Heise A (2015) Star-shaped polypeptides: synthesis and opportunities for delivery of therapeutics. Macromol Rapid Commun 36:1862–1876
282. Qi Y, Chilkoti A (2014) Growing polymers from peptides and proteins: a biomedical perspective. Polym Chem 5:266–276
283. Kuo S-W, Tsai H-T (2010) Control of peptide secondary structure on star shape polypeptides tethered to polyhedral oligomeric silsesquioxane nanoparticle through click chemistry. Polymer 51:5695–5704
284. Fabritz S, Hörner S, Könning D, Empting M, Reinwarth M, Dietz C, Glotzbach B, Frauendorf H, Kolmar H, Avrutina O (2012) From pico to nano: biofunctionalization of cube-octameric silsesquioxanes by peptides and miniproteins. Org Biomol Chem 10:6287–6293
285. Lin Y-C, Kuo S-W (2012) Hierarchical self-assembly and secondary structures of linear polypeptides graft onto POSS in the side chain through click chemistry. Polym Chem 3:162–171
286. Lin Y-C, Kuo S-W (2011) Self-assembly and secondary structures of linear polypeptides tethered to polyhedral oligomeric silsesquioxane nanoparticles through click chemistry. J Polym Sci Part A Polym Chem 49:2127–2137
287. Kuo S-W, Lee H-F, Huang W-J, Jeong K-U, Chang F-C (2009) Solid state and solution self-assembly of helical polypeptides tethered to polyhedral oligomeric silsesquioxanes. Macromolecules 42:1619–1626
288. Haldar U, Pan A, Mukherjee I, De P (2016) POSS semitelechelic Aβ17–19 peptide initiated helical polypeptides and their structural diversity in aqueous medium. Polym Chem 7:6231–6240
289. Rinkenauer AC, Schubert S, Traeger A, Schubert US (2015) The influence of polymer architecture on in vitro pDNA transfection. J Mater Chem B 3:7477–7493
290. Yang YY, Wang X, Hu Y, Hu H, Wu D-C, Xu F-J (2014) Bioreducible POSS-cored star-shaped polycation for efficient gene delivery. ACS Appl Mater Interfaces 6:1044–1052
291. Jiang S, Poh YZ, Loh XJ (2014) POSS-based hybrid cationic copolymers with low aggregation potential for efficient gene delivery. Org Biomol Chem 12:6500–6506
292. Jiang S, Poh YZ, Loh XJ (2015) POSS-based hybrid cationic copolymers with low aggregation potential for efficient gene delivery. RSC Adv 5:71322–71328
293. Loh XJ, Zhang Z-X, Mya KY, Wu Y-I, Hea CB, Li J (2010) Efficient gene delivery with paclitaxel-loaded DNA-hybrid polyplexes based on cationic polyhedral oligomeric silsesquioxanes. J Mater Chem 20:10634–10642
294. Cui L, Chen D, Zhu L (2008) Conformation transformation determined by different self-assembled phases in a DNA complex with cationic polyhedral oligomeric silsesquioxane lipid. ACS Nano 2:921–927

295. Zou Q-C, Yan Q-J, Song G-W, Zhang S-L, Wu L-M (2007) Detection of DNA using cationic polyhedral oligomeric silsesquioxane nanoparticles as the probe by resonance light scattering technique. Biosens Bioelectron 22:1461–1465
296. Jeon J-H, Kakuta T, Tanaka K, Chujo Y (2015) Facile design of organic–inorganic hybrid gels for molecular recognition of nucleoside triphosphates. Bioorganic Med Chem Lett 25:2050–2055
297. Liu Y-L, Liu C-S, Cho C-I, Hwu M-J (2007) Polyhedral oligomeric silsequioxane monolayer as a nanoporous interlayer for preparation of low-k dielectric films. Nanotechnology 18:225701
298. Wu G, Su Z (2006) Polyhedral oligomeric silsesquioxane nanocomposite thin films via layer-by-layer electrostatic self-assembly. Chem Mater 18:3726–3732
299. Ariga K, Yamauchi Y, Mori T, Hill JP (2013) 25th anniversary article: what can be done with the Langmuir-Blodgett method? Recent developments and its critical role in materials science. Adv Mater 25:6477–6512
300. Esker AR, Yu H (2012) Langmuir monolayers of siloxanes and silsesquioxanes. In: Owen MJ, Dvornic PR (eds) Silicone surface science, advances in silicon science. Springer Science + Business Media, Dordrecht
301. Deng J, Polidan JT, Hottle JR, Farmer-Creely CE, Viers BD, Esker AE (2002) Polyhedral oligomeric silsesquioxanes: a new class of amphiphiles at the air/water interface. J Am Chem Soc 124:15194–15195
302. Deng J, Hottle JR, Polidan JT, Kim H-J, Farmer-Creely CE, Viers BD, Esker AE (2004) Polyhedral oligomeric silsesquioxane amphiphiles: isotherm and Brewster angle microscopy studies of trisilanolisobutyl-POSS at the air/water interface. Langmuir 20:109–115
303. Deng J, Viers BD, Esker AR, Anseth JW, Fuller GG (2005) Phase behavior and viscoelastic properties of trisilanolcyclohexyl-POSS at the air/water interface. Langmuir 21:2375–2385
304. Wamke A, Dopierała K, Prochaska K, Maciejewski H, Biadasz A, Dudkowiak A (2015) Characterization of Langmuir monolayer, Langmuir-Blodgett and Langmuir-Schaefer films formed by POSS compounds. Colloids Surf A 464:110–120
305. Banerjee R, Sanya MK, Bera MK, Gibaud A, Lin B, Meron M (2015) Reversible monolayer-to-crystalline phase transition in amphiphilic silsesquioxane at the air–water interface. Sci Rep 5, No. 8497
306. Dutkiewicz M, Karasiewicz J, Rojewska M, Skrzypiec M, Dopierała K, Prochaska K, Maciejewski H (2016) Synthesis of an open-cage structure POSS containing various functional groups and their effect on the formation and properties of Langmuir monolayers. Chem Eur J 22:13275–13286
307. Dopierała K, Bojakowska K, Karasiewicz J, Maciejewski H, Prochaska K (2016) Interfacial behaviour of cubic silsesquioxane and silica nanoparticles in Langmuir and Langmuir-Blodgett films. RSC Adv 6:94934–94941
308. Paczesny J, Binkiewicz I, Janczuk M, Wybrańska K, Richter Ł, Hołyst R (2015) Langmuir and Langmuir–Blodgett films of unsymmetrical and fully condensed polyhedral oligomeric silsesquioxanes (POSS). J Phys Chem C 119:27007–27017
309. Kraus-Ophir S, Jerman I, Orel B, Mandler D (2011) Symmetrical thiol functionalized polyhedral oligomeric silsesquioxanes as building blocks for LB films. Soft Matter 7:8862–8869
310. Dopierala K, Wamke A, Dutkiewicz M, Maciejewski H, Prochaska K (2014) Interfacial properties of fully condensed functional silsesquioxane: a Langmuir monolayer study. J Phys Chem C 118:24548–24555
311. Gunawidjaja R, Huang F, Gumenna M, Klimenko N, Nunnery GA, Shevchenko V, Tannenbaum R, Tsukruk VV (2009) Bulk and surface assembly of branched amphiphilic polyhedral oligomer silsesquioxane compounds. Langmuir 25:1196–1209
312. Dopierała K, Maciejewski H, Prochaska K (2016) Interaction of polyhedral oligomeric silsesquioxane containing epoxycyclohexyl groups with cholesterol at the air/water interface. Colloids Surf B 140:135–141
313. Li Z, Ma X, Guan X, Qiang X, Zang D, Chen F (2017) Aggregation behavior of star-shaped fluoropolymers containing polyhedral oligomeric silsesquioxane (POSS) at the air–water interface. Colloid Polym Sci 295:157–170

314. Zhang W, Huang M, Su H, Zhang S, Yue K, Dong X-H, Li X, Liu H, Zhang S, Wesdemiotis C, Bernard Lotz B, Zhang W-B, Li Y, Cheng SZD (2016) Toward controlled hierarchical heterogeneities in giant molecules with precisely arranged nano building blocks. ACS Cent Sci 2:48–54
315. Raftopoulos KN, Pielichowski K (2016) Segmental dynamics in hybrid polymer/POSS nanomaterials. Progr Polym Sci 52:136–187
316. Zhou H, Ye Q, Xu J (2017) Polyhedral oligomeric silsesquioxane-based hybrid materials and their applications. Mater Chem Front 1:212–230
317. Chiu C-W, Huang T-K, Wang Y-C, Alamani BG, Lin J-J (2014) Intercalation strategies in clay/polymer hybrids. Progr Polym Sci 39:443–485
318. Kai J, Teo H, Toh CL, Lu X (2011) Catalytic and reinforcing effects of polyhedral oligomeric silsesquioxane (POSS)-imidazolium modified clay in an anhydride-cured epoxy. Polymer 52:1975–1982
319. Hojiyev R, Ulcay Y, Hojamberdiev M, Çelik MS, Carty WM (2017) Hydrophobicity and polymer compatibility of POSS-modified Wyoming Na-montmorillonite for developing polymer-clay nanocomposites. J Colloid Interf Sci 497:393–401
320. Zhao Y, Jiang X, Zhang X, Hou L (2017) Toughened elastomer/polyhedral oligomeric Ssilsesquioxane (POSS)-intercalated rectorite nanocomposites: preparation, microstructure, and mechanical properties. Polym Compos 38:E443–E450
321. Yei D-Y, Kuo S-W, Su Y-C, Chang F-C (2004) Enhanced thermal properties of PS nanocomposites formed from inorganic POSS-treated montmorillonite. Polymer 45:2633–2640
322. Zhao F, Wan C, Bao X, Kandasubramanian B (2009) Modification of montmorillonite with aminopropylisooctyl polyhedral oligomeric silsequioxane. J Colloid Interface Sci 333:164–170
323. Zhao F, Bao X, McLauchlin AR, Gu J, Wan C, Kandasubramanian B (2010) Effect of POSS on morphology and mechanical properties of polyamide 12/montmorillonite nanocomposites. Appl Clay Sci 47:249–256
324. Wan C, Zhao F, Bao X, Kandasubramanian B, Duggan M (2008) Surface characteristics of polyhedral oligomeric silsesquioxane modified clay and its application in polymerization of macrocyclic polyester oligomers. J Phys Chem B 112:11915–11922
325. Fox DM, Maupin PH, Harris RH Jr, Gilman JW, Eldred DV, Katsoulis D, Trulove PC, De Long HC (2007) Use of a polyhedral oligomeric silsesquioxane (POSS)-imidazolium cation as an organic modifier for montmorillonite. Langmuir 23:7707–7714
326. Toh CL, Xi L, Lau SK, Pramoda KP, Chua YC, Lu X (2010) Packing behaviors of structurally different polyhedral oligomeric silsesquioxane-imidazolium surfactants in clay. J Phys Chem B 114:207–214
327. Lee JH, Jeong YG (2011) Preparation and crystallization behavior of polylactide nanocomposites reinforced with POSS-modified montmorillonite. Fibers Polym 12:180–189
328. Toh CL, Yang L, Pramoda KP, Lauc SK, Lu X (2013) Poly(ethylene terephthalate)/clay nanocomposites with trisilanolphenyl polyhedral oligomeric silsesquioxane as dispersant: simultaneously enhanced reinforcing and stabilizing effects. Polym Int 62:1492–1499
329. Cui H-W, Kuo S-W (2012) Using a polyhedral oligomeric silsesquioxane surfactant and click chemistry to exfoliate montmorillonite. RSC Adv 2:12148–12152